CONTINUOUS PROXIMATE TIME-OPTIMAL CONTROL FOR A THIRD ORDER SERVOMECHANISM HAVING A PLANT WITH THREE REAL ROOTS

By

Mohammad Samer Charifa

A Thesis presented to the

DEANSHIP OF GRADUATE STUDIES

In Partial Fulfillment of the Requirements
for the degree

MASTER OF SCIENCE

IN

MECHANICAL ENGINEERING

KING FAHD UNIVERSITY
OF PETROLEUM AND MINERALS

Dhahran, Saudi Arabia

June 2005

KING FAHD UNIVERSITY OF PETROLEUM AND MINERALS
DHAHRAN 31261, SAUDI ARABIA

DEANSHIP OF GRADUATE STUDIES

This thesis, written by **MOHAMMAD SAMER CHARIFA** under the direction of his Thesis Advisor and approved by his Thesis Committee, has been presented to and accepted by the Dean of Graduate Studies, in partial fulfillment of the requirements for the degree of **MASTER OF SCIENCE IN MECHANICAL ENGINEERING.**

Thesis Committee

Dr. Muammer Kalyon (Advisor)

Dr. Faleh Al-.Sulaiman (Member)

Dr. Amin El-Sinawi (Member)

Dr. Faleh Al-.Sulaiman
Department Chairman

Dr. Mohammad A. Al-Ohali
Dean of Graduate Studies

١٤٢٦/٥/١٥

Date 22-6-2005

Dedicated to my beloved parents, Mr. Badea and Mrs. Inaam Sharifa,
whose constant prayers and sacrifice led to this accomplishment

ACKNOWLEDGEMENTS

First and foremost, all praise is due to Allah *subhana-wa-ta'ala* for bestowing me with health, knowledge and patience to complete this work.

Acknowledgements are due to the wonderful university, which I will never forget, King Fahd University of Petroleum & Minerals.

I acknowledge, with deep gratitude and appreciation, the inspiration, encouragement, remarkable assistance and continuous support given to me by my thesis advisor, Dr. Muammar Kalyon. His guidance taught me that *"professionalism is vitally important and with patience and hard working can be achievable"*. I greatly appreciate dedication, attention and patience provided by him throughout the course of this study.

Thanks are due to my thesis committee members, Dr. Faleh Al-Sulaiman and Dr. Amin El-Sinawi for their help and guidance.

I owe very deep appreciations to Dr. M. Hawwa for his comments, encouragements and for giving me the motivation. I am, highly, grateful to Dr. Maan Kousa, who directed me to KFUPM, and introduced me to the world of higher studies.

Special thanks are due to my colleagues at the university, Fahad El-Sulaiman, Salem Bashmal, Firas Tuffaha, Naji Almusabi, Basel Alsaeed, Ahmad Nobah, Khaled Afnan, Omar Molhem, Basem El-shahhat, Qasem Mayowa and Mansour Alharbi.

Last but not the least I am grateful to my parents, brothers, brother-in-law, and sisters for their extreme moral support.

TABLE OF CONTENTS

LIST OF FIGURES

THESIS ABSTRACT

NAME: **MOHAMMAD SAMER CHARIFA**

TITLE: **CONTINUOUS PROXIMATE TIME-OPTIMAL CONTROL FOR A THIRD ORDER SERVOMECHANISM HAVING A PLANT WITH THREE REAL ROOTS**

DEPARTMENT: **MECHANICAL ENGINEERING**

DATE: **JUNE 15, 2005**

A servomechanism is a system that controls the position or velocity of a mechanical devise. In many applications, such as disk-drive head positioning and pick-and-place robots, it is desirable to have servomechanisms effect a minimum time response. Since there is a limit on the magnitude of the control signal in every control system, this leads to time-optimal controllers that are bang-bang. Truly bang-bang time-optimal control systems are not practical, due to the poor overall behavior such as the instantaneous switching and the limit cycles about the target state. In order to eliminate such undesirable behavior, we apply Continuous Proximate Time-Optimal (CPTO) controller to a third order servomechanism having three real roots, which represents our modeling of the hard disk drive servomechanism. We have shown that the CPTO controller gives near time-optimal response for large states, and provides smooth and stable response with near linear control for small states.

To overcome the mathematical difficulties of solving the time-optimal control problem of the model of the plant, new approach based on similarity transformation has been used.

A saturated linear state-feedback controller has been designed for comparison and assessment.

It has been shown through the simulation results that response times are indeed near time-optimal. Moreover, it has been shown though specific examples that the CPTO behaves well in the presence of certain unmodeled dynamics, also it behaves well in the presence of a plant parameter variation providing that the control law is based on the worst-case consideration.

A comparison of the performance of the CPTO controller when changing the design criterion of the linear gain constants has been made.

This work was supported by King Fahd University of Petroleum & Minerals under Project #: FT 2003/5.

ملخص الرسالة

الاسم : **محمد سامر شريفة**

العنوان: **تصميم تحكم مستمر ذو أفضل زمن استجابة تقريبا لنموذج رياضي ذي ثلاثة جذور**

قسم : **الهندسة الميكانيكية**

التاريخ: **8 جمادى الاولى، 1426**

السيرفو هو نظام يتحكم بموقع أو سرعة أداة ميكانيكة ما. يطلب في كثير من تطبيقات السيرفو مثل الذراع القارئة/الكاتبة في سواقة القرص الصلب أو روبوتات الرفع والوضع، أن تكون الإستجابة بأقل وقت ممكن. بما أنه لكل نظام تحكم، يوجد حد للإشارة التحكمية هذا يقودنا الى استخدام التحكم ذي أفضل وقت استجابة والذي يسمى بالبانغ بانغ. فعليا، إن استخدام تحكم البانغ بانغ غير عملي، وذلك بسبب الإداء السيء اجماليا مثل التبديل اللحظي والدوران المحدود حول الحالة المطلوبة. من أجل التخلص من هذا الأداء السيء، نحن طبقنا تقنية التحكم المستمر التقريبي ذي أفضل زمن (CPTO) على نظام سيرفو من الدرجة الثالثة والذي يمثل نمذجتنا لنظام السيرفو في سواقة القرص الصلب (Hard Disk Drive). لقد بينا أن هذا التحكم يعطي استجابة أفضل زمن تقريبا عندما تكون متحولات الحالة ذات قيمة عالية ويعطي استجابة تحكم خطي عندما تكون متحولات الحالة ذات قيمة قليلة.

للتغلب على الصعوبات الرياضية لحل مسألة التحكم ذو أفضل زمن، استخدمنا طريقة جديدة تعتمد على مبدأ التحويل المثلي. وقد تم تصميم تحكم خطي مشبع يعمل على مبدأ التغذية العكسية للحالة، وذلك من أجل المقارنة والتقييم. لقد بينا من خلال المحاكات على الحاسوب أن التحكم (CPTO) يمتلك أفضل زمن استجابة تقريبا، أكثر من ذلك، تم إثبات أن تحكم (CPTO) يعمل بشكل جيد من أجل بعض الديناميكا الغير منمذجة، وأيضا يعمل بشكل جيد عند حصول بعض التغيرات في ثوابت النموذج الرياضي إذا أخذنا بعين الإعتبار التصميم على اساس الحالة الأسوء. تم مقارنة أداء تحكم (CPTO) من أجل أهداف تصميمية مختلفة للتحكم الخطي.

هذه الدراسة اعدت لنيل درجة الماجستير في العلوم
في جامعة الملك فهد للبترول والمعادن
الظهران 31261

CHAPTER 1

INTRODUCTION

1.1. Overview of Time Optimal Control

The objective of optimal control theory is to determine the control signals that will cause a process to satisfy the physical constraints and at the same time minimize (or maximize) some performance criterion [1], such as minimizing the fuel, energy, or time required to perform a process, which it is called the Time-Optimal Control (TOC).

The TOC is a special case of optimization problems and is defined as *the transfer of the system from an arbitrary initial state to a specific target set point in minimum time*. TOC problems are a common research area in analytical and numerical control system synthesis. Current research in robotics, radar, missiles tracking, and even some chemical processes, is fraught with TOC optimization problems. Moreover, the subject of the TOC is very important in the study of nonlinear motion control systems.

One of the most common areas of application of the TOC is the servomechanism. A servomechanism is a system that controls the position or velocity of a mechanical devise. In many applications, such as the hard disk drive head positioning system, pick-and-place robots and positioning of the plotter pen in either axis, it is desirable to have servomechanisms effect a minimum time response to set point changes.

Since the control signal is usually saturated, the time optimal controller is bang-bang, according to the well-known Pontryagin principle introduced in [2]. Bang-bang control systems operate by switching its value between an upper limit and a lower limit according to switching criteria obtained from the TOC. Time-optimal bang-bang control systems are often impractical because unavoidable measurement noise, disturbances and nonideal components cause the bang-bang control to switch when the state does not exactly meet the switching criteria. Hence, the robust TOC is needed.

Workman [3], [4] proposed a controller called PTOS (Proximate Time-Optimal Servomechanism). The controller approximates the switching curve with a strip. Unlike the bang-bang controller, PTOS is continuous in the neighborhood of the strip. Near the origin PTOS switches to a linear feedback law; in this sense PTOS has a dual mode behavior. That is, the control is switched between two different controllers to achieve the two conflicting requirement. It has been shown that PTOS functions well in the presence of disturbances and modeling errors. Consequently, PTOS is widely used nowadays in designing HDD servomechanisms [5], [6].

Since PTOS has dual mode behavior, this may cause undesired transients between the modes, which are familiar in mode switching controllers like PTOS [7], [5].

In this study, we proposed an analytical solution of the TOC problem of a third order system, consists of one integrator and two stable real poles, which is our modeling of the HDD servomechanism. Using the similarity transformation, we will study the application of the Continuous Proximate Time-Optimal Control (CPTO) technique, which was developed by Kalyon [8], [9], [10], and [11], on that system and we will show that our controller has a smooth switching between the TOC and the designed linear controller.

We begin our study by giving a description of the disk drive, which is one of the major applications in the TOC and we will make use if it in this thesis to give a better understanding of the controller behavior through the simulation results.

1.2. Hard Disk Drives (HDD)

Briefly, we will give a description of the HDD components and some basic terminologies used in the state of the art in the HDD.

A hard disk drive (also called a fixed disk) is the primary medium for storing information on computers, because it combines high capacity, relatively fast access and low price. As can be seen from Figure 1.1, the hard disk drive is made up of four basic components: A voice coil motor (head actuator), a spinning disk platter, a head arm with a read/write head on its end, and electronics to tie everything together and connect it to the outside world.

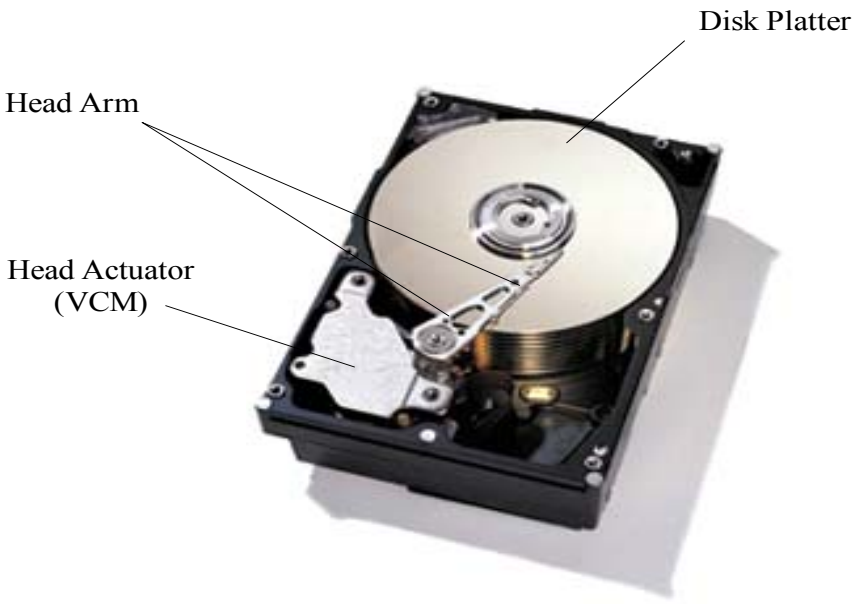

Figure 1.1 Basic components of the hard disk drive

The voice coil motor (VCM) is a dc motor, which drives the arm [12]. The Read/Write head is mounted on a slider device, which is connected to the head arm shown in Figure 1.1.

The variable to accurately control is the position of the Read/Write head. The disk rotates at a speed of between 1800 and 7200 rpm, and the head flies above the disk at a distance of less than 100 nm. The two main function of the Read/Write head positioning servomechanism in disk drives are track seeking and track following, where track as definition is a thin circular magnetic path where the data is written on. Each track is located on a specific radius measured from the disk center. In average, the width of a track is approximately 1/40,000 inch [12].

Track seeking moves the R/W head from the present track a specified destination track in minimum time using a bounded control effort. *Track following* maintains the head as close as possible to the destination track center while information is being read from or written to the disk. Track density is the reciprocal of the track width. It is

suggested that on a disk surface, tracks should be written as closely spaces as possible so that we can maximize the usage of the disk surface [13].

The prevalent trend in hard disk design is toward smaller hard disks with increasingly larger capacities. This implies that the track width has to be smaller leading to lower error tolerance in the positioning of the head, and the ability of the actuator to seek from one track to another quickly and adequately is very important because the data retrieval performance of the drive is directly affected by how fast the head seeks from one track to another. During seeking, the actuator get driven by a bang-bang current profile to achieve time-optimal, but due to the presence of resonance, the ideal bang-bang profile needs to be smoothed out, particularly at the switching stage (arrival stage).

In this study we will investigate the application of the CPTO algorithm, which serves to smooth out the switching of the TOC.

CHAPTER 2

LITERATURE REVIEW

So far, we have introduced some of the features of the TOC technique that can be used to design control laws to track certain target reference for systems with actuator saturations. The TOC technique is believed to be non-robust to system uncertainties and noise, and thus cannot be used in tackling real problems, although it has also been regarded as a method that would, at least theoretically, yield the best performance in terms of settling time [5].

To conserve the time-optimality of the TOC and handle the problem of robustness, the dual-mode operation of controllers has been widely adopted in the literature. In which, the controller changes its nature when needed so that we gain features of both controllers.

McDonald [14], [15] applied dual-mode concept to servos where there are two classes of inputs: one class consisting of continuous signals with small acceleration, the second class consisting of signals with large step discontinuities in the position and/or the

velocity. This dual-mode operation is accomplished by using a separate controller for each mode and connecting the appropriate controller to the actuator in accordance with the commands for a unit called a mode selector. The mode selector calls for the linear mode when the operating point is within a certain neighborhood of the origin in the phase plane and for the non linear mode when the operating point elsewhere.

The most popular control technique, which uses the dual mode concept, is the Proximate Time-Optimal Servomechanism (PTOS) proposed by Workman [3], [4], which achieves near time-optimal performance for a large class of motion control systems characterized a double integrator. The PTOS actually replaced the signum function in the TOC switching algorithm by the saturation function which, together with a gain factor, can be thought as a finite slope approximation of the signum function. Thus, it is made to yield a minimum variance with smooth switching from the track seeking to track following modes via mode switching controller (MSC) [16]. Pao and Franklin [17], [18] extended the application of PTOS on the triple integrator, third order systems by constructing a "slab" in 3-dimensional state space that approximates the switching surface for the TOC. Within the "slab" is a "tube" which approximates the switching curve that lies on the switching surface for the TOC [19]. Their approximate time-optimal controller utilizes the dual-mode concept of McDonald [14], [15] with the following exception: when far from the neighborhood of the origin, they apply their proximate TOC law instead of the ideal nonlinear TOC law.

Ho [20] introduced an alternative dual mode concept by combining TOC and input shaping method. He has shown through simulation results that the algorithm

achieves near optimal bang-bang performance with minimal excitation of the resonance mode.

Yamaguchi et al in [21], [22], proposed a method called initial value compensation is proposed. In this, when the switch is transferred from track seeking mode to track following mode, the final states of the track seeking controller become the initial states for the track following controller, and hence, affect the settling performance of the track following mode. In order to reduce the impact of these initial values during mode switching, some compensation must be worked out.

Iwashiro et al [23] applied Deadbeat control, which was introduced in [6], to model following seek control, in which single control architecture covers seeking and tracking control, and they experimented it with 2.5 inch HDD. Wu [16] introduced high gain linear state feedback law to achieve minimum-time control based on equivalent switching line, switching plane, and switching hyper plane instead of switching curve, switching surface and switching hyper surface, respectively, for a class of second, third, and higher order systems. However, the usage of high gain feedback coefficient, and that the feedback coefficients are reselected for each initial condition, limit the application of this approach.

Newman [24] proposed a near time-optimal state-feedback scheme combining the bang-bang control with the sliding mode control for double integrator system.

Lee and You [25], Zhou et al [26], and Zhang and Guo [27] have been working in designing PTOC for nonlinear and linear second order dynamics combined with the sliding mode control, which is called SMPTOS.

Choi et al [28] attempted to solve the problem of robustness by introducing a control system, which consists of two controllers; PTOS for high speed motion, and one of robust control approaches, which is disturbance observer technique (DOB). DOB is used for robustness and saturation handling element. They applied their design to a double integrator system.

Yi and Tomizuka [7] proposed a new method called a two-degree-of-freedom (2DOF) servomechanism. They used two types of robust control scheme in the feedback to the system for rejection of the disturbances; one scheme uses a disturbance observer (DOB), and the other uses adaptive robust control (ARC). They showed in simulation studies the advantage of the 2DOF servomechanism over MSC with the PTOS method, and the ARC approach compared with the DOB approach in the 2DOF structure.

Chen et al [5] proposed MSC law that combines the PTOS and so-called Robust Perfect Tracking (RPT) controllers [29], [30], so that PTOS will work in the track seek mode and RPT will work in the track following mode. They have applied it for a second order system and proved the stability and robustness of their method.

The main issue in the MSC's is the design of the switching mechanism, this problem has not yet been completely resolved, and many heuristic approaches have been tried so far [5]. Moreover, switching from seeking mode to following mode is often problematic and may cause undesired transients at the beginning of the following mode. Such transients make the effective seek time longer [7].

Maintaining the combination of the linear feedback controller in the track following and the ideal time-optimal controller in the track seeking, Kalyon in [8], [9],

[10], and [11], addressed this problem by introducing a class of *continuous* PTOS, which has a smooth switching between the modes that gave near time-optimal response.

In this study, we will apply this approach to HDD servo-system, which has a third order model with an integrator and two real roots, and we will compare the simulation results with the designed saturated linear controller and the ideal time-optimal controller.

CHAPTER 3

MATHEMATICAL MODELING

3.1. List of Assumptions

We start by listing number of assumptions, which have been made in the modeling of the HDD servomechanism and throughout the rest of the thesis.

1. In this thesis, we consider only the rigid body dynamics in the model of the HDD servomechanism. However, the flexibility will be considered in the robustness analysis section.
2. We assume that the poles of the open loop transfer function are all stable real poles.
3. When the state is near the origin, we assume that:

$z_i^n \cong 0$ if $n > 1$,

where,

z_i (i =1, 2, 3) are the state variables.

4. In this thesis, we assume that all the states are measurable and the measurements are error free.

3.2. Model Description

As a good approximation of the model of the hard disk drive servomechanism, we use the model of the armature-controlled dc motor, which is found in many control text books and technical papers [12], [31], [32], [33]. The mechanical structure of a typical modern hard disk drive is depicted in Figure 3.1.

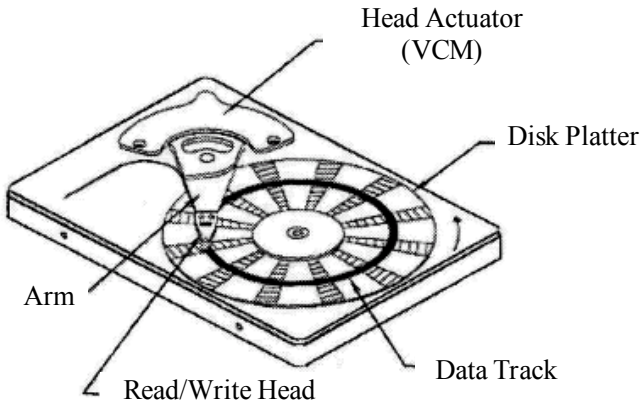

Figure 3.1 Hard disk drive head positioning system

We consider the block diagram in Figure 3.2, which represents a typical open-loop system of a HDD head positioning including flexible body [9]. Here, the bounded input, u, is ranging from -12 to +12 volt and the output, y, is the head position (track number). In this model description, we will use the similar approach as in [9].

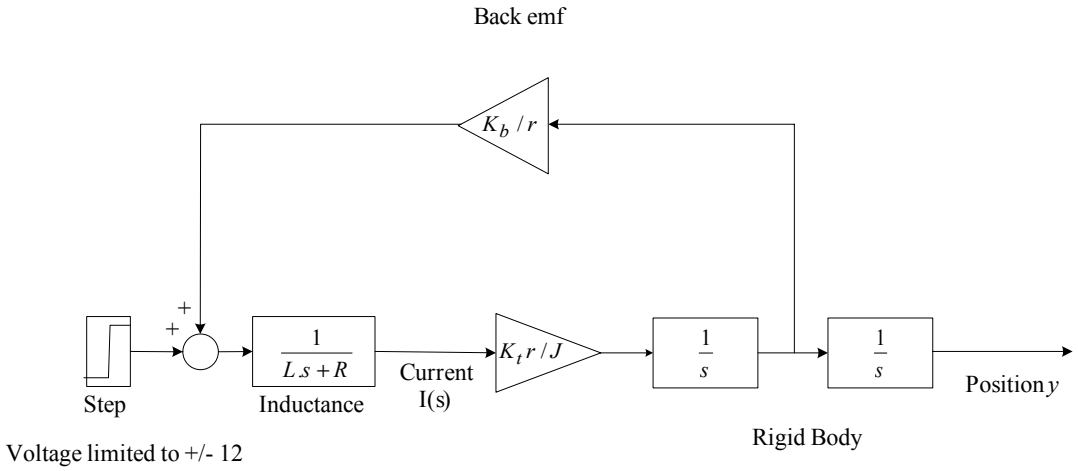

Figure 3.2 The open-loop system of HDD head positioning system

Where,

L = Inductance (H – Henry).

R = resistance (Ω --Ohm).

r = length of the head carriage (m).

J = moment of inertia of the head and head carriage ($Kg\ m^2$).

K_t = overall armature constant ($N\ m/\ A$).

K_b = back electromotive force gain ($volt\ sec$).

From, Figure 3.2, the open-loop plant transfer function, $G_p(s) = \frac{y(s)}{u(s)}$ becomes

$$\frac{y(s)}{u(s)} = G_p(s) = \frac{K_t\ r\ s}{[J\ L\ s^2 + J\ R\ s + K_t K_b]}\left[\frac{1}{s^2}\right] \tag{3.1}$$

$$\Rightarrow\ G_p(s) = \frac{\frac{K_t\ r}{J\ L}}{s\ [s^2 + \frac{R}{L}s + \frac{K_t K_b}{J\ L}]} \tag{3.2}$$

Letting

$$K_0 = \frac{K_t r}{JL}, \qquad b_1 = \frac{R}{L}, \qquad \text{and} \qquad b_0 = \frac{K_t K_b}{JL},$$

this yields,

$$G_p(s) = \frac{K_0}{s(s^2 + b_1 s + b_0)} \tag{3.3}$$

Consequently, the closed loop system will be:

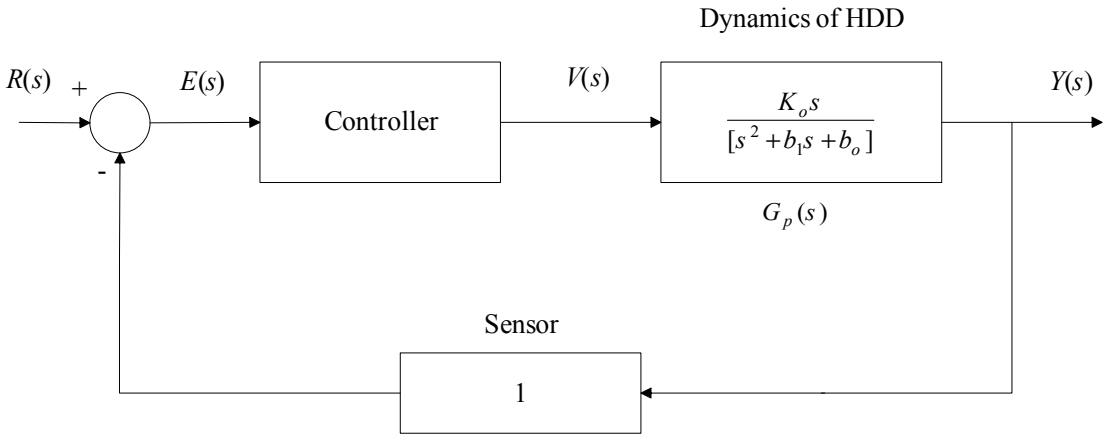

Figure 3.3 Closed-loop block diagram

As an example, we consider the following representative numerical values for the HDD:

L = 10^{-3} *H*, J = 10^{-6} *Kg* m^2, r = 0.03 *m*,

R = 10 Ω , K_t = 0.1 *N m/A*, K_b = 0.1 *volt sec*.

We note that these values are commonly used in the industry.

Thus, K_0, b_1 and b_0 will be

$$K_0 = 3\ 10^6 \quad \frac{N}{Kg.A.H} \tag{3.4}$$

$$b_1 = 10^4 \quad \Omega / H \tag{3.5}$$

$$b_0 = 10^7 \quad \frac{N}{Kg.m} \tag{3.6}$$

The corresponding poles of the plant become,

$s_0 = 0$, $s_1 = 1127.0166$, and $s_2 = 8873.9833$.

Note that the poles as well as the gain of the plant are so huge. Clearly, using time (in second) and the position (in meter) is not suitable and changing the dimensions by using more appropriate units is essential [9]. We know that the seek distance can be anything from 1 track to 50,000 tracks, where the width of a track is 1/50000 *inch*, and the accuracy at the end of seek should be below 0.1 track. Therefore, using **track (*track*)** as position unit and **millisecond (*msec*)** as time unit seems to be the best choice.

3.3. Change of Units

Here, our objective, as mentioned above, is to change the unit time to millisecond [*msec*] and the distance unit to [*track*], which are more convenient than [*second*] and [*meter*] respectively.

Considering $T = \frac{N}{A.m}$ and $H = \frac{T.m^2}{A}$ [34] (T stands for *Tesla*, the magnetic field unit), this yields,

$$H = \frac{N.m}{A^2} \tag{3.7}$$

Substituting (3.7) into (3.4) gives

$$K_0 = 3*10^6 \quad \frac{A}{Kg.m} \tag{3.8}$$

Note that, since we are considering 50000 track per inch (TPI), therefore,

$$1\ meter = 39.37\ inch = 39.37*50000\ track = 1.9685*10^6\ track \tag{3.9}$$

This gives

$$K_0 = 1.524 \ \frac{A}{Kg.track} \tag{3.10}$$

Again, substituting (3.7) into (3.5) and (3.6) for the other parameters of the model,

$$b_1 = 10^4 \Omega / H = 10^4 \frac{\frac{Volt}{A}}{\frac{N.m}{A^2}} = 10 \ \frac{1}{msec}$$

$$b_0 = 10^7 \frac{N}{Kg.m} = 10 \frac{1}{msec^2}$$

Writing the parameters of the model again after modifying theirs units:

$$K_0 = 1.524 \ \frac{A}{Kg.track}, \quad b_0 = 10 \ \frac{1}{msec} \quad \text{and} \quad b_1 = 10 \frac{1}{msec^2} \tag{3.11}$$

Replacing K_0, b_0 and b_1 in (3.3) by their values of (3.11), gives

$$G_p(s) = \frac{1.524}{s[s^2 + 10s + 10]} \tag{3.12}$$

or

$$G_p(s) = \frac{k}{s(s + s_1)(s + s_2)} \tag{3.13}$$

where

$$\text{k} = 1.524, \ s_0 = 0, \ s_1 = 5 + \sqrt{15} \ \text{ and } \ s_2 = 5 - \sqrt{15}$$

Since we have changed all the unit time to *msec* and the unit length to *track*, the unit of the control effort should be changed also to correlate these unit changes. We know from the previous section that,

$$u_{\max} = 12 \ Volts \ . \tag{3.14}$$

We have,

$$1\ volt = 1\frac{m.N}{sec.A} = \frac{1.9685*10^3 track.N}{msec.A} = 3.875*10^3\frac{Kg.track^2}{msec^3.A}$$

Thus, substituting into (3.14), the control boundary will be equal to:

$$u_{\max} = 46500\ \frac{Kg.track^2}{msec^3.A} \tag{3.15}$$

3.4. State-Space Representation

Writing the model of the system in state space representation is of a great importance for the design and application of modern control systems, since most of the control techniques nowadays rely on this way of representing the systems.

In the previous section, we found that the model of the system is described by:

$$G_p(s) = \frac{Y(s)}{U(s)} = \frac{k}{s(s^2 + bs + c)} \tag{3.16}$$

where,

$Y(s)$: is the output, which is the position of the armature,

$U(s)$: is the control signal.

From (3.16), the differential equation of this model can be written as:

$$\dddot{y}(t) = -b\ddot{y}(t) - c\dot{y}(t) + ku(t) \tag{3.17}$$

Defining the state space variables to be as follows:

$$\left.\begin{aligned} x_1(t) &= r(t) - y(t) \\ x_2(t) &= \dot{r}(t) - \dot{y}(t) \\ x_3(t) &= \ddot{r}(t) - \ddot{y}(t) \end{aligned}\right\} \tag{3.18}$$

The state space variables $x_1(t)$, $x_2(t)$, and $x_3(t)$ represent the error in position, error in speed, and error in acceleration, respectively. Assuming that our reference signal $r(t)$ has a *constant* value, then $\dot{r}(t) = 0$ and $\ddot{r}(t) = 0$, and the previous equations become:

$$\begin{aligned} x_1(t) &= r(t) - y(t) \\ x_2(t) &= -\dot{y}(t) \\ x_3(t) &= -\ddot{y}(t) \end{aligned} \tag{3.19}$$

Taking the time derivative of (3.19) and substituting the value of $\dddot{y}(t)$ in (3.17), into the resulting equation, yields

$$\begin{aligned} \dot{x}_1(t) &= x_2(t) \\ \dot{x}_2(t) &= x_3(t) \\ \dot{x}_3(t) &= b\ddot{y}(t) + c\dot{y}(t) - ku(t) \end{aligned} \tag{3.20}$$

Substituting the values of $\dot{y}(t)$ and $\ddot{y}(t)$ from (3.19) into (3.20) and simplifying, we obtain the state equation as

$$\begin{aligned} \dot{x}_1(t) &= x_2(t) \\ \dot{x}_2(t) &= x_3(t) \\ \dot{x}_3(t) &= -bx_3(t) - cx_2(t) - ku(t) \end{aligned} \tag{3.21}$$

Writing the last equations in state space matrix representation:

$$\left.\begin{aligned} \dot{\mathbf{x}}(t) &= \mathrm{A}\,\mathbf{x} + \mathrm{B}u \\ y &= \mathrm{C}\,\mathbf{x} \end{aligned}\right\} \tag{3.22}$$

where:

$$\mathbf{x} = \begin{pmatrix} x_1 \\ x_2 \\ x_3 \end{pmatrix}, \qquad \mathrm{A} = \begin{pmatrix} 0 & 1 & 0 \\ 0 & 0 & 1 \\ 0 & -c & -b \end{pmatrix}, \quad \mathrm{B} = \begin{pmatrix} 0 \\ 0 \\ -k \end{pmatrix}, \quad \text{and} \quad \mathrm{C} = \begin{bmatrix} 1 & 0 & 0 \end{bmatrix}.$$

Note that the output is chosen as the position's error x_1, that is,

$$Y = x_1$$

CHAPTER 4

TIME-OPTIMAL CONTROL

4.1. Introduction

Before we start solving the TOC problem, we need to consider some definitions that are common in TOC theory.

Definition 4.1: Performance Index

A performance index, in general, is a quantitative measure of the performance of a system and is chosen so that emphasis is given to the importance system specification. It can have the general formulation [12],

$$J = \int_{t_0}^{t_f} f_0(\mathbf{x}, u, t)dt \tag{4.1}$$

where t_f and t_0 are the final and the initial time of the process, respectively, and $\mathbf{x}$ and u, respectively, are the state vector and the single control input of the system [35], [36].

In the TOC, the goal is to determine the control signals such that the time is minimized, at the same time, the physical constraints (4.3), are satisfied. Thus, the performance index for the TOC is given by

$$J = \int_{t_0}^{t_f} 1 \, dt \tag{4.2}$$

Definition 4.2: Hamiltonian and Costate Variables

We consider the following general optimization problem:

Obtain u(t) such that the performance index (4.1) is minimized subject to the equations of motion (constrains equations)

$$\dot{x}_i = f_i(\mathbf{x}, u, t); \ (i = 1, 2, ..., n) \tag{4.3}$$

The ***Hamiltonian*** (H), in general, is given by

$$H = f_0(x, u, t) + \sum_{i=1}^{n} p_i(t) f_i(x, u, t) \tag{4.4-a}$$

where $p_i(t)$, $(i = 1, 2, ..., n)$, are called ***costate variables*** (Lagrange multipliers. The Hamiltonian expression for the TOC problem, thus, is given by replacing $f_0(x, u, t)$ in (4.4-a) with 1. That is,

$$H = 1 + \sum_{i=1}^{n} p_i(t) f_i(x, u, t) \tag{4.4-b}$$

Considering the Hamiltonian (4.4-b) and assuming that the single control u(t) in (4.6) is unbounded, the necessary conditions for a time-optimal solution are:

$$\frac{\partial H}{\partial x_i} = -\dot{p}_i \ ; \ (i = 1, 2, ..., n) \tag{4.5}$$

$$\frac{\partial H}{\partial u} = 0 \tag{4.6}$$

These two equations, together with the equations of motion (4.3), govern the optimal paths. Hence, solving the set of equations (4.3), (4.5), and (4.6) will lead to the solution of the TOC problem [36]. We remark here that if the control input is bounded, then, equation (4.6) is not applied and the control equation has a special form, which will be treated in the next section.

4.2. Ideal Time-Optimal Control of Double Integrator System:

As an illustrative example consider the following double integrator system

$$\ddot{y}(t) = a\ u(t) \tag{4.7}$$

where y is the position output, a is the acceleration constant and u is the input to the system, which is assumed to be constrained as follows;

$$|u(t)| \le u_{\max}$$

For the tracking purpose, we define:

$$\begin{aligned} x_1(t) &:= r(t) - y(t) \\ x_2(t) &:= \dot{r}(t) - \dot{y}(t) \end{aligned} \tag{4.8}$$

Here, $x_1(t)$ is the position error with $r(t)$ being the desired final position, and $x_2(t)$ is the error rate.

Assuming that $\ddot{r}(t) = 0$, the equations describing the system (4.7) then become

$$\begin{aligned} \dot{x}_1(t) &= x_2(t) \\ \dot{x}_2(t) &= -au(t) \end{aligned} \tag{4.9}$$

In order to obtain the TOC law, we use Pontryagin's principle and calculus of variation. Consequently, the Hamiltonian (H) for (4.9) is given by:

$$H(x(t),u(t),p(t)) = 1 + p_1(t)x_2(t) + p_2(t)[-au(t)] \tag{4.10}$$

where $p = (p_1 \quad p_2)^T$ is a vector of the time-varying costate variables. Note from (4.10) that the control $u(t)$ is involved in the last term only. Hence, to minimize the Hamiltonian, the last term must be, always, minimum. We, thus, have the following optimal control law,

$$u(t) = \left\{ \begin{matrix} +u_{\max,} & \text{for} \quad p_2(t) > 0 \\ -u_{\max,} & \text{for} \quad p_2(t) < 0 \end{matrix} \right\} := \text{sgn}(p_2(t))u_{\max} \tag{4.11}$$

We note from (4.11) that $u(t)$ depends on the polarity of $p_2(t)$. Therefore, the form of $p_2(t)$, which is obtained below, is necessary for the time optimal control.

Applying the necessary conditions (4.5) to the Hamiltonian (4.10), we get

$$\left. \begin{matrix} \dot{p}_1(t) = 0 \\ \dot{p}_2(t) = -p_1(t) \end{matrix} \right\} \tag{4.12}$$

Solving these two ordinary differential equations in time, we get

$$\left. \begin{matrix} p_1(t) = c_1 \\ p_2(t) = -c_1 t + c_2 \end{matrix} \right\} \tag{4.13}$$

Here, c_1 and c_2 are the integration's constants.

From equation (4.13), we note that $p_2(t)$ is linear in time and can have at most one sign change, therefore $u(t)$ can change sign at most once. Since there can be at most one switching in the sign of $p_2(t)$, the optimal control for a specified initial state must be one of the following forms:

$$
\left.
\begin{aligned}
&1: \quad u(t) = \{+u_{\max} && \forall t \in [t_0, t^*] \\
&2: \quad u(t) = \begin{cases} -u_{\max} & \forall t \in [t_0, t_1) \\ +u_{\max} & \forall t \in [t_1, t^*] \end{cases} \\
&3: \quad u(t) = \{-u_{\max} && \forall t \in [t_0, t^*] \\
&4: \quad u(t) = \begin{cases} +u_{\max} & \forall t \in [t_0, t_1) \\ -u_{\max} & \forall t \in [t_1, t^*] \end{cases}
\end{aligned}
\right\} \tag{4.14}
$$

Here, t_1 and t^* are the time when the states reach the switching curve which is defined in Definition 4.3, and the time when the states reach the origin, respectively.

It is to be noted that if the initial state lies on the switching curve define by equations (4.20) in the state plane, then the control will be either the case (1) or (3) in equation (4.14) depending on the direction of motion. On the other hand, for if the state is not on the switching curve then the control law will be either case (2) or (4) depends on the location of the state.

Definition 4.3: The Switching Curve [V_2] is a set of points, at which the control switches from a maximum (or minimum) value to the other extremum, according to the dynamics of the system, It has the property that any state on it can be forced to the origin in a minimum time by application of the full control effort (either maximum or minimum) [38].

Each segment of the switching curve can be found by integrating (4.9) backward in time. Let τ represent negative time, as opposed to t, which represents positive time, then,

$$\frac{d(\ )}{d\tau} = -\frac{d(\ )}{dt}$$

Thus, for backward integration (4.9) becomes

$$\begin{aligned} \frac{dx_1(\tau)}{d\tau} &= -x_2(\tau) \\ \frac{dx_2(\tau)}{d\tau} &= a\,u(\tau) \end{aligned} \tag{4.15}$$

We solve (4.15) by setting $u(\tau) \equiv \Delta^*$ and $[x_1(0) \quad x_2(0)] = [0 \quad 0]$, where $\Delta^* = \pm u_{\max}$.

Thus,

$$x_1(t) = -\frac{1}{2} a.\Delta^* \tau^2 \tag{4.16}$$

$$x_2(t) = a.\Delta^* \tau \tag{4.17}$$

Eliminating the time from (4.16) and (4.17), we obtain

$$x_1 = -\frac{{x_2}^2}{2a\Delta^*} \tag{4.18}$$

From (2.17) we note that for τ to be positive, the polarity of x_2 and the polarity of Δ^* must be the same. Therefore, we have

$$\Delta^* = \frac{x_2}{|x_2|} u_{\max} \ ; \quad (x_2 \neq 0). \tag{4.19}$$

Consequently, from (4.18) and (4.19), we obtain an expression describing the switching curve, Figure 4.1,

$$\mathrm{V}: \{X_1(x_2) = -\frac{x_2 |x_2|}{2a u_{\max}}\} \tag{4.20}$$

Now we can summarize the TOC sequence in two control laws as explained in [38]:

Control Law 4.2.1

If $\mathbf{x}(t) \in \mathrm{V}$, where V is described in Definition 4.3, then $u(\tau) \equiv \Delta^*$ is the time-optimal control, where Δ^* is given by (4.19).

Control Law 4.2.2

If the state $\mathbf{x}(t)$ lies above the curve V, then $u(\tau) = +u_{\max}$ is the control. If the state $\mathbf{x}(t)$ lies below the curve V, then $u(\tau) = -u_{\max}$ is the control. Combining these two control laws results in the following discontinuous time-optimal, bang-bang controller:

$$U^* = \begin{cases} u_{\max} \operatorname{sgn}\{x_1 - X_1(x_2)\} & \text{if} \quad x_1 - X_1(x_2) \neq 0 \\ u_{\max} \operatorname{sgn}(x_2) & \text{if} \quad x_1 - X_1(x_2) = 0 \end{cases} \tag{4.21}$$

The mechanism of the control laws (4.2.1) and (4.2.2) can be illustrated in graphical form as given in Figure 4.1.

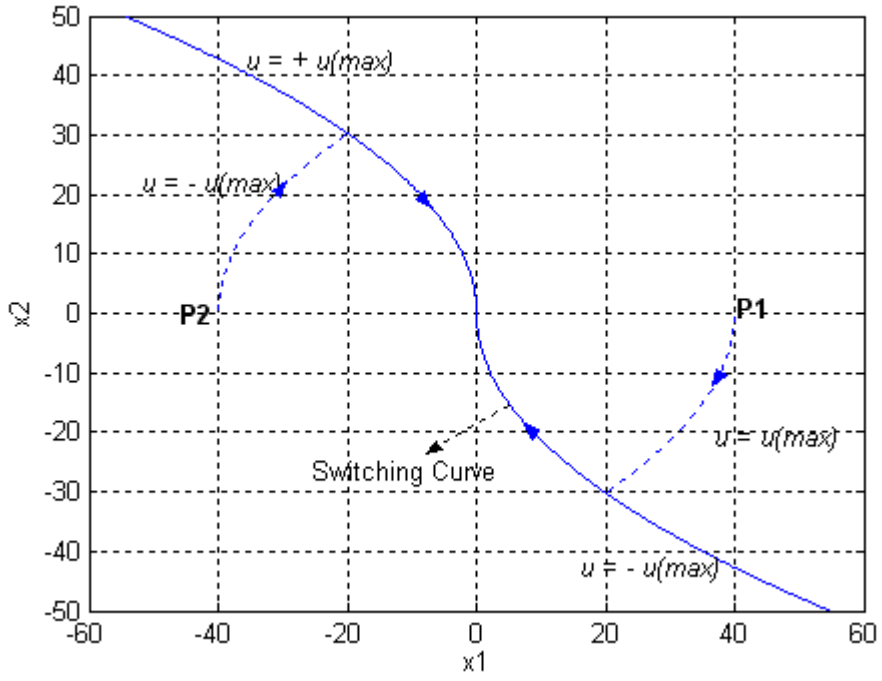

Figure 4.1 Switching trajectories of the double integrator system

Clearly, any initial state lying above the curve, in terms of x_1-axis, like P_1 in Figure 4.1, is to be driven by the positive acceleration force to bring the state to deceleration trajectory when hits the switching curve. On the other hand, any initial state lying below the curve, point P_2 in Figure 4.1, is to be accelerated by negative force to the deceleration trajectory.

In following, we will apply TOC law to the HDD servomechanism.

4.3. Ideal Time-Optimal Control of Third Order System Having Two Real Roots and an Integrator

Rewriting HDD model that was derived in Chapter 3, equation (3.16)

$$G_p(s) = \frac{k}{s(s^2 + bs + c)} \tag{4.22}$$

According to La-orpacharapan and Pao [32], the third order rigid body system (4.22) does not have any analytical solution. Ananthanarayanan [33] has solved it partially, by ignoring some terms. Pao and Franklin [17] worked out a solution of a triple integrator system. Kalyon [8] proposed a solution of two integrators and first order lag system.

In this chapter, we proposed a general analytical solution of the problem using similarity transformation.

Objective: Given the system (4.22), determine the control [subject to constrain $|u(t)| \le u_{\max}$] that forces any given initial state $x(0)$ to the origin in *minimum time.*

4.3.1. Calculus of Variation

We recall the state equations describing the system, equations (3.21),

$$\begin{aligned} \dot{x}_1(t) &= x_2(t) \\ \dot{x}_2(t) &= x_3(t) \\ \dot{x}_3(t) &= -bx_3(t) - cx_2(t) - ku(t) \end{aligned} \tag{4.23}$$

Taking into consideration TOC performance index, equation (4.2), and the set of equations 4.23 as the constraints on the system performance, the Hamiltonian (*H*) for the minimum time control of the system, will be:

$$H = 1 + p_1(t)x_2(t) + p_2(t)x_3(t) + p_3(t)[-bx_3(t) - cx_2(t) - ku(t)] \tag{4.24}$$

Arranging (4.24), we get

$$H = 1 + x_2(t)[p_1(t) - cp_3(t)] + x_3(t)[p_2(t) - bp_3(t)] - ku(t)p_3(t) \tag{4.25}$$

where $P = (p_1 \;\; p_2 \;\; p_3)^T$ is time-varying costate vector. Note from (4.25) that the control is involved in the last term only. Hence, to minimize the Hamiltonian, the last term must be, always, minimum. We, thus, have the following optimal control law;

$$u(t) = \left.\begin{cases} +u_{\max,} & \text{for} \quad p_3(t) > 0 \\ -u_{\max,} & \text{for} \quad p_3(t) < 0 \end{cases}\right\} := u_{\max} \operatorname{sgn}\{p_3(t)\} \tag{4.26}$$

We note from (4.26) that $u(t)$ depends on the polarity of $p_3(t)$. Therefore, the form of $p_3(t)$, which is obtained below, is necessary for the optimal control.

4.3.2 Number of Switches

Equation (4.26) shows that the sign of the control *u* should be the same as the sign of the costate variable $p_3(t)$. Thus, the number of sign changes of $p_3(t)$ implies the number of switches of the control *u.* We, now, obtain the form of $p_3(t)$ as follows:

The calculus of variation yields the following necessary conditions for a time-optimal solution:

$$\dot{p}_1(t) = -\frac{\partial H}{\partial x_1} = 0 \tag{4.27-a}$$

$$\dot{p}_2(t) = -\frac{\partial H}{\partial x_2} = -[p_1(t) - cp_3(t)] \tag{4.27-b}$$

$$\dot{p}_3(t) = -\frac{\partial H}{\partial x_3} = -[p_2(t) - bp_3(t)] \tag{4.27-c}$$

Solving (4.27-a), yields

$$p_1(t) = constant = p_{01} \tag{4.28}$$

We take the time derivative of (4.27-c) and substitute (4.27-b) into the resulting equation yields

$$\ddot{p}_3(t) - b\dot{p}_3(t) + cp_3(t) = p_{01} \tag{4.29}$$

Solving the last linear differential equation of (4.29), with constant coefficient, we obtain

$$p_3(t) = p_{02}e^{s_1 t} + p_{03}e^{s_2 t} + \frac{p_{01}}{c} \tag{4.30}$$

where,

$$s_1 = \frac{b + \sqrt{b^2 - 4c}}{2} \tag{4.31}$$

and

$$s_2 = \frac{b - \sqrt{b^2 - 4c}}{2} \tag{4.32}$$

Here P_{01}, P_{02}, and P_{03} are the initial values of $P_1(t)$, $P_2(t)$, and $P_3(t)$, respectively.

Note that $b^2 > 4c$ for the assumption of the real roots.

Apparently, by examining the extremum of $P_3(t)$, we get the maximum number of sign changes that the function $p_3(t)$ might have. Thus,

$$\dot{p}_3(t) = s_1 p_{02} e^{s_1 t} + s_2 p_{03} e^{s_2 t} = 0 \Rightarrow \quad e^{s_1 t} = -\frac{s_2 p_{03}}{s_1 p_{02}} e^{s_2 t} \tag{4.33}$$

Then, the unique solution of (4.33) will be

$$t = -\frac{1}{s_2 - s_1} \ln\{-\frac{s_1 p_{02}}{s_2 p_{03}}\} \tag{4.34}$$

Since, (4.33) has a unique solution, $\dot{p}_3(t)$ has only one extremum (maximum or minimum). This implies that $p_3(t)$ has at most two zeros, which also implies that $p_3(t)$ has *at most* three sign changes for all possible values of P_{01}, P_{02}, and P_{03}. Hence, from (4.26), we can immediately conclude that there are the following possible control sequences for the TOC:

{+1}, {-1}, {+1,-1}, {-1+1}, {+1,-1,+1}, {-1,+1,-1}

In details, the possible control sequences can be presented as follows:

$$
\left.
\begin{aligned}
&1: \quad u^*(t) = \{+u_{\max} && \forall t \in [t_0, t^*] \\
&2: \quad u^*(t) = \{-u_{\max} && \forall t \in [t_0, t^*] \\
&3: \quad u^*(t) = \begin{cases} -u_{\max} & \forall t \in [t_0, t_1) \\ +u_{\max} & \forall t \in [t_1, t^*] \end{cases} \\
&4: \quad u^*(t) = \begin{cases} +u_{\max} & \forall t \in [t_0, t_1) \\ -u_{\max} & \forall t \in [t_1, t^*] \end{cases} \\
&5: \quad u^*(t) = \begin{cases} -u_{\max} & \forall t \in [t_0, t_2) \\ +u_{\max} & \forall t \in [t_2, t_1) \\ -u_{\max} & \forall t \in [t_1, t^*] \end{cases} \\
&6: \quad u^*(t) = \begin{cases} +u_{\max} & \forall t \in [t_0, t_2) \\ -u_{\max} & \forall t \in [t_2, t_1) \\ +u_{\max} & \forall t \in [t_1, t^*] \end{cases}
\end{aligned}
\right\} \qquad (4.35)
$$

where t_0, t_1, t_2 and t^* are the starting time, the time at which the state meets the switching curve, the time at which the state meets the switching surface, which is defined below, and the final time.

Definition 4.4: The Switching Surface is a set of points [V_1], surface shaped, at which the control switches from a maximum (or minimum) value to the other extremum, according to the third-order dynamics of the system [38]. We note that V_1 divides the states space into two regions, the switching curve [V_2]**,** which is belongs to V_1, divides the switching surface into two parts.

From equation (4.35), basically, we can have three different cases depending on the location of the initial state:

- First, if the initial state lies exactly at the switching curve, then the control should follow either the case 1 or 2, depending on its location.
- Second, if the initial state lies exactly on the switching surface, then the control should follow either the case 3 or 4, depending on its location with respect to the switching curve, noting that, in this case, the segment $[t_0, t_1]$ belongs to the switching surface and the segment $[t_1, t^*]$ belongs to both the switching surface and the switching curve, as shown in Figure 4.3.
- Third, if the initial state lies neither on the switching surface nor on the switching curve, then the control should follow either the case 5 or 6, depending on its location, that is weather it is above or below the switching surface. Note that in the last case, the trajectory passes through three segments, until it reaches the target.

In the following section, we will introduce an approach for determining mathematical expressions of the switching curve V_2 and switching surface V_1, and the corresponding control sequence, which drives any initial state to the origin in minimum time.

4.3.3. Equivalence Transformation of the System

It can be observed that obtaining the TOC solution of the system (4.22) with the bounded control (4.26) is not easy due to the coupling of the equations. To overcome this problem, we introduce equivalence transformation for the system, which will make the problem solvable by decoupling the equations in (4.22). Hence, we will transfer the state $\mathbf{x}$ into the state $\mathbf{z}$ with the following transformation:

$$\mathbf{z} = \mathbf{P}^{-1}\mathbf{x} \tag{4.36}$$

where the transformation matrix is given by,

$$\mathbf{P} = \begin{pmatrix} \frac{1}{c^2}(-c + \lambda_1 b + b^2) & \frac{1}{c^2}(-c + \lambda_2 b + b^2) & 1 \\ \frac{\lambda_2}{c} & \frac{\lambda_1}{c} & 0 \\ 1 & 1 & 0 \end{pmatrix} \tag{4.37}$$

Similarly, each state in z-domain can be transformed back to x-domain by the transformation

$$\mathbf{x} = \mathbf{P}\ \mathbf{z} \tag{4.38}$$

Note that the columns of $\mathbf{P}$ are the eigenvectors of the matrix $\mathbf{A}$ in (3.22). The details of the similarity transformation are the following:

Recall, from (3.21)-(3.23), that the state space representation of the system is given by

$$\left.\begin{aligned} \dot{\mathbf{x}}(t) &= \mathrm{A}\mathbf{x} + \mathrm{B}u \\ y(t) &= \mathrm{C}\mathbf{x} \end{aligned}\right\} \tag{4.39}$$

where

$$\mathrm{A} = \begin{pmatrix} 0 & 1 & 0 \\ 0 & 0 & 1 \\ 0 & -c & -b \end{pmatrix}, \quad \mathrm{B} = \begin{pmatrix} 0 \\ 0 \\ -k \end{pmatrix}, \quad \text{and } \mathrm{C} = [1 \quad 0 \quad 0]$$

Let

$$\mathbf{x} = \mathbf{P}\ \mathbf{z} \quad \Rightarrow \quad \dot{\mathbf{x}} = \mathbf{P}\ \dot{\mathbf{z}}$$

Substituting $\mathbf{x}$ and $\dot{\mathbf{x}}$ into (4.39), we get

$$\left.\begin{aligned} \mathbf{P}\dot{\mathbf{z}} &= \mathrm{A}\mathbf{P}\mathbf{z} + \mathrm{B}u \\ y(t) &= \mathrm{C}\mathbf{P}\mathbf{z} \end{aligned}\right\} \quad \Rightarrow \quad \left.\begin{aligned} \mathbf{P}^{-1}\mathbf{P}\dot{\mathbf{z}} &= \mathbf{P}^{-1}\mathrm{A}\mathbf{P}\mathbf{z} + \mathbf{P}^{-1}\mathrm{B}u \\ y(t) &= \mathrm{C}\mathbf{P}\mathbf{z} \end{aligned}\right\} \tag{4.40}$$

or

$$\dot{\mathbf{z}} = \mathrm{A}_z\,\mathbf{z} + \mathrm{B}_z\,u \tag{4.41}$$

where

$$\mathrm{A}_z = \mathbf{P^{-1}}\,\mathrm{A}\,\mathbf{P} = \begin{pmatrix} \lambda_1 & 0 & 0 \\ 0 & \lambda_2 & 0 \\ 0 & 0 & 0 \end{pmatrix} \tag{4.42}$$

and

$$\mathrm{B}_z = \mathrm{P}^{-1}\,\mathrm{B} = \begin{pmatrix} -\dfrac{k\,\lambda_1}{m} \\ \dfrac{k\,\lambda_2}{m} \\ -\dfrac{k}{c} \end{pmatrix} \tag{4.43}$$

Note that, the eigenvalues of the matrix A are:

$\lambda_1 = 0.5(-b + \sqrt{b^2 - 4c})$, $\lambda_2 = 0.5(-b - \sqrt{b^2 - 4c})$ and $\lambda_3 = 0$

For the convenience, we introduce the following abbreviation, $m = \sqrt{b^2 - 4c}$ in (4.43), and throughout the rest of this thesis.

Note here that the matrix A_z in the transformed system (4.40) is a diagonal matrix. Hence, the decoupled system can be written in the z-domain as follow:

$$\begin{aligned} \dot{z}_1(t) &= \lambda_1 z_1(t) - \frac{k\,\lambda_1}{m} u(t) \\ \dot{z}_2(t) &= \lambda_2 z_2(t) + \frac{k\,\lambda_2}{m} u(t) \\ \dot{z}_3(t) &= -\frac{k}{c} u(t) \end{aligned} \tag{4.44}$$

Having decoupled the system, we will try to get the analytical equations describing the switching curve and the switching surface.

4.3.4. Switching Criteria

Bonger and Kazda [37] and Athan and Falb [38] established a switching criterion for third and higher order TOC systems with real roots from the simultaneous solution of a number of equations representing trajectory projections, where the first trajectory passes through a point defined by the initial conditions, and the final trajectory passes through the origin. Kalyon [8] and Wu [16] have used a simpler approach to determine the switching criteria by using the backward integration technique and applied it on third order system with two real roots and integrator, and we are going to follow this technique for our model.

Let τ represent negative time, as opposed to t, which represents positive time, then

$$\frac{d(\ )}{d\tau} = -\frac{d(\ )}{dt}$$

Thus, for backward integration (4.44) becomes,

$$\begin{aligned}
\frac{z_1(\tau)}{d\tau} &= -\lambda_1 z_1(\tau) + \frac{k\lambda_1}{m}u(\tau) \\
\frac{z_2(\tau)}{d\tau} &= -\lambda_2 z_2(\tau) - \frac{k\lambda_2}{m}u(\tau) \\
\frac{z_3(\tau)}{d\tau} &= \frac{k}{c}u(\tau)
\end{aligned} \tag{4.45}$$

We assume $u(\tau) = \Delta^*$, $\Delta^* \equiv \pm u_{\max}$ for $0 \le \tau \le t_1$, where t_1 is the time at which the state hits the switching curve backward in time, and integrate (4.45) to obtain

$$z_1(\tau) = c_{11} e^{-\lambda_1 \tau} + \frac{k\Delta^*}{m}$$

$$z_2(\tau) = c_{21} e^{-\lambda_2 \tau} - \frac{k\Delta^*}{m} \tag{4.46}$$

$$z_3(\tau) = \frac{k\Delta^*}{c}\tau + c_{31}$$

where c_{11}, c_{21} and c_{31} are the integration constants.

Since we are moving backward in time, the final state becomes the initial state, and $z_1(0)$, $z_2(0)$ and $z_3(0)$ are all equal to zero, this leads that the constants of integration in equations (4.46) are:

$$c_{11} = -\frac{k\Delta^*}{m}$$

$$c_{21} = \frac{k\Delta^*}{m} \tag{4.47}$$

$$c_{31} = 0$$

Then, equations (4.46) will be

$$z_1(\tau) = \frac{k\Delta^*}{m}(1 - e^{-\lambda_1 \tau}) \tag{4.48-a}$$

$$z_2(\tau) = \frac{k\Delta^*}{m}(-1 + e^{-\lambda_2 \tau}) \tag{4.48-b}$$

$$z_3(\tau) = \frac{k\Delta^*}{c}\tau \tag{4.48-c}$$

From (4.48-c), we obtain for the backward time τ as

$$\tau = \frac{c}{k\Delta^*} z_3 \tag{4.49}$$

We note from (4.49) that for positive τ, Δ^* and z_3 must have the same polarity. Hence, we get,

$$\Delta^* = u_{\max}\,\mathrm{sgn}(z_3) \tag{4.50}$$

We substitute (4.49) into (4.48) to solve z_1 and z_2 in terms of z_3. We, thus, obtain

$$\begin{aligned} \mathrm{z}_1 &= \frac{k\Delta^*}{m}(1-e^{-\lambda_1\frac{c}{k\Delta^*}\mathrm{z}_3}) \\ \mathrm{z}_2 &= \frac{k\Delta^*}{m}(-1+e^{-\lambda_2\frac{c}{k\Delta^*}\mathrm{z}_3}) \end{aligned} \tag{4.51}$$

Substituting (4.50) into (4.51), the switching curve V_2, Figure 4.2, is given explicitly by;

$$\begin{aligned} \mathrm{V}_2 = \{\, \mathrm{z}:\, \mathrm{Z}_1(z_3) &= \frac{k\,u_{\max}\,\mathrm{sgn}(z_3)}{m}(1-e^{-\lambda_1\frac{c}{k\,u_{\max}\,\mathrm{sgn}(z_3)}z_3}), \\ \mathrm{Z}_2(z_3) &= \frac{k\,u_{\max}\,\mathrm{sgn}(z_3)}{m}(-1+e^{-\lambda_2\frac{c}{k\,u_{\max}\,\mathrm{sgn}(z_3)}z_3})\} \end{aligned} \tag{4.52}$$

Note that we have used the symbol Z to differentiate the functions describing V_2,

Evaluating (4.48) at $\tau = t_1$, we have,

$$\begin{aligned} z_1(t_1) &= \frac{k\Delta^*}{m}(1-e^{-\lambda_1 t_1}) \\ z_2(t_1) &= \frac{k\Delta^*}{m}(-1+e^{-\lambda_2 t_1}) \\ z_3(t_1) &= \frac{k\Delta^*}{c}t_1 \end{aligned} \tag{4.53}$$

Here t_1 and $\mathbf{z}(t_1)$ represent, respectively, the backward time and state, at which the trajectory leaves the set V_2.

Next, we assume $u(t) = -\Delta^*$ for $t_1 \le \tau \le t_2$, and integrate (4.45) to obtain,

$$
\begin{aligned}
z_1(\tau) &= c_{12} e^{-\lambda_1 \tau} - \frac{k\Delta^*}{m} \\
z_2(\tau) &= c_{22} e^{-\lambda_2 \tau} + \frac{k\Delta^*}{m} \\
z_3(\tau) &= -\frac{k\Delta^*}{c}\tau + c_{32}
\end{aligned}
\tag{4.54}
$$

where t_2 is the time at which the state leaves the switching curve backward in time, and c_{12}, c_{22} and c_{32} are the integration constants. Applying the initial conditions of (4.53) and solving the integration constants, we get,

$$
\begin{aligned}
c_{12} &= \frac{k\Delta^*}{m}(2e^{\lambda_1 t_1} - 1) \\
c_{22} &= \frac{k\Delta^*}{m}(-2e^{\lambda_2 t_1} + 1) \\
c_{32} &= \frac{2k\Delta^*}{c} t_1
\end{aligned}
\tag{4.55}
$$

Substituting the integration constants into (4.54), yields,

$$
\begin{aligned}
z_1(\tau) &= \frac{k\Delta^*}{m}[2e^{-\lambda_1(\tau - t_1)} - e^{-\lambda_1 \tau} - 1] \\
z_2(\tau) &= \frac{k\Delta^*}{m}[-2e^{-\lambda_2(\tau - t_1)} + e^{-\lambda_2 \tau} + 1] \\
z_3(\tau) &= \frac{k\Delta^*}{c}(2t_1 - \tau)
\end{aligned}
\tag{4.56}
$$

Note that $\tau = t_2$ and $\mathbf{z} = \mathbf{z}(t_2)$ represent the time and corresponding state, at which the trajectory leaves the switching surface V_1 during backward integration. Substituting $\tau = t_2$ into (4.56), we have,

$$z_1(t_2) = \frac{k\Delta^*}{m}[2e^{-\lambda_1(t_2-t_1)} - e^{-\lambda_1 t_2} - 1]$$

$$z_2(t_2) = \frac{k\Delta^*}{m}[-2e^{-\lambda_2(t_2-t_1)} + e^{-\lambda_2 t_2} + 1] \tag{4.57}$$

$$z_3(t_2) = \frac{k\Delta^*}{c}(2t_1 - t_2)$$

Let,

$$\Delta t_1 = t_1, \quad \Delta t_2 = t_2 - t_1, \tag{4.58}$$

where, Δt_1 and Δt_2 represent the time intervals, over which the trajectory moves on the switching curve V_2 and the switching surface V_1, respectively. Writing (4.57) in terms of Δt_1 and Δt_2, we obtain,

$$z_1(t_2) = \frac{k\Delta^*}{m}[2e^{-\lambda_1\Delta t_2} - e^{-\lambda_1(\Delta t_1+\Delta t_2)} - 1] \tag{4.59-a}$$

$$z_2(t_2) = \frac{k\Delta^*}{m}[-2e^{-\lambda_2\Delta t_2} + e^{-\lambda_2(\Delta t_1+\Delta t_2)} + 1] \tag{4.59-b}$$

$$z_3(t_2) = \frac{k\Delta^*}{c}(\Delta t_1 - \Delta t_2) \tag{4.59-c}$$

We, now, try to solve the set of equations (4.59) in terms of time intervals Δt_1 and Δt_2, in order to get the equations describing the surface V_1. From (4.59-c), we have

$$\Delta t_1 = \Delta t_2 + z_3 \frac{c}{k\Delta^*} \tag{4.60}$$

Substituting (4.60) into (4.59-b), we have

$$z_2 = \frac{k\Delta^*}{m}[-2e^{-\lambda_2\Delta t_2} + e^{-\lambda_2(2\Delta t_2 + z_3\frac{c}{k\Delta^*})} + 1] \tag{4.61}$$

To simplify (4.61), we define the following parameters:

$$\beta = e^{-\lambda_2 (z_3 \frac{c}{k\Delta^*})} \tag{4.62}$$

and

$$\gamma = e^{-\lambda_2 (\Delta t_2)} \tag{4.63}$$

Substituting (4.62) and (4.63) into (4.61), to obtain

$$z_2 = \frac{k\Delta^*}{m}[-2\gamma + \beta\gamma^2 + 1] \tag{4.64}$$

We rewrite (4.64) as a second order equation in terms of γ;

$$\beta\gamma^2 - 2\gamma + (1 - z_2 \frac{m}{k\Delta^*}) = 0 \tag{4.65}$$

Solving (4.65) with respect to the variable γ, we get two solutions

$$\gamma_1 = \frac{2 + \sqrt{4 - 4\beta(1 - z_2 \frac{m}{k\Delta^*})}}{2\beta} \tag{4.66}$$

$$\gamma_2 = \frac{2 - \sqrt{4 - 4\beta(1 - z_2 \frac{m}{k\Delta^*})}}{2\beta} \tag{4.67}$$

We note from (4.66) and (4.67) that, to conserve the realness of the roots, we must assume that

$$1 - \beta(1 - z_2 \frac{m}{k\Delta^*}) = 1 - e^{-\lambda_2 (z_3 \frac{c}{k\Delta^*})}(1 - z_2 \frac{m}{k\Delta^*}) > 0 \tag{4.68}$$

Note, also, from (4.62) and (4.63), that the values of γ and β are always positive, which implies that γ_1 is the only solution to the equation (4.65).

Substituting back the values of β and γ into equation (4.67), we have

$$e^{-\lambda_2(\Delta t_2)} = \frac{2+\sqrt{4-4e^{-\lambda_2(z_3\frac{c}{k\Delta^*})}(1-z_2\frac{m}{k\Delta^*})}}{2e^{-\lambda_2(z_3\frac{c}{k\Delta^*})}} \tag{4.69}$$

Simplifying (4.69)

$$e^{-\lambda_2(\Delta t_2)} = e^{\lambda_2(z_3\frac{c}{k\Delta^*})}\{1+\sqrt{[1-e^{-\lambda_2(z_3\frac{c}{k\Delta^*})}(1-z_2\frac{m}{k\Delta^*})]}\} \tag{4.70}$$

Taking the logarithm of both sides and simplifying, we get an expression of Δt_2 in terms of z_2 and z_3,

$$\Delta t_2 = -(z_3\frac{c}{k\Delta^*}) - \frac{1}{\lambda_2}\ln\{1+\sqrt{1-e^{-\lambda_2(z_3\frac{c}{k\Delta^*})}(1-z_2\frac{m}{k\Delta^*})}\} \tag{4.71}$$

Substituting (4.71) into (4.61), we obtain,

$$\Delta t_1 = -\frac{1}{\lambda_2}\ln\{1+\sqrt{1-e^{-\lambda_2(z_3\frac{c}{k\Delta^*})}(1-z_2\frac{m}{k\Delta^*})}\} \tag{4.72}$$

Finally, substituting (4.71) and (4.72) into (4.59-a) and simplifying, we get an equation describing the switching surface (V_1),

$$\mathbb{Z}_1(z_2,z_3) = -\frac{k\Delta^*}{m}\{e^{(\frac{\lambda_1 c z_3}{k\Delta^*})}[(g(z_2,z_3)-1)^2-1]+1\} \tag{4.73}$$

where,

$$g(z_2,z_3) = \{1+\sqrt{[1+(\frac{mz_2}{k\Delta^*}-1)e^{-\lambda_2(z_3\frac{c}{k\Delta^*})}]}\}^{\frac{\lambda_1}{\lambda_2}} \tag{4.74}$$

Here, Δ^* determines the control sequence to reach the state $\mathbf{z} \in \mathrm{V}_1$ by moving backwards in time from the origin. For instance, $\Delta^* = +u_{\max}$ means the state $\mathbf{z} \in \mathrm{V}_1$ can be reached from the origin with the control sequence $\{+u_{\max}, -u_{\max}\}$. Similarity $\Delta^* = -u_{\max}$ implies that the control sequence to reach the state $\mathbf{z} \in \mathrm{V}_1$ is $\{-u_{\max}, +u_{\max}\}$. Therefore, once Δ^* is determined, then, the control sequence to reach a given state is also determined. Specifically, if $\Delta^* = +u_{\max}$, then the control sequence to reach a given state from the origin is $\{+u_{\max}, -u_{\max}, +u_{\max}\}$, and if $\Delta^* = -u_{\max}$ then the control sequence to reach a given state from the origin is $\{-u_{\max}, +u_{\max}, -u_{\max}\}$.

Now we shall introduce a scheme to determine Δ^* in equations (4.73) and (4.74).

Scheme 4.1

Consider equations (4.71) and (4.72). Using the fact that Δt_1 in (4.72) and Δt_2 in (4.71) must be real and non-negative, we obtain, after a lengthy algebra, the following explicit relation for Δ^* as a function of the state

$$\Delta^* = u_{\max} \operatorname{sgn}\{z_2 - \mathrm{Z}_2(z_3)\} \tag{4.75}$$

Hence, we get three different equations (4.73), (4.74), and (4.75), to describe the switching surface V_1. Figure 4.3 shows an illustrative plot of the switching surface and switching curve within the switching surface.

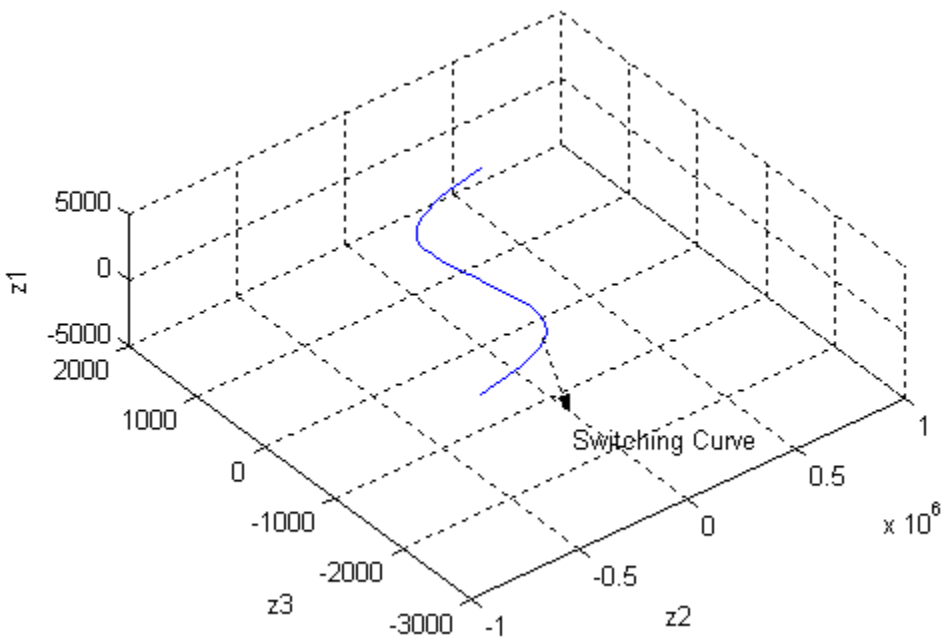

Figure 4.2 Switching Curve

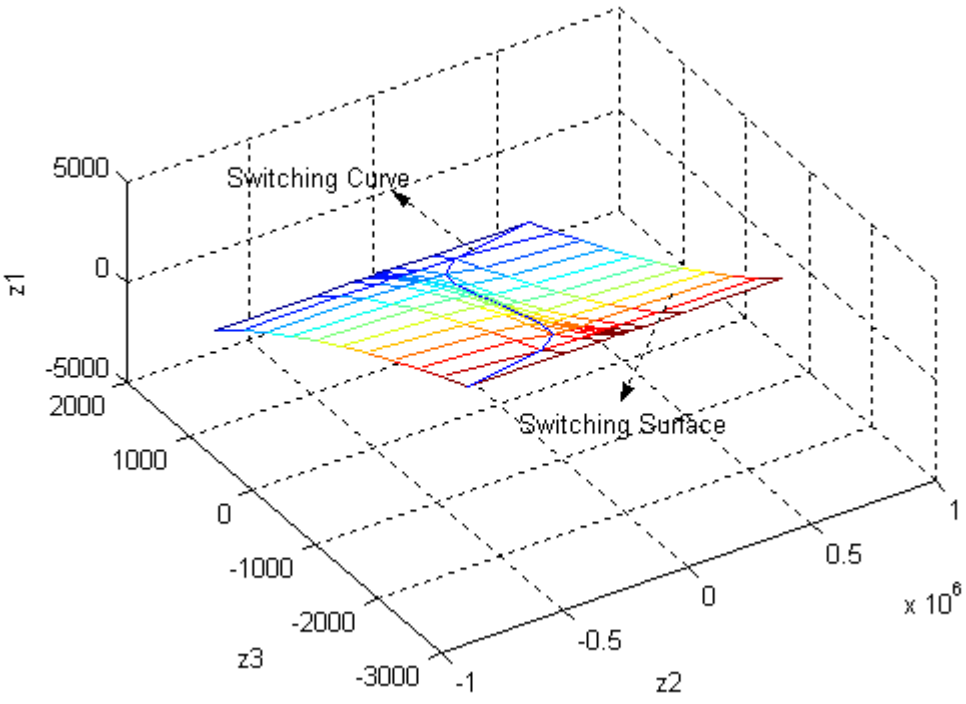

Figure 4.3 Switching Surface

4.3.5. The Control Strategy

The surface V_1 has the following properties [38]:

- The set V_1 can be reduced to the set V_2 by setting $\Delta t_2 = 0$ in (4.59) and the set V_1 can be reduced to the origin by setting $\Delta t_1 = 0$ and $\Delta t_2 = 0$ in (4.59). Thus, $0 \subset V_2 \subset V_1$.
- From (4.73), it is clear that for every pair (z_2, z_3), $\mathbb{Z}_1(z_2, z_3)$ is uniquely determined.
- The set V_1 is union of two subsets, namely V_1^1 and V_1^2 which are constructed by similar procedures; that is, V_1^1 is obtained by varying Δt_1 and Δt_2 from zero to infinity with the control sequence u $=\{+u_{\max}, -u_{\max}\}$ and V_1^2 is obtained by varying Δt_1 and Δt_2 from zero to infinity with the control sequence u $=\{-u_{\max}, +u_{\max}\}$.
- The surface V_1 partitions R^3 into three disjoint sets: V_1 and two sets that either lay "above" V_1 or "below" V_1 along the z_1 axis.

The remainder of the TOC policy is constructed based on the last property of V_1 [38]. To explain this, we define three control laws corresponding to three different cases.

Control Law 4.3.1

Consider an arbitrary state $\mathbf{z} \in \mathbf{R}^3$ and let $\mathbb{Z}_1(z_2, z_3)$ be determined by (4.73)-(4.75).

If $z_1 - \mathbb{Z}_1(z_2, z_3) > 0$, it means that $\mathbf{z}$ lies above the surface V_1, then $u = u_{\max}$.

If $z_1 - \mathbb{Z}_1(z_2, z_3) < 0$, it means that $\mathbf{z}$ lies below the surface V_1, then $u = -u_{max}$.

In short, if the state $\mathbf{z}$ is arbitrary and does not belong to V_1, the control will be

$u = u_{max}\, \text{sgn}\{z_1 - \mathbb{Z}_1(z_2, z_3)\}$

Control Law 4.3.2

Similar to the previous Control Law, consider the case where $\mathbf{z} \in V_1$, which means that $z_1 - \mathbb{Z}_1(z_2, z_3) = 0$, and let $Z_2(z_3)$ be determined by (4.52).

If $z_2 - Z_2(z_3) > 0$, it means that $\mathbf{z}$ lies on one side of the curve V_2, then $u = -u_{max}$.

If $z_2 - Z_2(z_3) < 0$, it means that $\mathbf{z}$ lies on another side the curve V_2, then $u = u_{max}$.

In short, if $\mathbf{z}$ belongs to V_1 but does not belong to the curve V_2, then the control law can be written as

$u = -u_{max}\, \text{sgn}\{z_2 - Z_2(z_3)\}$

Control Law 4.3.3

Similarly, consider the case where $\mathbf{z} \in V_2$, then the control law will be determined using (4.50), which gives;

If $z_3 > 0$, it means that $\mathbf{z}$ lies on one side of the origin, then $u = u_{max}$.

If $z_3 < 0$, it means that $\mathbf{z}$ lies another side of origin, then $u = -u_{max}$.

Thus, the expression of the control law when the state is on the switching curve is given by:

$u = u_{max}\, \text{sgn}\{z_3\}$

The combination of these three control laws results in the following time-optimal bang-bang controller:

$$U^*(z)=\begin{cases} u_{\max}\,\mathrm{sgn}\{z_1-\mathbb{Z}_1(z_2,z_3)\} & \text{if} \quad z_1-\mathbb{Z}_1(z_2,z_3)\neq 0 \\ -u_{\max}\,\mathrm{sgn}\{z_2-Z_2(z_3)\} & \text{if} \quad z_1-\mathbb{Z}_1(z_2,z_3)=0,\ z_2-Z_2(z_3)\neq 0 \\ u_{\max}\,\mathrm{sgn}\{z_3\} & \text{if} \quad z_1-\mathbb{Z}_1(z_2,z_3)=0,\ z_2-Z_2(z_3)=0 \end{cases}$$

(4.76)

It is clear that the ideal TOC law $U^*(z)$ is defined everywhere except at the origin.

We, now, outline the operation of the control law (4.76) as follows:

- Consider any initial state **x**(0).
- Use the transformation (4.36), compute **z**(0) as

$$\mathbf{z}(0)=\mathbf{P}^{-1}\mathbf{x}(0)$$

- Use the controller (4.76) in the equation of motion (4.44) to obtain $\mathbf{z}(t)$ for $0\le t\le t^*$.
- Finally, use the inverse transformation (4.37) to obtain $\mathbf{x}(t)$ for $0\le t\le t^*$.

As an illustration, Figure 4.4 shows the response of the system, in *x*-domain, with the TOC (4.79), for an initial state $\mathbf{x}(0) = [5000\ 0\ 0]^T$.

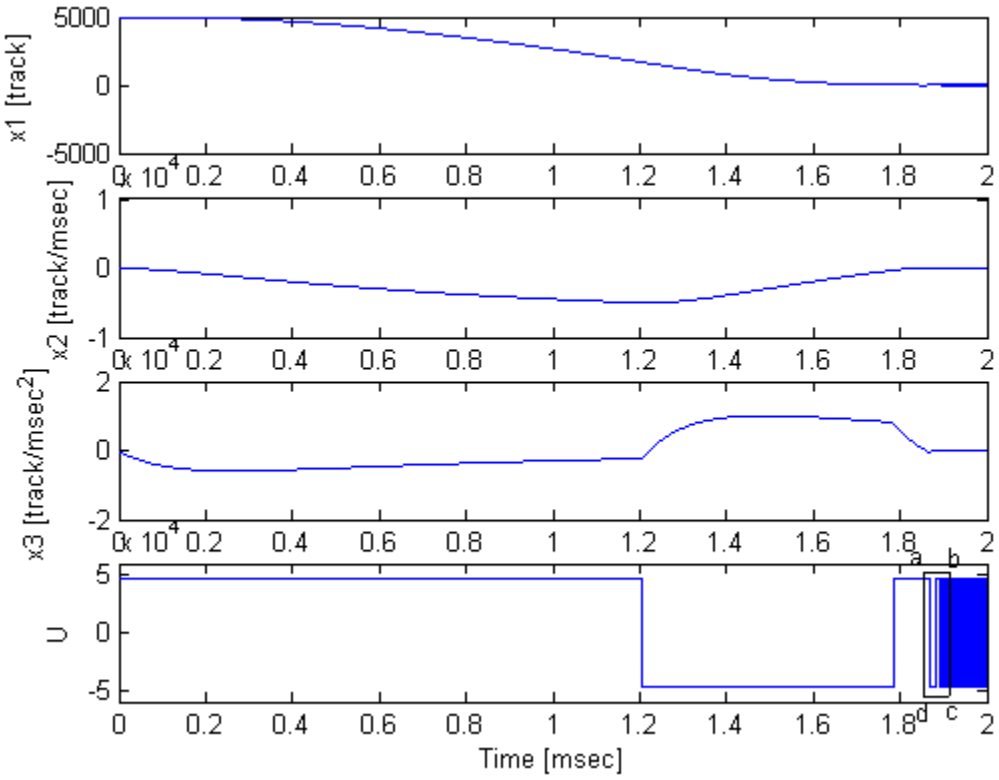

Figure 4.4 The response of the TOC

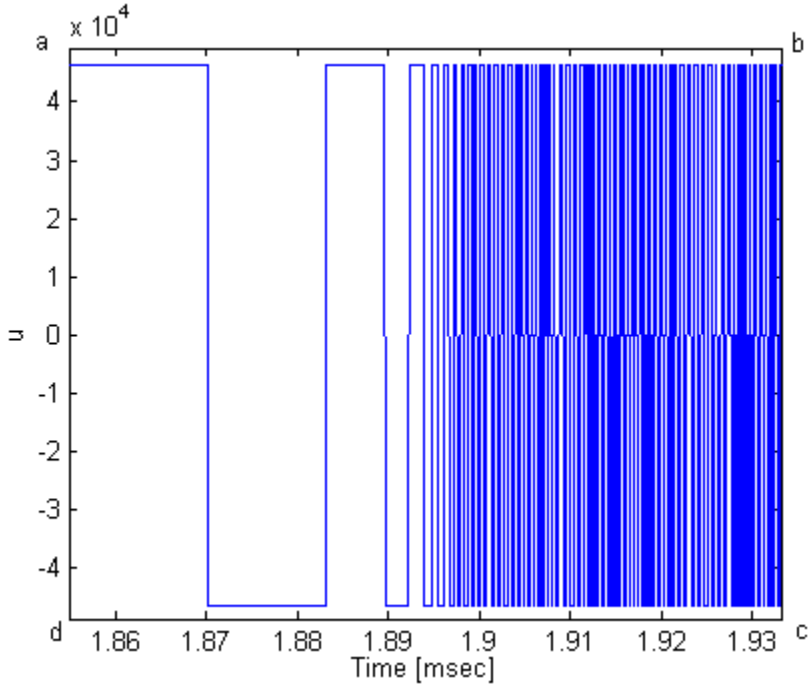

Figure 4.5 The TOC chattering (zoomed version of Figure 4.4)

Apparently, the control law given by (4.76) for the third order system (3.16) is not practical, as can be seen in Figures 4.4 and 4.5, Due to the fact that the TOC applies only the maximum or minimum control effort to the plant to be controlled even for a small error. Moreover, this algorithm is not suited for hard disk drive applications for the following reasons [5]:

1. Even the smallest system process or measurement noise will cause control "chatter", Figure 4.5.
2. Any error in the plant model will cause limit cycling to occur.

As such, the TOC given above has to be modified to suit the model that we have. In the following chapter, we will apply a modified version of TOC called the CPTO control, which was initiated by Rauch and Howe [39] and extended by Kalyon [8], [9], [10].

CHAPTER 5

CONTINUOUS PROXIMATE TIME-OPTIMAL (CPTO) CONTROL

5.1. CPTO Control of Third Order System Having Two Real Roots and an Integrator

The infinite gain of the signum function in the TOC causes control chatter [5], as seen in Figure 4.4. To overcome such a drawback, Kalyon [8], [9], [10], proposed a modification of the TOC, the so-called CPTO controller. The CPTO controller essentially uses the maximum effort if the state is large and uses the linear control law if the state is small. Moreover, the CPTO controller, smoothly, switches between the maximum and minimum control effort, rather then the sharp chop as in the TOC. In the CPTO control, the ideal switching surface for the third-order system becomes “slab” of finite thickness

in the neighborhood of the ideal switching surface, and the ideal switching curve becomes a tube in the neighborhood of the ideal switching curve [8]. The tube, lying within the slab, encloses the origin.

We will apply the CPTO technique on a third order model having two real roots and an integrator, which we have derived in Chapter 3 as a model of the HDD. We, thus, propose the following control law:

$$U(z) = \text{sat}\{k_1\{[z_1 - \mathbb{Z}_1(z_2, z_3)] - \frac{1}{k_1}\text{sat}\{k_2 k_1[z_2 - \text{Z}_2(z_3)] - \text{sat}(k_3 k_1 z_3)\}\}\} \tag{5.1}$$

where from (4.52), (4.74), (4.75), and (4.78)

$$\mathbb{Z}_1(z_2, z_3) = -\frac{k\Delta^*}{m}\{e^{(\frac{\lambda_1 c z_3}{k\Delta^*})}[(g(z_2, z_3) - 1)^2 - 1] + 1\} \tag{5.2}$$

$$g(z_2, z_3) = \{1 + \sqrt{[1 + (\frac{m z_2}{k\Delta^*} - 1)\, e^{-\lambda_2 (z_3 \frac{c}{k\Delta^*})}]}\}^{\frac{\lambda_1}{\lambda_2}} \tag{5.3}$$

$$\Delta^* = u_{\max}\,\text{sgn}\{z_2 - \text{Z}_2(z_3)\} \tag{5.4}$$

$$\text{Z}_2(z_3) = \frac{k\, u_{\max}\,\text{sgn}(z_3)}{m}(-1 + e^{-\lambda_2 \frac{c}{k\, u_{\max}\,\text{sgn}(z_3)} z_3}) \tag{5.5}$$

Here k_1, k_2 and k_3 are the controller gain constants, which will be computed later in this chapter, and where, the *sat* function in (5.1) is defined as followed,

$$\text{sat}(x) = \begin{cases} u_{\max}\,\text{sgn}(x) & \text{for} \quad |x| \geq u_{\max} \\ x & \text{for} \quad |x| < u_{\max} \end{cases} \tag{5.6}$$

We remark that the CPTO control law (5.1)-(5.6) is an approximation of the ideal discontinuous time-optimal control law (4.79) when k_1 is sufficiently large, which is proven below.

Claim 5.1

For all $z \neq 0$, $U(z) \rightarrow U^*(z)$ as $k_1 \rightarrow \infty$.

Proof: Since $U^*(z)$, defined in Equation (4.79), apparently depends on three different cases, we will consider each of these cases to prove that indeed $U(z)$ approaches $U^*(z)$ as $k_1 \rightarrow \infty$.

I) Set $z_1 - \mathbb{Z}_1(z_2, z_2) = 0$, $z_1 - \mathrm{Z}_2(z_2) = 0$ and $z_3 \neq 0$. Substituting into (5.1)-(5.6), we get

$U(z) = \mathrm{sat}\{\mathrm{sat}\{\mathrm{sat}(k_1 k_3 z_3)\}\}$

Clearly, as $k_1 \rightarrow \infty$, $U(z) = u_{\max}\,\mathrm{sgn}(z_3)$, which verifies the third part of $U^*(z)$, (4.79).

II) Set $z_1 - \mathbb{Z}_1(z_2, z_2) = 0$ and $z_1 - \mathrm{Z}_2(z_2) \neq 0$. Substituting into (5.1)-(5.6), we get

$U(z) = \mathrm{sat}\{-\mathrm{sat}\{k_2 k_1 [z_2 - \mathrm{Z}_2(z_3)] - \mathrm{sat}(k_3 k_1 z_3)\}\}$

As $k_1 \rightarrow \infty \Rightarrow \left| k_2 k_1 [z_2 - \mathrm{Z}_2(z_3)] \right| \gg \mathrm{sat}(k_3 k_1 z_3)$,

which gives that

$U(z) = -u_{\max}\,\mathrm{sgn}\{[z_2 - \mathrm{Z}_2(z_3)]\}$

Similar to the previous case, equation (5.6) verifies the second part of $U^*(z)$.

III) Set $z_1 - \mathbb{Z}_1(z_2, z_2) \neq 0$, then we have

$$U(z) = \text{sat}\{\{k_1[z_1 - \mathbb{Z}_1(z_2, z_3)] - \text{sat}\{k_2 k_1[z_2 - \mathrm{Z}_2(z_3)]$$
$$-\text{sat}(k_3 k_1 z_3)\}\}.$$

As $k_1 \to \infty \Rightarrow$

$$\left|k_1[z_1 - \mathbb{Z}_1(z_2, z_3)]\right| \gg \text{sat}\{k_2 k_1[z_2 - \mathrm{Z}_2(z_3)] - \text{sat}(k_3 k_1 z_3)\}.$$

Thus, we obtain

$$U(z) \to \text{sat}\{k_1[z_1 - \mathbb{Z}_1(z_2, z_3)]\} \to u_{\max}\, \text{sgn}\{z_1 - \mathbb{Z}_1(z_2, z_3)\},$$

which verifies the first part of (4.79).

We, thus, conclude from Claim 5.1 that the ideal TOC is a special case of the CPTO control. We, further, state the following claim in order to prove that the linear control is a special case of the CPTO control, as well.

Claim 5.2

If $\|\mathbf{z}\|$ is small, then $U(z) = \hat{k}_1(z_1 + \hat{k}_2 z_2 + \hat{k}_3 z_3)$.

Proof:

Here, we are going to find an approximation of $\mathbb{Z}_1(z_2, z_3)$ and $\mathrm{Z}_2(z_3)$ if $\|\mathbf{z}\|$ is small, that is, if z_1, z_2 and z_3 are small. We, thus, assume that $z_i = \varepsilon_i$, $i = 1, 2, 3$ and $z_i^n = \varepsilon_i^n \cong 0$ if $n > 1$.

Substituting these values into (5.3), we get

$$g(\varepsilon_2,\varepsilon_3)=\{1+\sqrt{[1+(\frac{m\varepsilon_2}{k\Delta^*}-1)\,e^{-\lambda_2(\varepsilon_3\frac{c}{k\Delta^*})}]}\}^{\frac{\lambda_1}{\lambda_2}} \tag{5.7}$$

Based on the small state assumption, we obtain the Taylor series expansion of the exponential term in equation (5.7),

$$e^{-\lambda_2(\varepsilon_3\frac{c}{k\Delta^*})}=1-\lambda_2(\varepsilon_3\frac{c}{k\Delta^*})+\text{HOT}\cong 1-\lambda_2(\varepsilon_3\frac{c}{k\Delta^*}) \tag{5.8}$$

Similar to the approximation of (5.8), we have

$$e^{(\frac{\lambda_1 c\varepsilon_3}{k\Delta^*})}\cong 1+\frac{\lambda_1 c\varepsilon_3}{k\Delta^*} \tag{5.9}$$

where the higher order terms (HOT) is negligible.

Substituting (5.8) into (5.7) and organizing the resulting equation by neglecting the HOT, we obtain,

$$g(\varepsilon_2,\varepsilon_3)\cong\{1+\sqrt{(\frac{m\varepsilon_2}{k\Delta^*}+\frac{c\lambda_2\varepsilon_3}{k\Delta^*})}\}^r \tag{5.10}$$

where

$$r=\frac{\lambda_1}{\lambda_2}$$

In order to approximate equation (5.10), we apply the following binomial expansion formula,

$$(1+w)^n=1+nw+\frac{n(n-1)}{2!}w^2+\frac{n(n-1)(n-2)}{3!}w^3+\frac{n(n-1)(n-2)(n-3)}{4!}w^4+\ldots+w^n$$

By neglecting the HOT, we, thus, have

$$g(\varepsilon_2,\varepsilon_3)\cong\{1+r\sqrt{(\frac{m\varepsilon_2}{k\Delta^*}+\frac{c\lambda_2\varepsilon_3}{k\Delta^*})}+\frac{r(r-1)}{2}(\frac{m\varepsilon_2}{k\Delta^*}+\frac{c\lambda_2\varepsilon_3}{k\Delta^*})\} \tag{5.11}$$

or

$$(g(\varepsilon_2,\varepsilon_3)-1)^2 \cong r^2(\frac{m\varepsilon_2}{k\Delta^*}+\frac{c\lambda_2\varepsilon_3}{k\Delta^*}) \tag{5.12}$$

We substitute (5.12) into (5.2) to obtain the proximate value of $\mathbb{Z}_1(z_2,z_3)$.

$$\mathbb{Z}_1(\varepsilon_2,\varepsilon_3) \cong -\frac{k\Delta^*}{m}\{\, e^{(\frac{\lambda_1 c\varepsilon_3}{k\Delta^*})}[r^2(\frac{m\varepsilon_2}{k\Delta^*}+\frac{c\lambda_2\varepsilon_3}{k\Delta^*})-1]+1\} \tag{5.13}$$

If we substitute, (5.9) into (5.13), we have,

$$\mathbb{Z}_1(\varepsilon_2,\varepsilon_3) \cong -\frac{k\Delta^*}{m}\{\, [1+(\frac{\lambda_1 c\varepsilon_3}{k\Delta^*})][r^2(\frac{m\varepsilon_2}{k\Delta^*}+\frac{c\lambda_2\varepsilon_3}{k\Delta^*})-1]+1\} \tag{5.14}$$

Organizing (5.14) by neglecting the HOT, we get,

$$\mathbb{Z}_1(\varepsilon_2,\varepsilon_3) \cong -r^2\varepsilon_2+(\frac{\lambda_1 c}{m}+\frac{\lambda_2 c}{m}r^2)\varepsilon_3 = -r^2\varepsilon_2+\frac{\lambda_1 c}{m}(1-r)\varepsilon_3$$

We, correspondingly, have,

$$\mathbb{Z}_1(z_2,z_3) \cong -r^2 z_2+\frac{\lambda_1 c}{m}(1-r)z_3 \tag{5.15}$$

for z_2 and z_3 are small. Clearly, from (5.15), we note that $\mathbb{Z}_1(z_2,z_3)$ is in linear form in terms of z_2 and z_3 when the state is near the origin, that is, when the state is small.

Similarly, we, now, obtain the approximation of $\mathrm{Z}_2(z_3)$ in (5.5).

$$\mathrm{Z}_2(z_3)=\frac{k\,u_{\max}\,\mathrm{sgn}(z_3)}{m}(-1+e^{-\lambda_2\frac{c}{k\,u_{\max}\,\mathrm{sgn}(z_3)}z_3})$$

Referring to (5.8), we can write the exponential term in (5.5) as,

$$e^{-\lambda_2\frac{c}{k\,u_{\max}\,\mathrm{sgn}(z_3)}z_3} \cong 1-\lambda_2\frac{c}{k\,u_{\max}\,\mathrm{sgn}(z_3)}z_3 \tag{5.16}$$

Substituting (5.16) into (5.5) and organizing, we get

$$\mathbf{Z}_2(z_3) \cong -\frac{\lambda_2 c}{m} z_3 \tag{5.17}$$

Thus, similar to $\mathbb{Z}_1(z_2, z_3)$, $\mathbf{Z}_2(z_3)$ can, also, be linearized near the origin when the state is small.

Now, let us prove that the CPTO control converges to a linear control when it is close to the origin. The linear controller gain constants, which will be designed, in the following section, can be expressed in terms of the state,

$$\hat{U}(\mathbf{z}) = \hat{k}_1(z_1 + \hat{k}_2 z_2 + \hat{k}_3 z_3) \tag{5.18}$$

When the state is near the origin that is $\|\mathbf{z}\|$ small, we can substitute the linear approximations of the equations describing the switching surface (5.15) and the switching curve (5.17) into (5.1), we have,

$$U(\mathbf{z}) \cong \text{sat}\{k_1[[z_1 + r^2 z_2 - \frac{\lambda_1 c}{m}(1-r)z_3)] - \text{sat}\{k_2[z_2 + \frac{c\lambda_2}{m} z_3] - \text{sat}(k_3 z_3)\}]\} \tag{5.19}$$

Since near the origin, the state will be in the linear region, the sat functions will be unsaturated, that is $sat(x) = x$. The equation (5.19), thus, will have the following form,

$$U(\mathbf{z}) \cong k_1\{[z_1 + r^2 z_2 - \frac{\lambda_1 c}{m}(1-r)z_3)] - \{k_2[z_2 + \frac{c\lambda_2}{m} z_3] - (k_3 z_3)\}\}. \tag{5.20}$$

Arranging (5.20), we get

$$U(\mathbf{z}) \cong k_1\{z_1 + (r^2 - k_2)z_2 + [k_3 - \frac{\lambda_2 c}{m} k_2 - \frac{\lambda_1 c}{m}(1-r)]z_3\} \tag{5.21}$$

To find the gain constants k_1, k_2, and k_3 used in (5.1), we compare (5.21) with the equation $\hat{U}(\mathbf{z}) = \hat{k}_1(z_1 + \hat{k}_2 z_2 + \hat{k}_3 z_3)$. We, thus, obtain

$$\hat{k}_1 = k_1$$
$$\hat{k}_2 = (r^2 - k_2) \tag{5.22}$$
$$\hat{k}_3 = k_3 - \frac{c\lambda_2}{m} k_2 - \frac{\lambda_1 c}{m}(1-r)$$

or

$$k_1 = \hat{k}_1$$
$$k_2 = r^2 - \hat{k}_2 \tag{5.23}$$
$$k_3 = \hat{k}_3 + \frac{\lambda_2 c}{m}(r^2 - \hat{k}_2) + \frac{\lambda_1 c}{m}(1-r)$$

As a result, we have proved that if the gain constants $k_1,\ k_2,$ and k_3 of the control law in equation (5.1) are chosen as in (5.23), then $U(z) \to \hat{U}(z)$ when $\|\mathbf{z}\|$ is small.

Figure 5.1 shows the response of the system (4.22) with the CPTO controller (5.1) for an initial state $\mathbf{x}(0) = [5000 \quad 0 \quad 0]^T$.

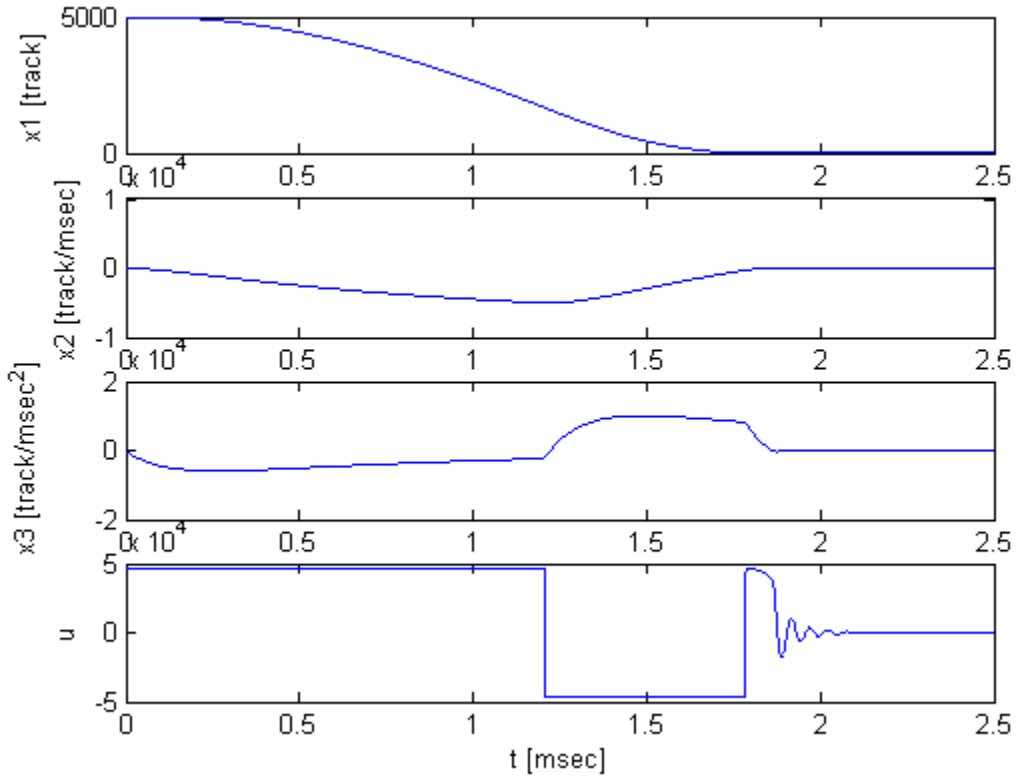

Figure 5.1 The response of the CPTO control

In Figure 5.1, all the state variables converge from $\mathbf{x}(0) = [5000 \quad 0 \quad 0]^T$ to zero, in around 2 *msec*, and remain there. Apparently, we note that the CPTO controller, unlike ideal TOC, shown in Figures 4.4 and 4.5, does not have any chattering. Moreover, it converges to a linear controller near the origin.

In the following section we are going to present the design of the linear controller $\hat{U}(z)$ in (5.15) in detail.

5.2. Linear Controller Design

The objective of this controller, mainly, is to determine the gain constants such that the design specifications are satisfied. The linear controller design is important since the CPTO controller converges to the linear controller when the state is small, as it is proven in the previous section (Claim 5.2), where we have obtained the relations (5.23) between the CPTO controller's gain constants (k_1, k_2 and k_3) and the linear controller's gain constants ($\hat{k}_1$, $\hat{k}_2$ and $\hat{k}_3$).

As an example for a linear controller design, we again consider the HDD servomechanism. For track following and track seeking, which are defined in Chapter 1, the following design criterion will be used:

I. Percent overshoot:

$$P.O. \leq 10\%, \tag{5.24}$$

II. Settling time:

$$T_s \leq 1\ msec\ , \tag{5.25}$$

The settling time T_s is defined [12] as the time required for the system to settle with a certain percentage δ of the input amplitude. Since the HDD needs very high accuracy, the error in the response should be $e_s \leq 0.1$, thus,

$$\delta = \frac{0.1}{50000} * 100 = 2 * 10^{-4}\% \tag{5.26}$$

We note here that we are considering the maximum reference input to be $r_{\max} = 50000$ *tracks*, which represents the "Full Stroke", when the armature moves from the first track

to the last track (number of a track = 50000), noting that the full stroke takes 15-20 *msec* to achieve it [40].

Hence, based on (5.24), (4.25) and (4.26) we design the gain constants of the linear controller.

5.3.1. Pole Placement

In the Linear Control practice, one of the commonly used methods in the design is called Pole Placement or Pole Assignment method, in which, briefly, we assign the poles of the system according to the design criterion, and then we compute the gain constants, accordingly. Due to its convenience, we are going to apply it regarding the linear controller design.

Because of the CPTO controller's structure, the linear controller (5.18) has to be state-feedback, thus, it should have the following form,

$$U_L(x) = k_{1L}x_1 + k_{2L}x_2 + k_{3L}x_3 \tag{5.27}$$

where,

k_{1L}, k_{2L}, and k_{3L} are the linear controller's gain constants.

Using the set of equations (3.18), we, thus, rewrite (5.27) in a transfer function form,

$$U_L(s) = k_{1L} + k_{2L}s + k_{3L}s^2 \tag{5.28}$$

We recall the HDD model,

$$G_p(s) = \frac{1.524}{s\ [s^2 + 10s + 10]} \tag{5.29}$$

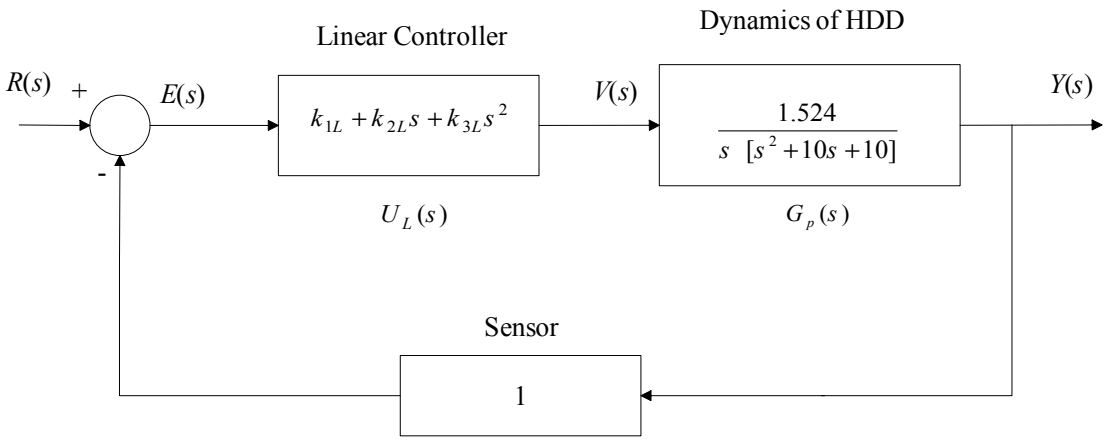

Figure 5.2 Closed loop block diagram of the system

Figure 5.2 shows the linear controller (5.28) and the HDD model in a closed-loop block diagram. From Figure 5.2, we get the closed loop transfer function,

$$G(s) = \frac{1.524(k_{1L} + k_{2L}s + k_{3L}s^2)}{s^3 + (10+1.524k_{3L})s^2 + (10+1.524k_{2L})s + 1.524k_{1L}} \tag{5.30}$$

Thus, the characteristic equation is given by

$$T(s) = s^3 + (10+1.524k_{3L})s^2 + (10+1.524k_{2L})s + 1.524k_{1L} = 0 \tag{5.31}$$

We note that (5.31) is in third-order. Thus, let us assume that it has the following general form,

$$T(s) = (s^2 + 2\zeta\omega_n s + \omega_n^2)(s+\mu) = 0 \tag{5.32}$$

Our objective is to compute the coefficients ζ, ω_n, and μ, such that, the response of (5.30) follows the design specifications in equations (5.24) and (5.25).

The response of a third order system can be approximated as the response of a second order system by using the *dominant roots*, of the second order system as long as the real part of the dominant roots is, approximately, ten times less than the real part of

the third root [12]. Since the real part of the complex poles of (5.32) is equal to $-\zeta\omega_n$, the third pole of (5.32) is, then, given by

$$\mu \cong -10\zeta\omega_n \tag{5.33}$$

Thus, we left with the designing of ω_n and ζ of the second order closed loop transfer function, which is easier to handle than the third order system, since there are ready expressions describing the performance measures. Therefore, we compute ζ from the following equation [12]:

$$P.O. = 100.e^{\frac{-\zeta\pi}{\sqrt{1-\zeta^2}}} \tag{5.34}$$

From (5.24) and (5.34) we solve for ζ as,

$$\zeta = 0.5911 \cong 0.6 \tag{5.35}$$

Moreover, we can compute ω_n from the following relation [12],

$$\delta = \frac{e^{-\zeta\omega_n T_s}}{100\sqrt{1-\zeta^2}} \tag{5.36}$$

Similarly, from (5.35), (5.25), and (5.26) and (5.36), and solve for ω_n as

$$\omega_n = 21.879\frac{1}{msec} \tag{5.37}$$

The corresponding μ can be obtained from (5.33) as,

$$\mu \cong 120 \tag{5.38}$$

Substituting these values of ζ, ω_n, and μ, into (5.32) and solving the roots, we get

$$\left.\begin{aligned} s_1 &= -12.9084 + 17.6649i \\ s_2 &= -12.9084 - 17.6649i \\ s_3 &= -120 \end{aligned}\right\} \tag{5.39}$$

Clearly, s_1 and s_2 are the dominant poles, since, the real part of both of them is almost 10 times less than the real part of the third pole. Rewriting (5.32), we have

$$T(s) = (s^3 + 12.58s^2 + 30.4225s + 46.225). \tag{5.40}$$

Comparing (5.40) with (5.31) and solving for k_{1L}, k_{2L} and k_{3L}, we get

$$\left.\begin{aligned} k_{1L} &= 37691 \\ k_{2L} &= 2340.4 \\ k_{3L} &= 89.119 \end{aligned}\right\} \tag{5.41}$$

Substituting the values of the controller's constants into (5.28), we obtain

$$U_L(s) = 37691 + 2340.4s + 89.119s^2 \tag{5.42}$$

or in a state space form of (5.27),

$$U_L(x) = \mathbf{k}_L \ \mathbf{x} \tag{5.43}$$

where,

$$\mathbf{k}_L = [k_{1L} \qquad k_{2L} \qquad k_{3L}]$$

Noting from (4.38) that $\mathbf{x} = \mathbf{P}\ \mathbf{z}$, we thus, obtain the linear controller in z-domain as,

$$U_L(z) = \mathbf{k}_L \mathbf{P}\ \mathbf{z} \tag{5.44}$$

Now, substituting the numerical values, we get

$$U_L(\mathbf{z}) = 27687\ z_1 + 304.1\ z_2 + 37691\ z_3 \tag{5.45}$$

or

$$U_L(\mathbf{z}) = \hat{k}_1(z_1 + \hat{k}_2 z_2 + \hat{k}_3 z_3)$$

where,

$$\left.\begin{aligned}\hat{k}_1 &= 27687\\ \hat{k}_2 &= 0.010984\\ \hat{k}_3 &= 1.3613\end{aligned}\right\} \tag{5.46}$$

Substituting the values in (5.46) into (5.23), we compute the gain constants of the CPTO controller,

$$\left.\begin{aligned}k_1 &= 27687\\ k_2 &= 0.032188\\ k_3 &= 0.0051497\end{aligned}\right\} \tag{5.47}$$

Lastly, by substituting (5.47) into (5.1), we obtain, fully, the gain constants of the CPTO controller as,

$$U(z) = \text{sat}\{k_1\{[z_1 - \mathbb{Z}_1(z_2, z_3)] - \frac{1}{k_1}\text{sat}\{k_2 k_1[z_2 - \mathbf{Z}_2(z_3)] - \text{sat}(k_3 k_1 z_3)\}\}\} \tag{5.48}$$

The simulation results of this CPTO controller are given in the following chapter.

To test the linear controller design, Figure 5.4 shows the response of the system (5.29) with the linear controller (5.42) for a unit step input of 50000 *tracks*. From Figure 5.3, we observe that, indeed, the response meets our design criterion, (5.24) and (5.25), that is, the maximum overshoot is less than 10% of the input and the settling time is less than 1 *msec*.

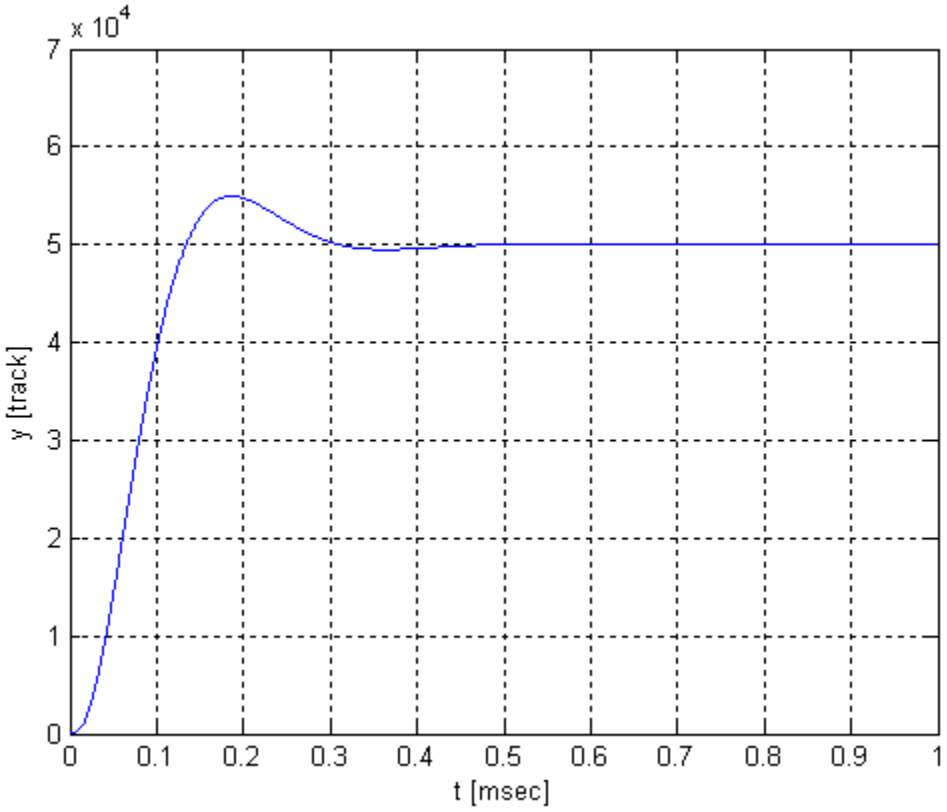

Figure 5.3 The response of the linear controller

CHAPTER 6

SIMULATION RESULTS

In this chapter, we test the performance of the CPTO controller through simulations. We have used Simulink software [41]. The Simulink block diagrams, which have been used for the simulations is given in Section 6.4.

Throughout the simulation, we assume that there is no disturbance acting on the system. Runge-Kutta-4 integration with step size h = 0.0001 was used to obtain the simulation results. Further reduction in step size had negligible effect on the simulation, so it is clear that the numerical solution with h = 0.0001 exhibit no significant errors.

6.1. The Performance of the CPTO Controller

The following simulations demonstrate the performance of the CPTO controller with initial conditions (1000, 0, 0), (10000, 0, 0) and (50000, 0, 0). In Figure 6.1, the responses of the error state (x_1, x_2, x_3) and the response of the CPTO controller with

the first initial conditions are shown. In Figure 6.2, we zoomed the switching part of the CPTO controller response. Figure 6.3, shows the corresponding responses (z_1, z_2, z_3) in z-domain (z_1, z_2, z_3). Clearly, all the state variables in *x*-domain, and correspondingly in z – domain, converge to zero and remain there. In Figures 6.1 and 6.3, we observe that the trajectory originating at $\mathbf{x}(0) = (1000\ \ 0\ \ 0)$, or, equivalently, at $\mathbf{z}(0) = (0\ \ 0\ \ 1000)$, reaches the slab with the control $u = +u_{\max}$. At this point, the z_1-distance from the slab $z_1 - \mathbb{Z}_1$ has diminished to near zero, as shown in Figure 6.4. At the same time the control decreases, from $u_{\max}$ to $-u_{\max}$. We note here that, unlike the ideal TOC, the switching from $u_{\max}$ to $-u_{\max}$ occurs gradually, as can be seen in Figure 6.2, where we have zoomed the switching part (a b c d) of the control response. After the trajectory reaches the slab, it moves within the slab until it reaches the tube. We note here that the concept of the slab and the tube have been discussed in the first paragraph of Chapter 5. At this point, the trajectory moves quickly across the tube until the z_2- distance, $z_2 - \mathrm{Z}_2$, has diminished nearly to zero as, shown in Figure 6.4. At the same time the control increases gradually from $-u_{\max}$ to nearly $u_{\max}$ be seen in Figure 6.4, the part (e f g h). After the control approaches $u_{\max}$, it remains near $u_{\max}$ until the trajectory enters the final region, within which all saturation functions are unsaturated, where the CPTO controller, proximately, functions as linear controller, as can be seen in Figure 6.1 and more clearly, in Figure 6.7. Thus, once the trajectory enters the final region, it converges to the origin smoothly and remains there. The same actions happen for other initial conditions, (10000, 0, 0) and (50000, 0, 0), as can be seen in Figures 6.5 and 6.6 respectively.

We observe from Figures 6.1, 6.5 and 6.6 that the settling times for the initial conditions 1000, 10000 and 50000 *tracks* error state are 0.87, 2.68, and 8.45, *milliseconds*, respectively, where all these settling times were observed when the error is less than or equal 0.1 *track*.

Figure 6.8 shows a comparison between the responses of three controllers, the CPTO controller (in the solid line), the saturated linear controller (PDD) (in the dotted-dashed line), and the TOC (in the dotted line). In Figure 6.9, for illustration purpose, we eliminate the control chattering, shown also in Figure 4.5, of the TOC from Figure 6.8, so that a clearer comparison can be conducted. We notice, from Figure 6.9, the linear behavior of the CPTO control near the origin, as it is explained in Chapter 5, Claim 2. Moreover, we observe that the CPTO control converges to the origin faster than the PDD control, while the TOC, due to its structure, can not go to zero at all, so that it has the chattering found in Figure 6.8. In Figure 6.10, we have zoomed the part, labeled with (p q r s) where the controllers switch from $u_{\max}$ to $-u_{\max}$. Clearly, the CPTO control does not have the sharp switching of the TOC. Figure 6.11 shows the error state x_1 response with the three controllers. Apparently, it can be observed that response of the system using the CPTO controller is essentially identical to the TOC response and it much faster than response of the system with the PDD controller.

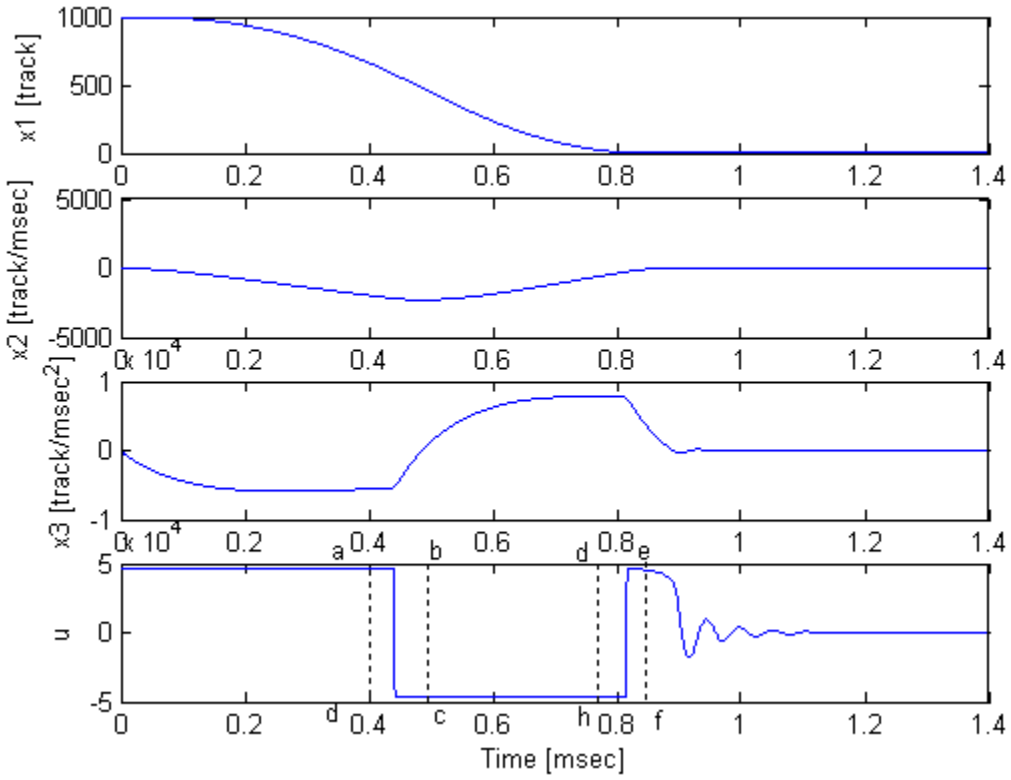

Figure 6.1 The response of the system to the CPTO controller for $\mathbf{x}(0) = (1000, 0, 0)$

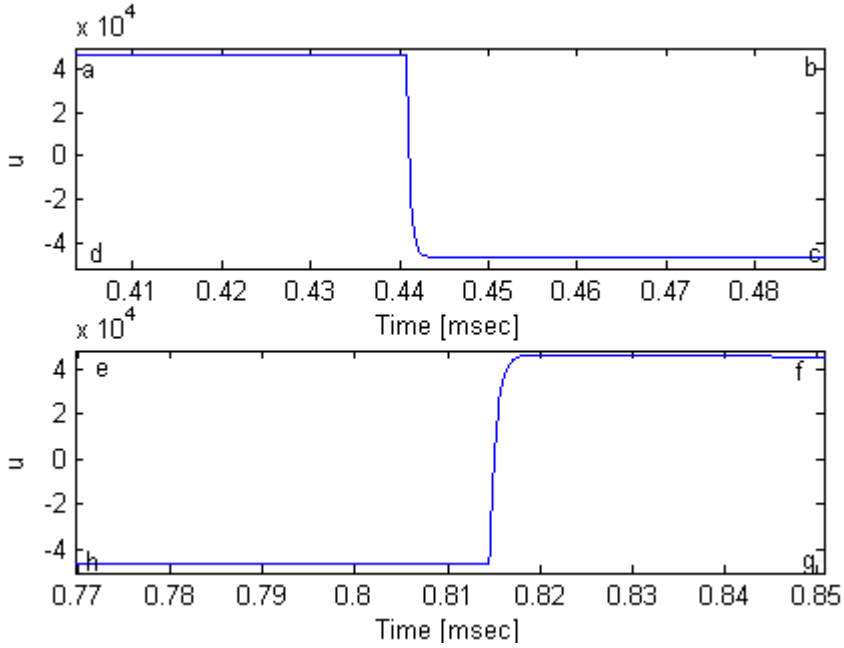

Figure 6.2 Zoomed version of the switching parts of the control response

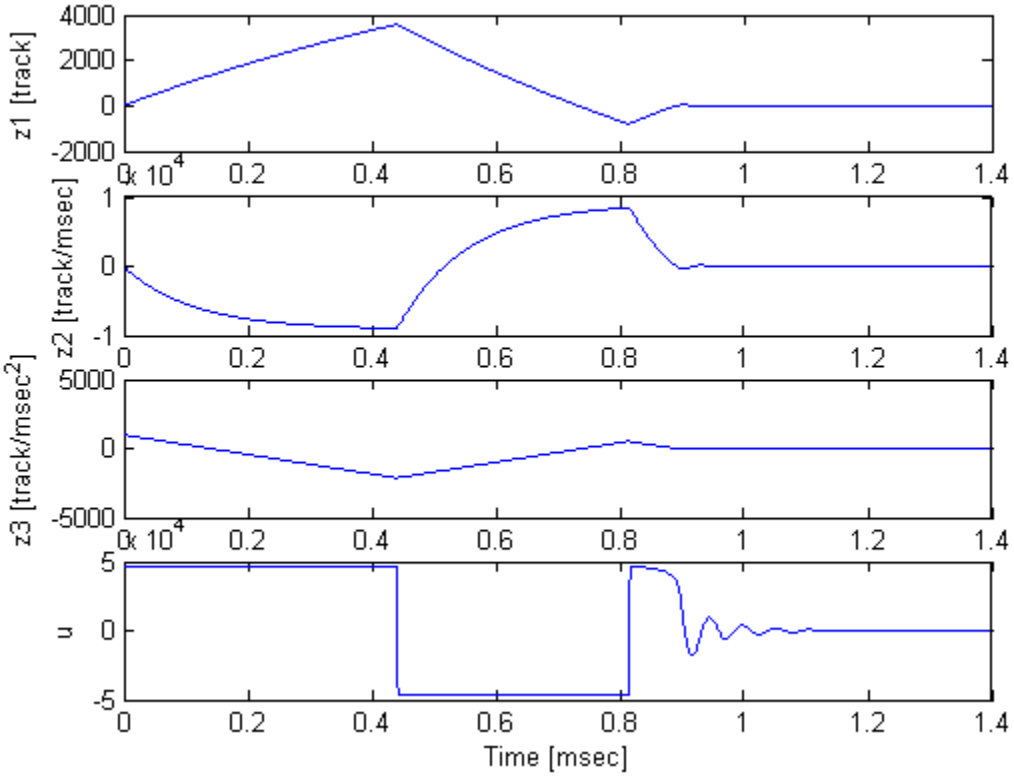

Figure 6.3 The response of the system to the CPTO controller in z-domain

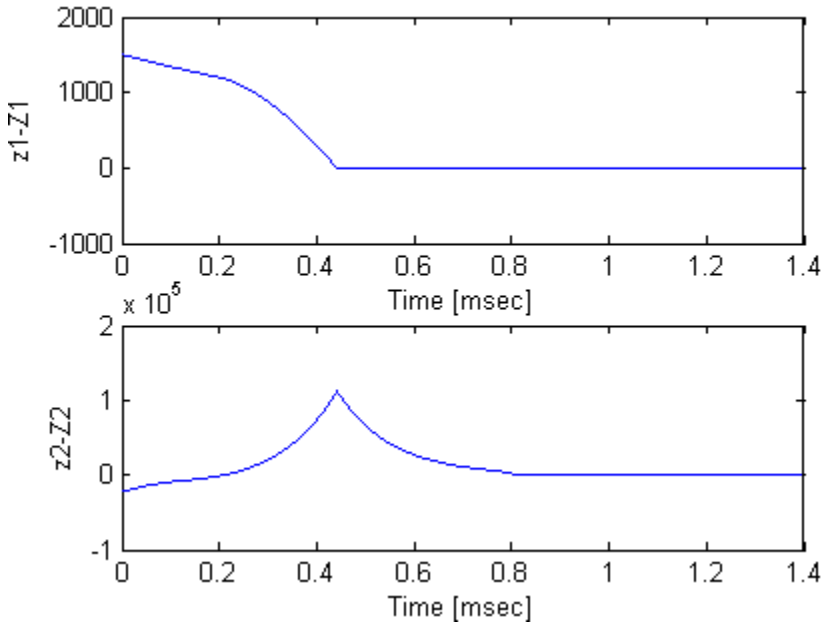

Figure 6.4 The history of the switching-surface function and the switching-curve function

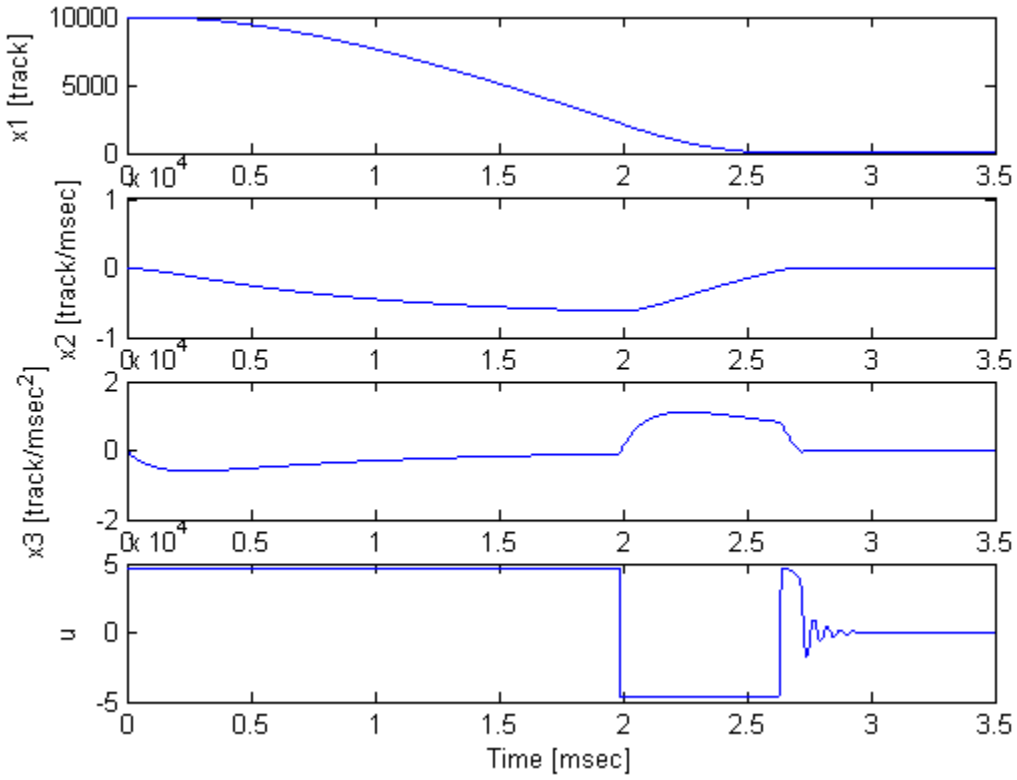

Figure 6.5 The response of the system to the CPTO controller for $\mathbf{x}(0) = (10000, 0, 0)$

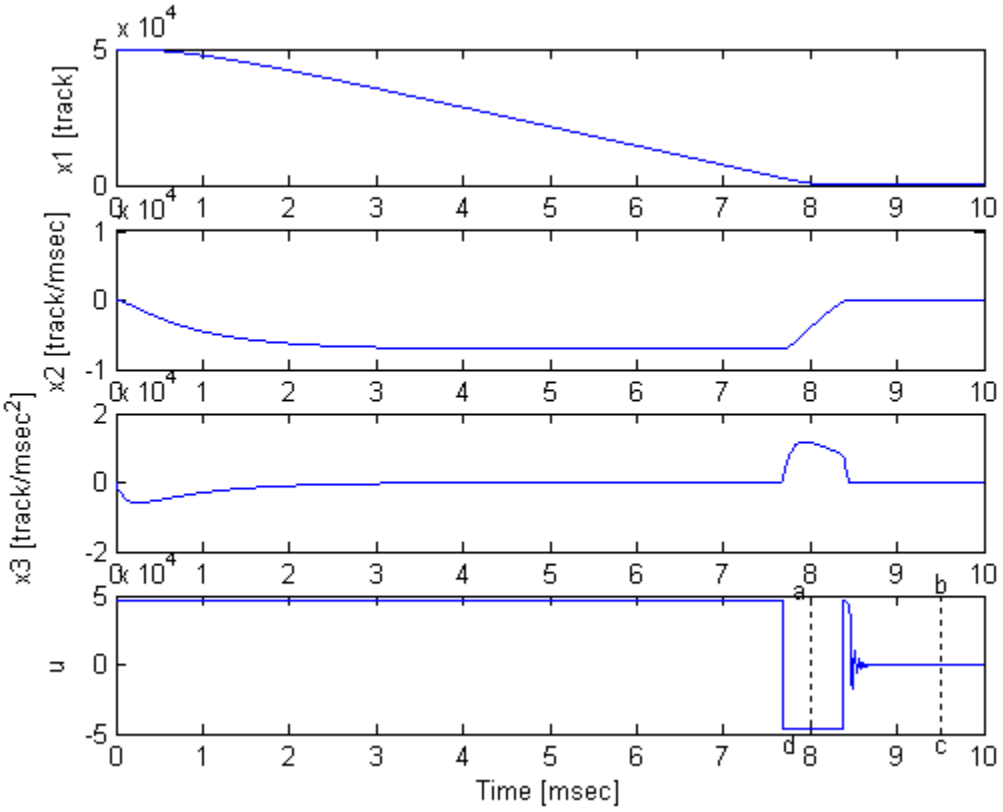

Figure 6.6 The response of the system to the CPTO controller for $\mathbf{x}(0) = (50000, 0, 0)$

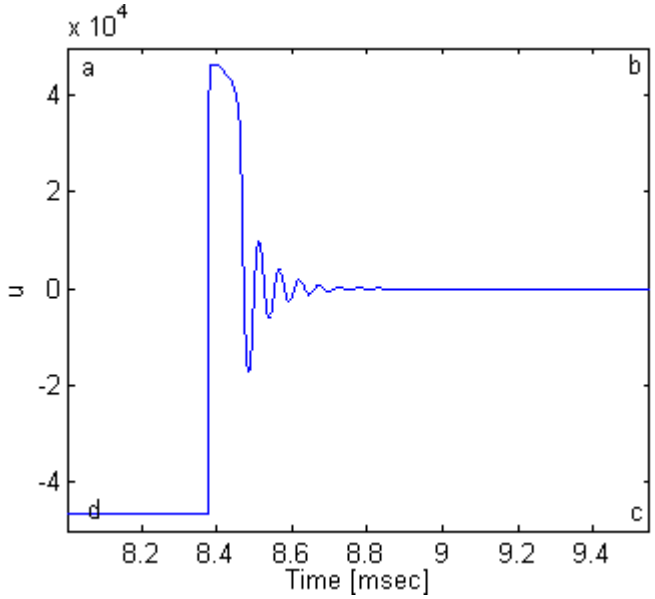

Figure 6.7 Zoomed version of the linear part of the control input of the CPTO controller

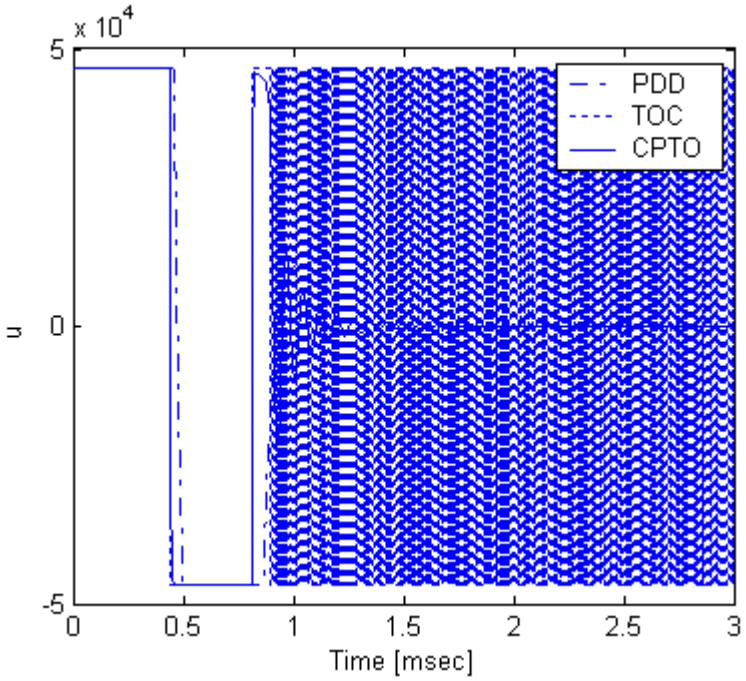

Figure 6.8 The responses of three different controllers

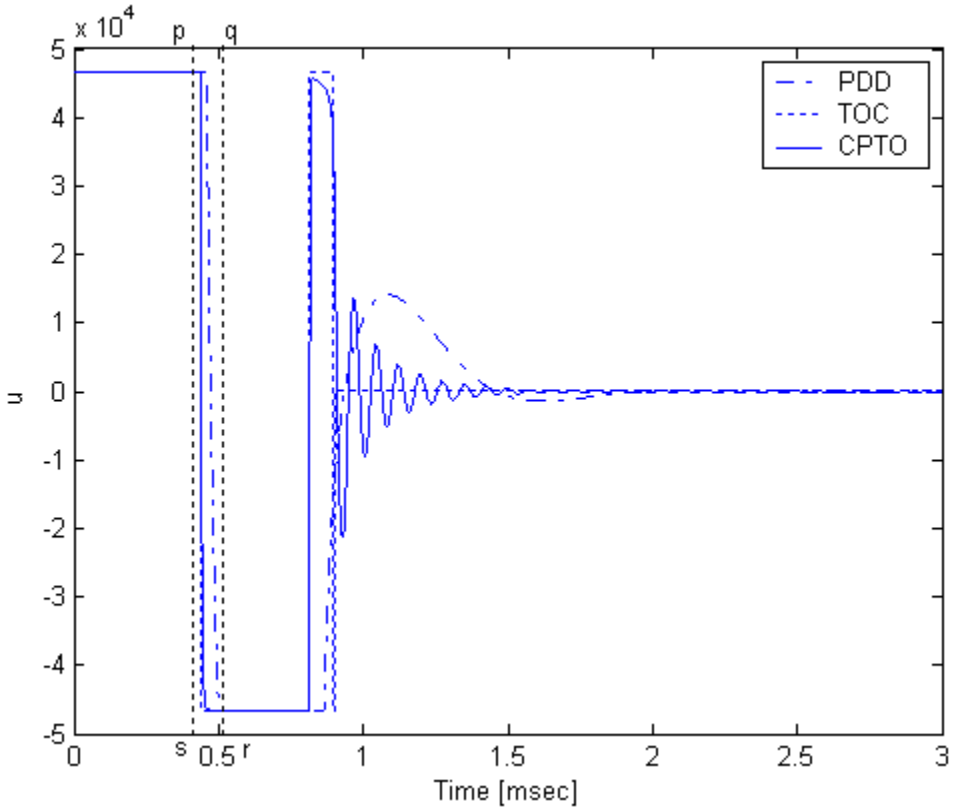

Figure 6.9 The responses of three different controllers, without chattering

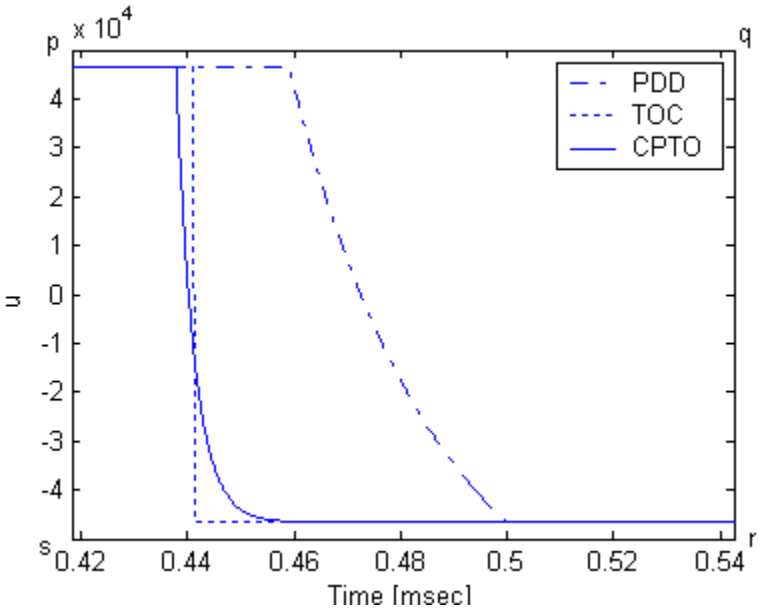

Figure 6.10 Zoomed version of the part (p q r s) of the Figure 6.9

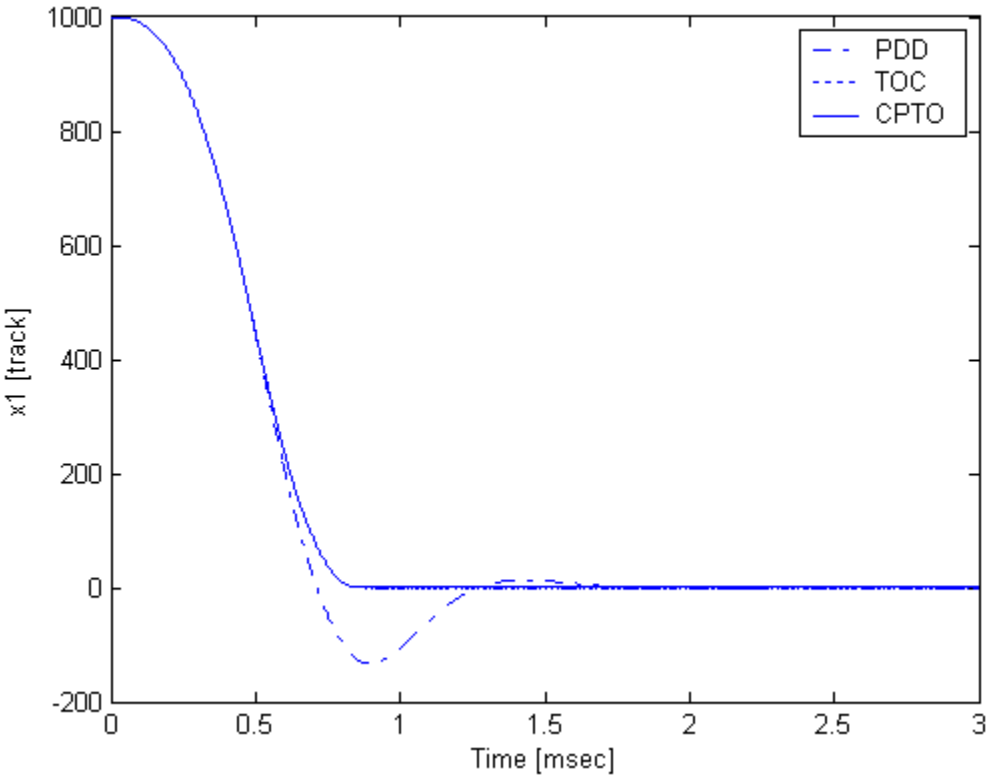

Figure 6.11 The x_1 response for three controllers

6.2. Effects of the Variation of the Gain Constants of the CPTO Controller

In the following, we will investigate the effect of changing the values of the gain constants $\mathbf{k} = [k_1 \;\; k_2 \;\; k_3]$ of the CPTO controller on the response of the controller. By choosing different criterions for the design of the linear controller, we get different values for the linear controller's gain constants $\mathbf{k}_L = [k_{1L} \;\; k_{2L} \;\; k_{3L}]$, thus, different gain constants of the CPTO controller k_1, k_2 and k_3, as were explained in Chapter 5. Changing the value of the settling time T_s of equation (5.25) and keeping the same 10% overshoot of equation (5.24), we get three different sets of gain constants, as follows,

A) $T_s = 3\ msec \;\Rightarrow\; \mathbf{k}_L = [1396 \;\; 254.21 \;\; 25.332] \Rightarrow \mathbf{k} = [898.82 \;\; 0.282 \;\; 1*10^{-4}]$

B) $T_s = 2\ msec \;\Rightarrow\; \mathbf{k}_L = [5025.5 \;\; 614.05 \;\; 43.903] \Rightarrow \mathbf{k} = [3455.6 \;\; 0.127 \;\; 0.005]$

C) $T_s = 1\ msec \;\Rightarrow\; \mathbf{k}_L = [37691 \;\; 2340.4 \;\; 89.12] \Rightarrow \mathbf{k} = [27687 \;\; 0.0322 \;\; 0.0052]$

The following figures show the simulations of the responses of the error state x_1 and the CPTO controller for three sets of gain constants A, B and C, with the same initial condition $\mathbf{x}(0) = (1000 \;\; 0 \;\; 0)$. From Figures 6.12 and 6.13, we notice that for lower values of the gain constants, it takes more time to switch from $+u_{\max}$ to $-u_{\max}$, which makes the switching "smoother", this is due to the higher thickness of the slab for lower values of the gain constants. Also, when switching from $-u_{\max}$ to $+u_{\max}$, the switching is smoother, due to the higher thickness of the tube as values of the gain constants are lower, as can be seen in Figure 6.14. On the other hand, from Figure 6.17, which is

zoomed twice of Figure 6.15, the time required for the x_1 to reach 0.1 of track error, the settling time criterion, is higher for higher values of the gain constants.

The previous results has a mathematical verification, in Chapter 5, Claim 5.1, where we have proven that the CPTO controller converges to the ideal TOC, Figure 4.4 as the gain constant k_1 goes to infinity.

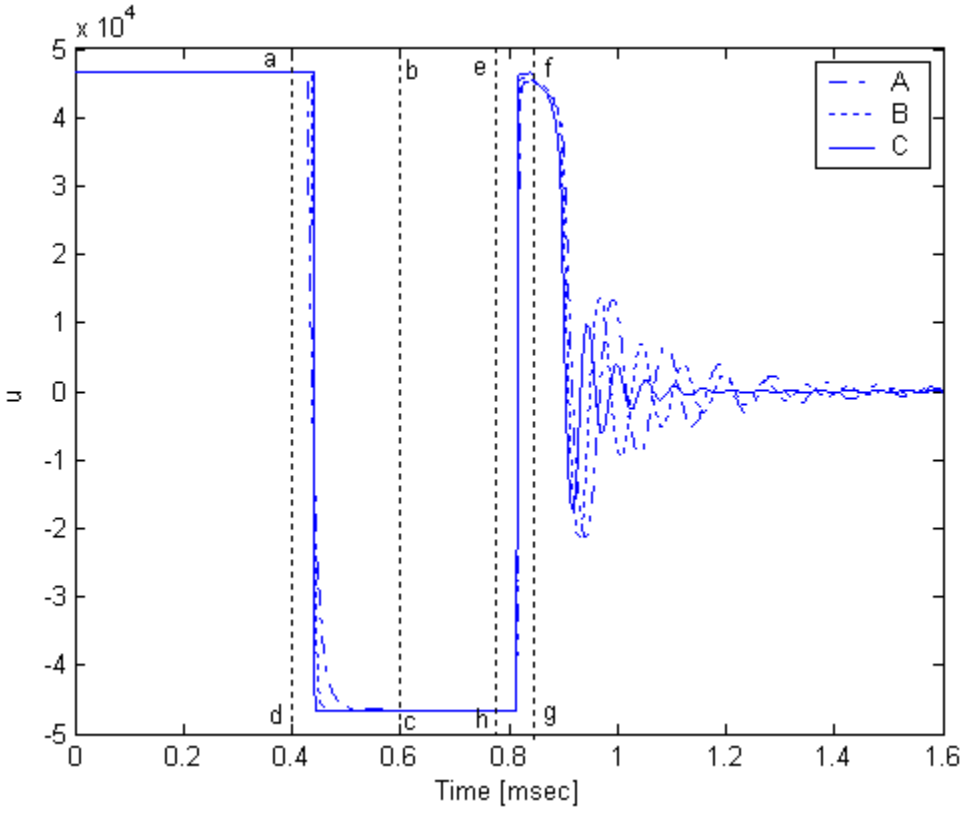

Figure 6.12 Comparison of the CPTO control for different sets of gain constants

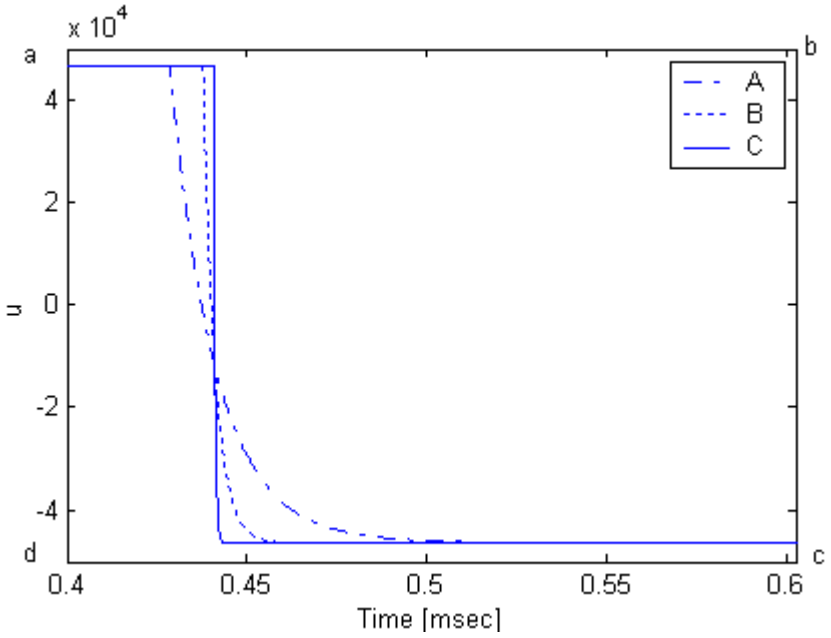

Figure 6.13 Zoomed version of the part (a b c d) of the response in Figure 6.8

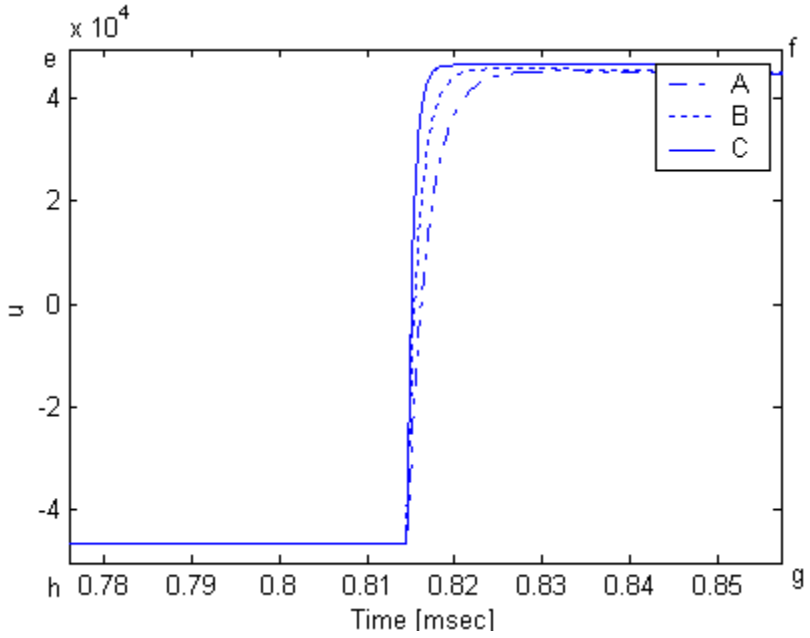

Figure 6.14 Zoomed version of the part (e f g h) of the response in Figure 6.8

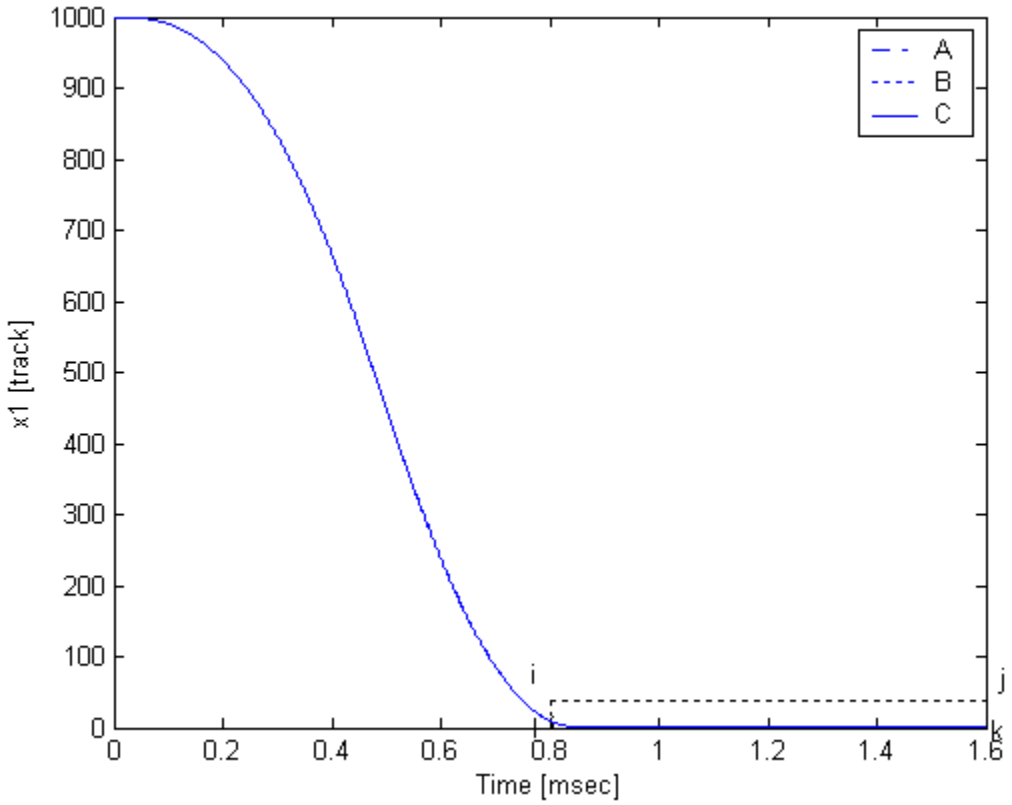

Figure 6.15 Comparison of the response of the system for the cases A, B and C

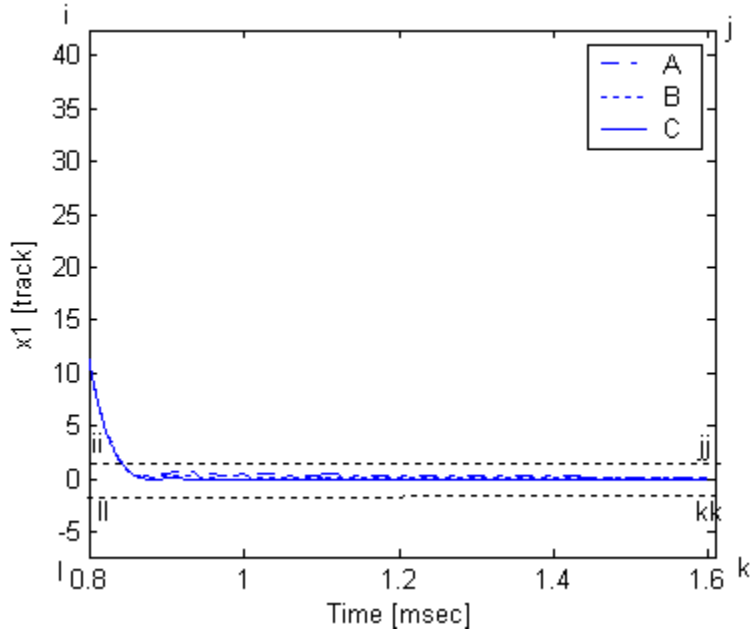

Figure 6.16 Zoomed version of the part (I j k l) of the response in Figure 6.15

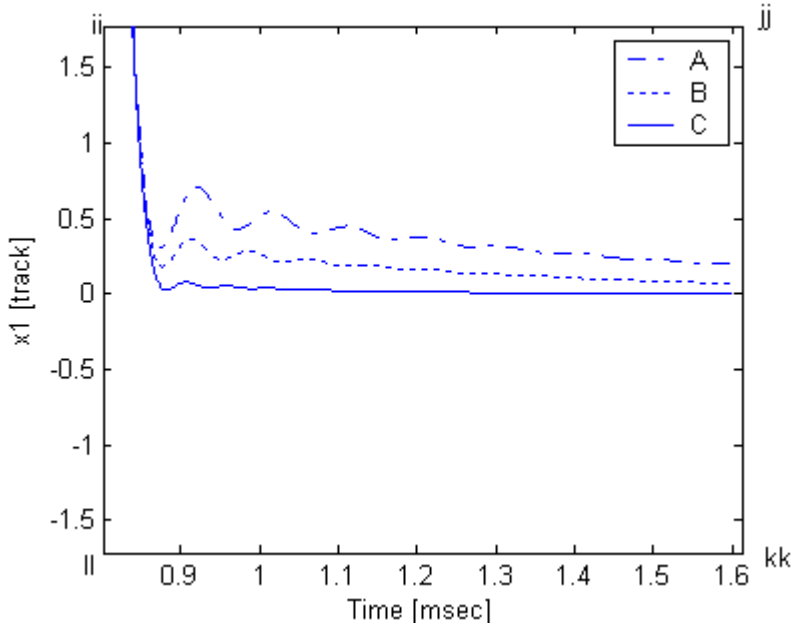

Figure 6.17 Further zoomed version of the part (ii jj kk ll) of the Figure 6.16

6.3. Robustness of the CPTO Controller

6.3.1. Robustness to Parameter Variations

The motivation behind variation analysis is provided by the fact that actual system parameters often differ from the nominal values used in the controller design. This can be due to many reasons most likely are modeling errors and environmental effects. In the case of the HDD servomechanism considered here, the higher-order dynamics are ignored or approximated [20]. Hence, studying modeling errors and parameter variations is important. In this section, we present some simulation results, which show that the proposed CPTO control system is robust to certain parameter variations. We note that we follow the similar analysis as in [8].

Let us examine first the effect on the performance of the proposed CPTO control law (5.1) due to changes in the plant gain constant, parameter *k*, in the model of the HDD servomechanism in (3.16). Assume that the actual plant gain constant is k_a, and the controller is designed for nominal plant gain constant $k_n \neq k_a$. Then the resulting system performance will be affected. Let us compare how much the performance of the proposed CPTO controller degrades as k_a deviates from k_n. Thus, we have the following two cases:

Case I: Assume that $k_a < k_n$. That is, there is less effective control than the nominal control effort. Figure 6.18 shows the error state x_1-response, with initial condition (1000, 0, 0), for a CPTO controller having parameter variation of $k_a = 0.8\, k_n$. We observe that the trajectory converges to the origin only after overshooting two times. Evidently, the response time is significantly greater than the response time of the plant with no parameter variation as can be seen in Figure 6.18. In Figure 6.19, the control varies from $+u_{\max}$ to $-u_{\max}$ continuously, more than the theoretically proven maximum number of switches, which is two. Then it experiences high fluctuation, before settling with settling time, almost, equal to 1.8 times of the settling time of the CPTO control without parameter variation.

Case II: Assume that $k_a > k_n$. That is, there is more effective control than the nominal control effort. In this case, we notice from Figure 6.20, for $k_a = 1.2\, k_n$, that there is no overshoot and the time to reach the neighborhood of the origin is less than the ideal case. From Figure 6.21, we observe that the CPTO control has faster response, for

parameter variation $k_a = 1.2\, k_n$, than the response without parameter variation. We found similar results even for $k_a = 1.4\, k_n$ in Figures 6.22 and 6.23.

Thus, we see that a larger than nominal plant gain constants actually causes a reduction in the response time. However, having a smaller than nominal plant gain constants causes one or more overshoots, which increases the response time significantly.

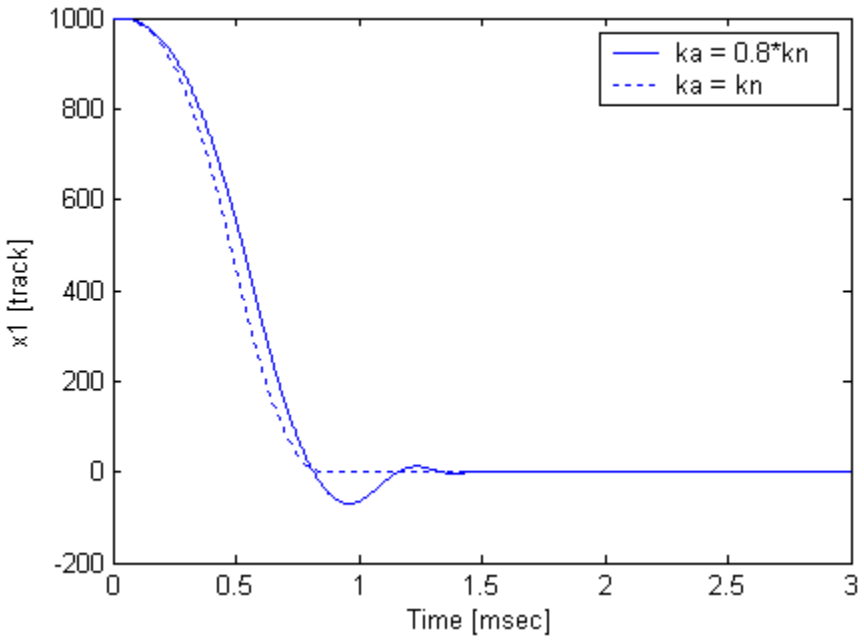

Figure 6.18 The x_1 - response of the system having $k_a = 0.8\, k_n$

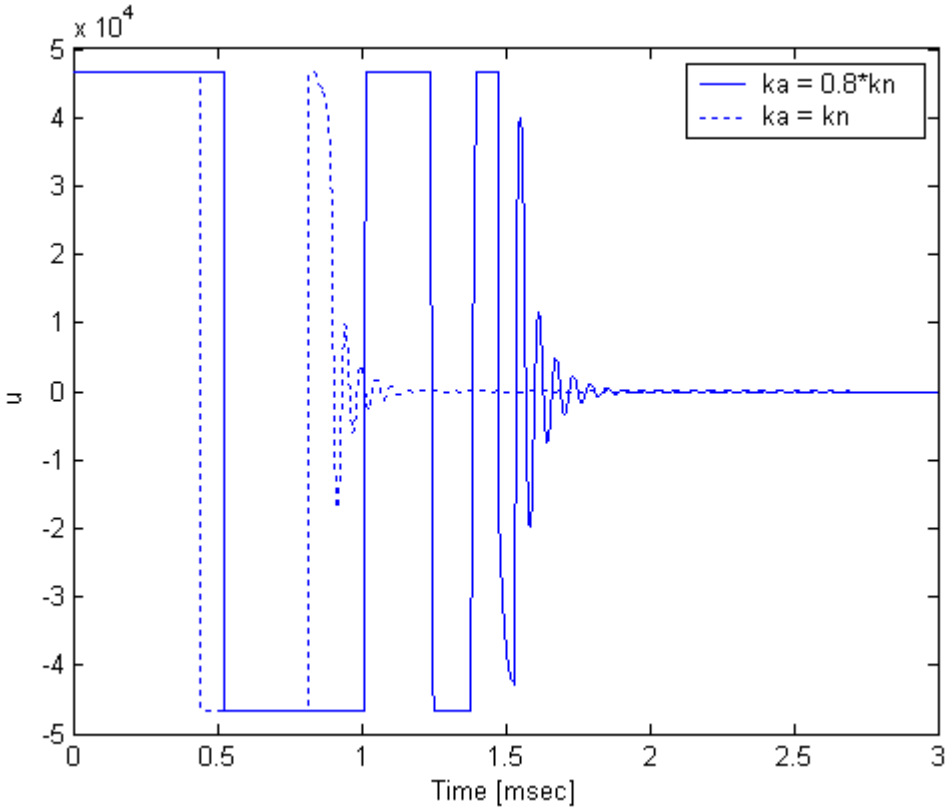

Figure 6.19 The CPTO control history for $k_a = 0.8\, k_n$

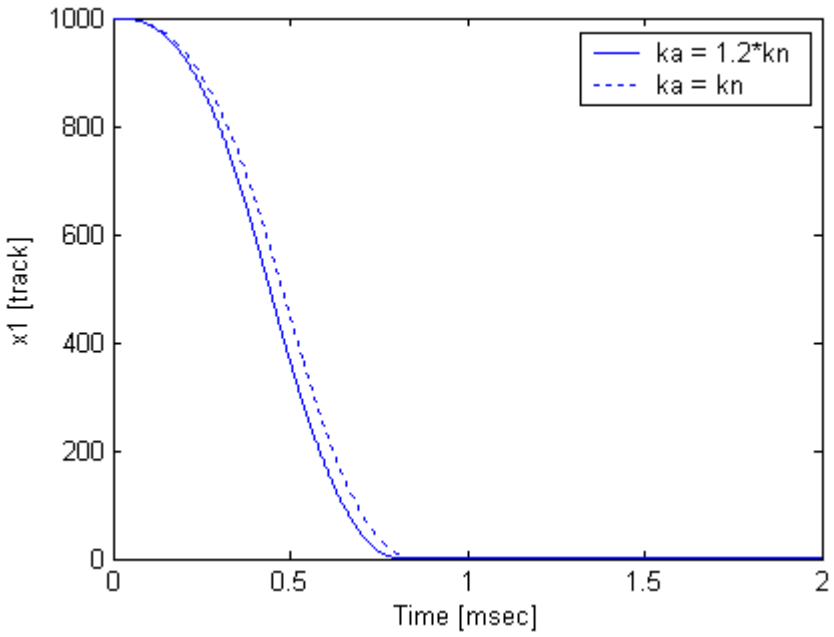

Figure 6.20 The x_1 - response of the system having $k_a = 1.2\, k_n$

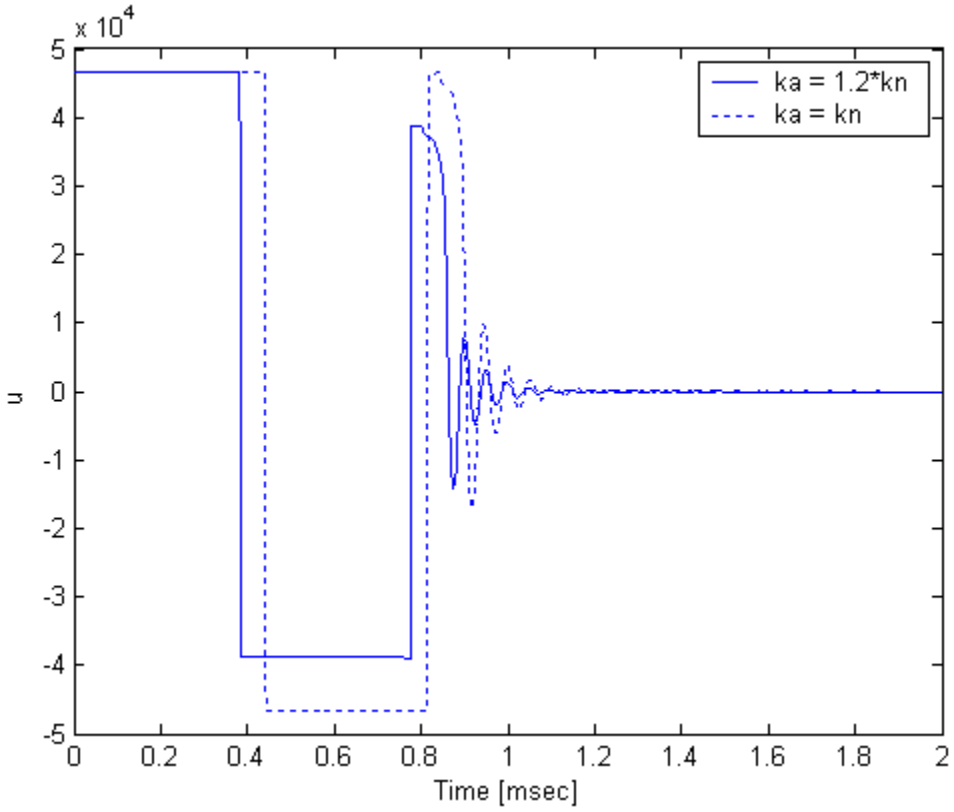

Figure 6.21 The CPTO control history for $k_a = 1.2\, k_n$

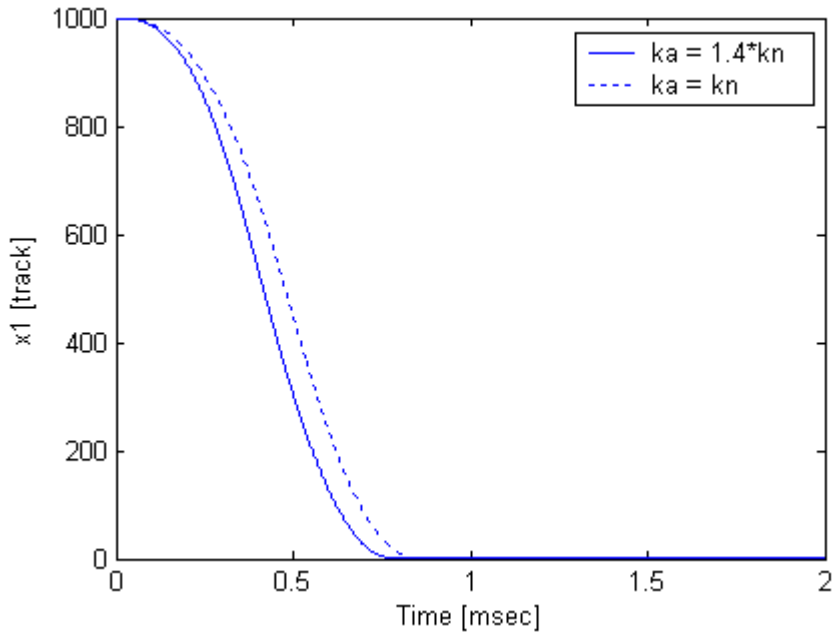

Figure 6.22 The x_1 - response of the system having $k_a = 1.4\, k_n$

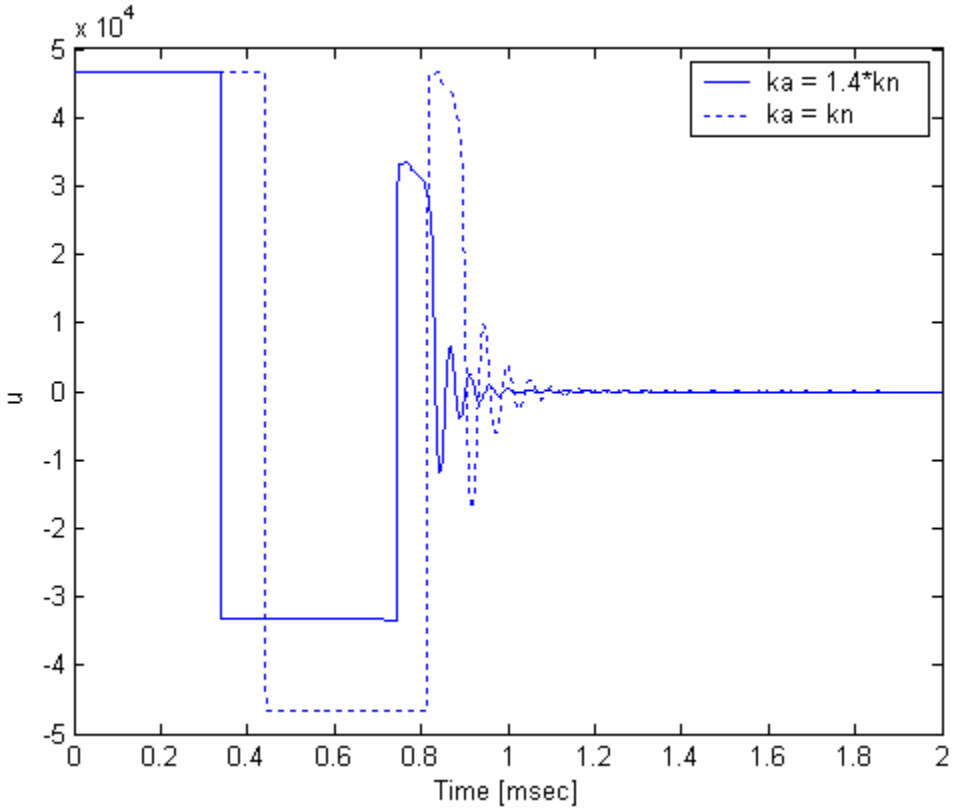

Figure 6.23 The CPTO control history for $k_a = 1.4\, k_n$

From the previous simulation results, we conclude that the control law should be designed for $k_n = k_a - d_\infty$, where d_∞ is the maximum positive uncertainty in the plant gain constant. Designing the control law in this manner is considered in [18], where it is called worst-case analysis [18].

We conclude that the designed CPTO controller is quite robust for the variations in plant gain constant k when the controller is based on the worst-case (minimum expected k) analysis.

6.3.2. Robustness due to unmodeled dynamics

In Chapter 3, we have considered that the effect of the flexibility of the read/ write arm on the performance of the system is negligible. Here, we will consider the flexibility of the arm and investigate its effect on the performance of the CPTO controller. The second order model of the flexibility, which we consider in this paper, is:

$$F(s) = \frac{\omega^2}{s^2 + 2\zeta\omega + \omega^2} \tag{6.1}$$

where ζ and ω are the damping ratio and the natural frequency, respectively. From [5], [42], the values of ω and ζ are $\omega = 15.7$ kHz and $\zeta = 0.08$.

Thus, from Figure 6.24, we can obtain the fifth order transfer function of the plant, as follows:

$$G_p(s) = \frac{K_0\omega^2}{s(s^2 + b_1 s + b_0)(s^2 + 2\zeta\omega + \omega^2)} \tag{6.2}$$

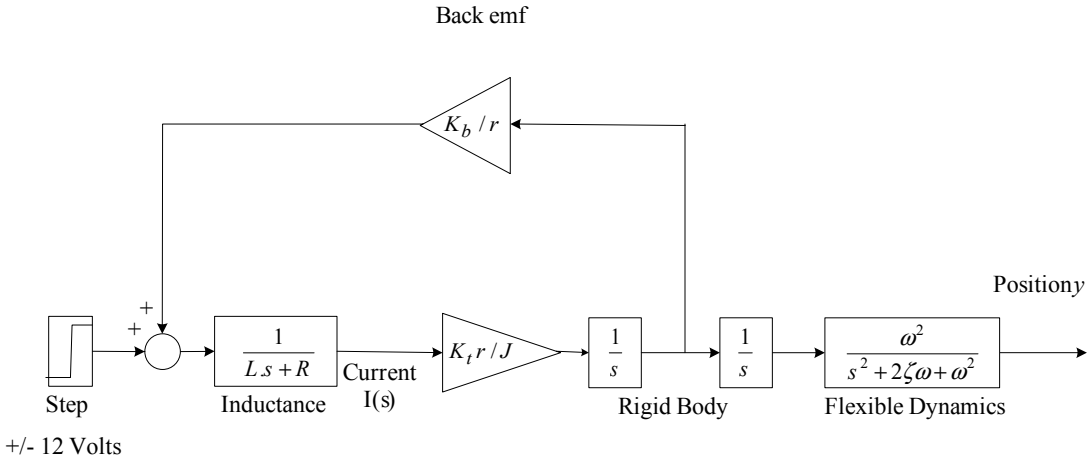

Figure 6.24 The open-loop system of HDD head positioning system considering the flexibility

The following simulations demonstrate the performance of the CPTO controller when the flexible dynamics (6.1) is considered in the model of the plant. In Figures 6.25 and 6.26, we notice that when $\omega = 15.7$ kHz, the flexibility, almost, has no real effect on the response of the system and the response of the CPTO control law. In Figures 6.27 and 6.28, we applied the same flexibility model for different initial conditions. We find that, again, it has no real effect on the performance of the system.

From [43], ω may have a range of (4-16) kHz. Thus, we simulate the response of the system when $\omega = 4$ kHz, from Figure 6.29, we can see the output of the system is still, almost, the same as the ideal system. In Figures 6.30 and 6.31, we observe from the two responses of the CPTO controller for the both cases that the response of the CPTO controller with flexibility has more overshooting and takes a little more time to settle down. In Figures 6.32 and 6.33 we tested the performance of the CPTO controller for smaller value of ω, $\omega = 0.8$ kHz, we notice that the output of the system with the considered flexibility has an overshooting but, still, the two responses have nearly the same settling time. For the CPTO controller output in Figure 6.33, the effect of the flexibility is real obvious, we notice that the controller response has some oscillation when switching between the upper and lower limit and it has it takes more time to settle down.

From the previous simulations, we conclude that for the values of the natural frequency higher than 0.8 kHz, the flexibility has no real effect on the performance of the HDD servomechanism with the CPTO controller.

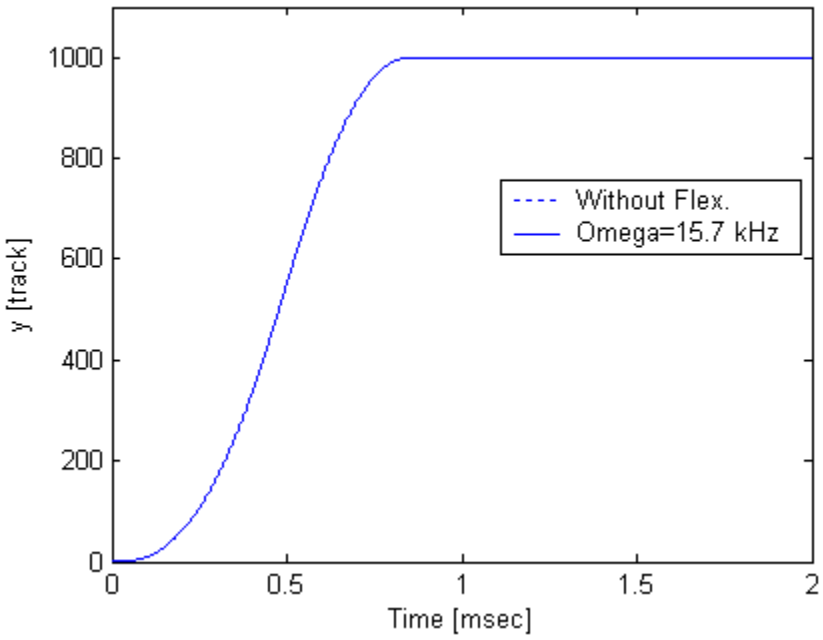

Figure 6. 25 The response of the system considering the flexibility ($\omega = 15.7$ kHz)

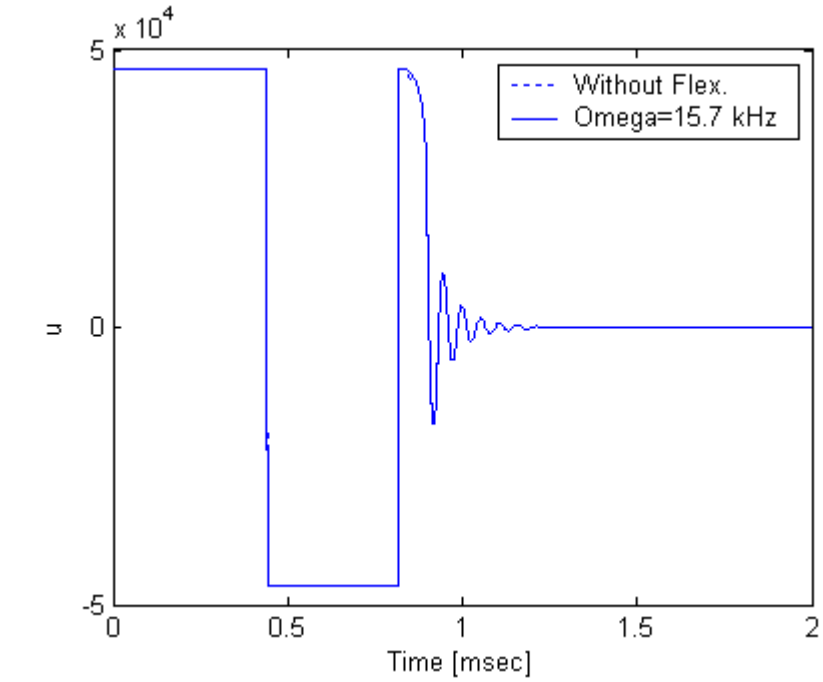

Figure 6. 26 The CPTO control history of the system considering the flexibility ($\omega = 15.7$ kHz)

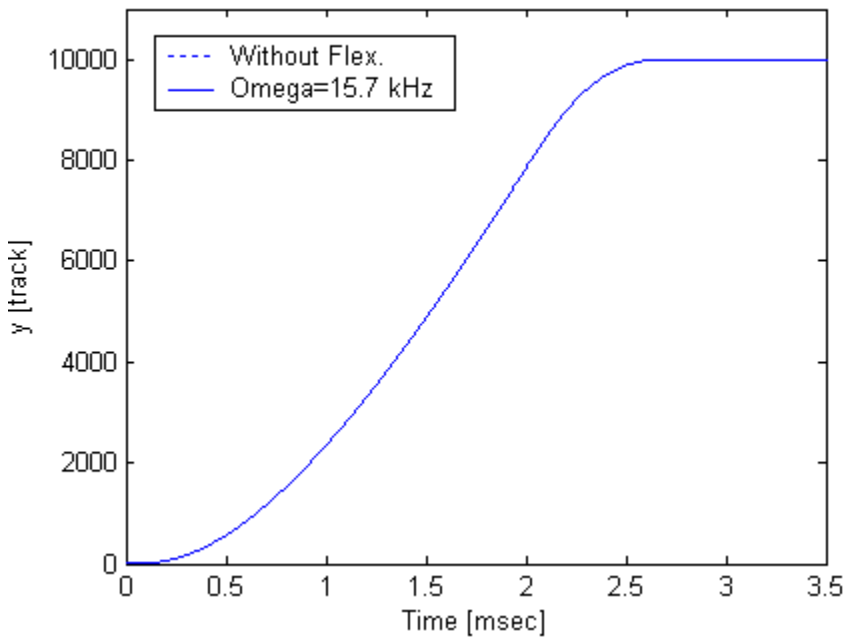

Figure 6. 27 The response of the system considering the flexibility ($\omega = 15.7$ kHz) for different initial conditions

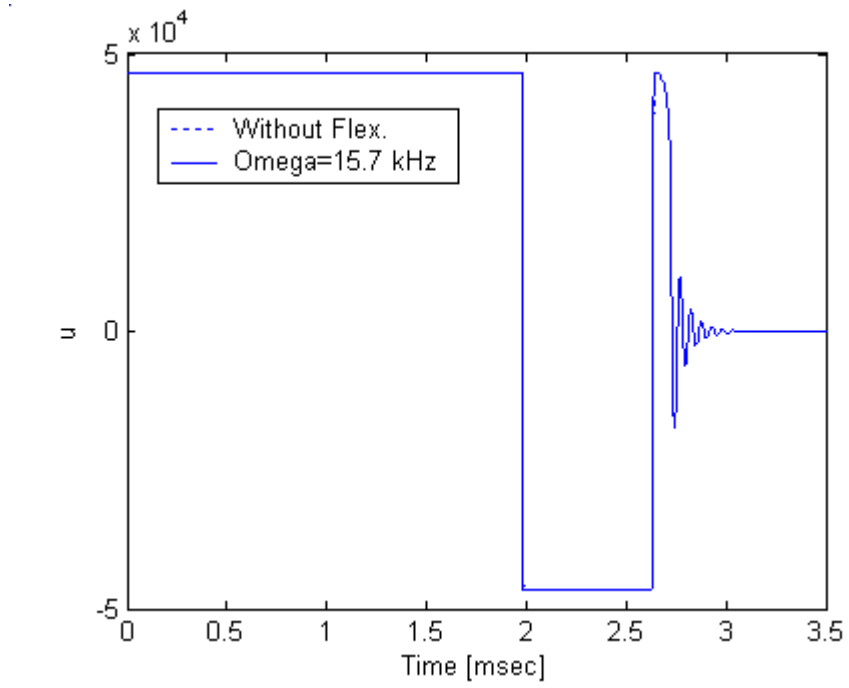

Figure 6. 28 The CPTO control history of the system considering the flexibility ($\omega = 15.7$ kHz) for different initial conditions

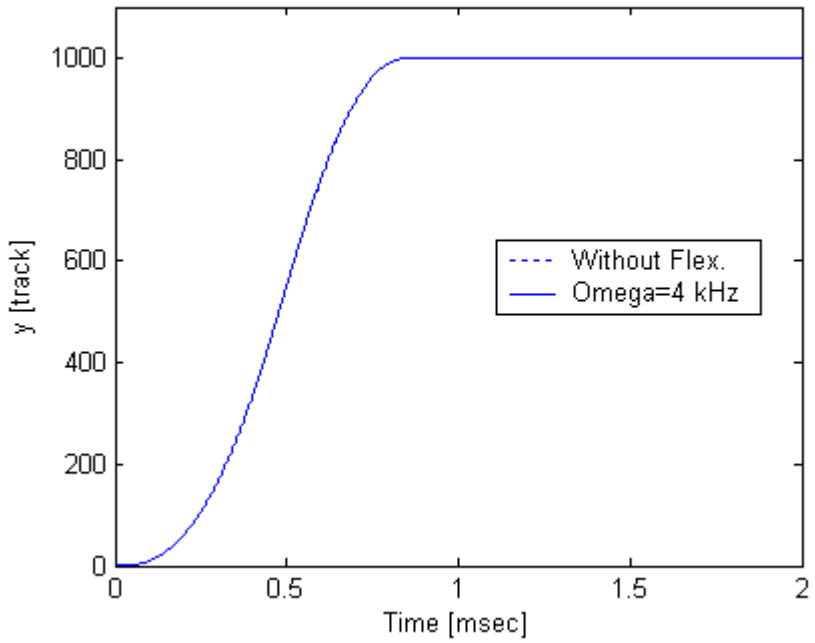

Figure 6. 29 The response of the system considering the flexibility ($\omega = 4$ kHz)

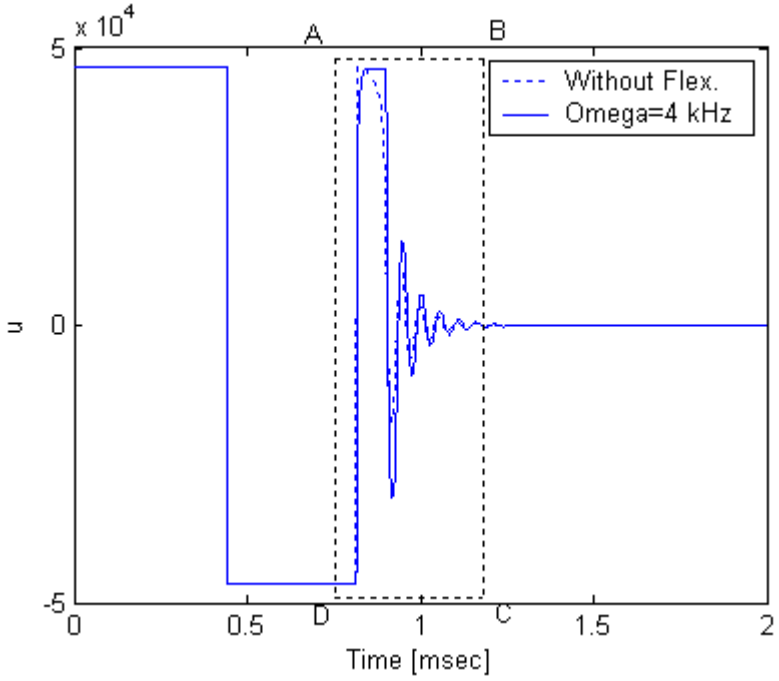

Figure 6. 30 The CPTO control history of the system considering the flexibility ($\omega = 4$ kHz)

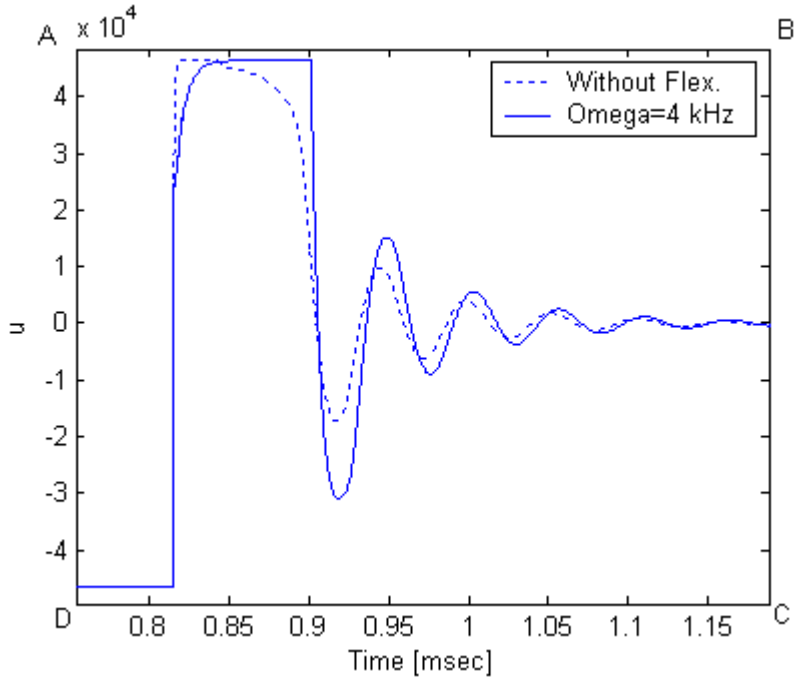

Figure 6. 31 Zoomed part of the CPTO control history of the system considering the flexibility ($\omega = 4$ kHz)

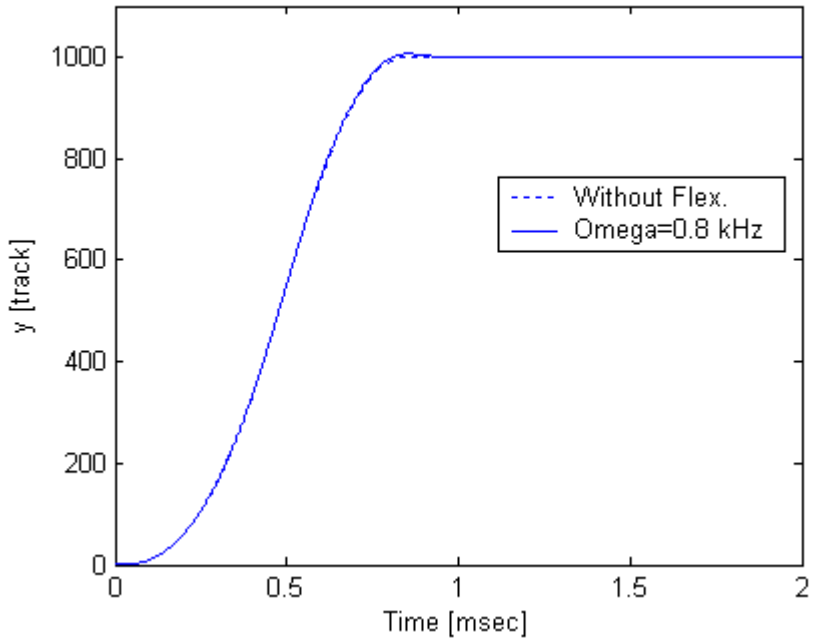

Figure 6. 32 The response of the system considering the flexibility ($\omega = 0.8$ kHz)

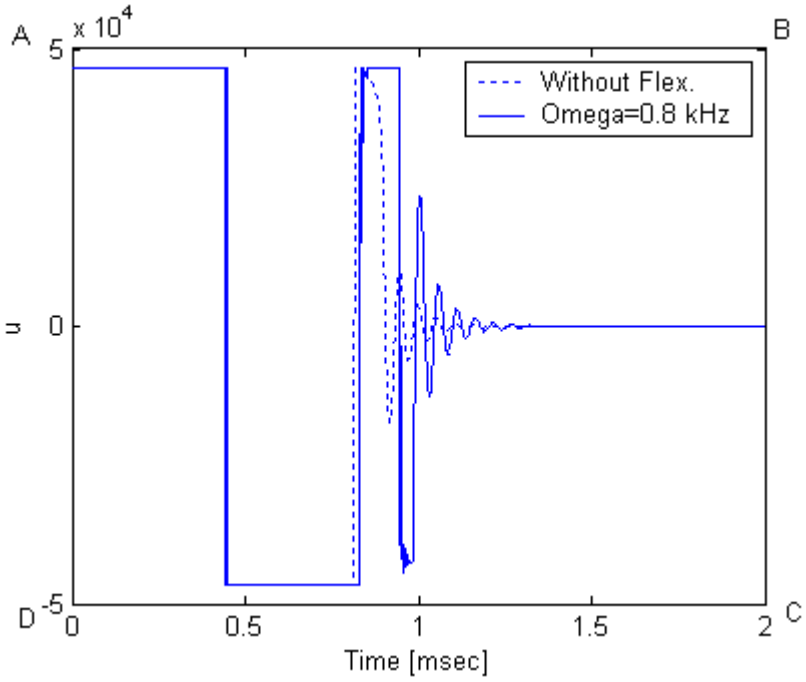

Figure 6. 33 The CPTO control history of the system considering the flexibility ($\omega = 0.8$ kHz)

6.4. Simulink Block Diagrams

In the following section, we will demonstrate the Simulink block diagrams, which have been used to get the previous simulation results,

6.4.1. CPTO controller block diagrams

For the simulation of the CPTO controller, the Simulink block diagram shown in Figure 6.24 is obtained. In this diagram, the plant dynamics and the CPTO controller, within a sub-block named "U subsystem", are indicated. A detailed block diagram of the subsystem "U subsystem" is shown in Figure 6.25. Note that the U subsystem contains a number of blocks representing the functions needed to compute s and w, where

$$s := z_1 - \mathbb{Z}_1(z_{2,}, z_3),$$

and

$$w := z_2 - Z_2(z_3).$$

Noting also that the values of *s* and *w* are the inputs the CPTO control subsystem. Figure 6.26 represents the CPTO control law (5.1).

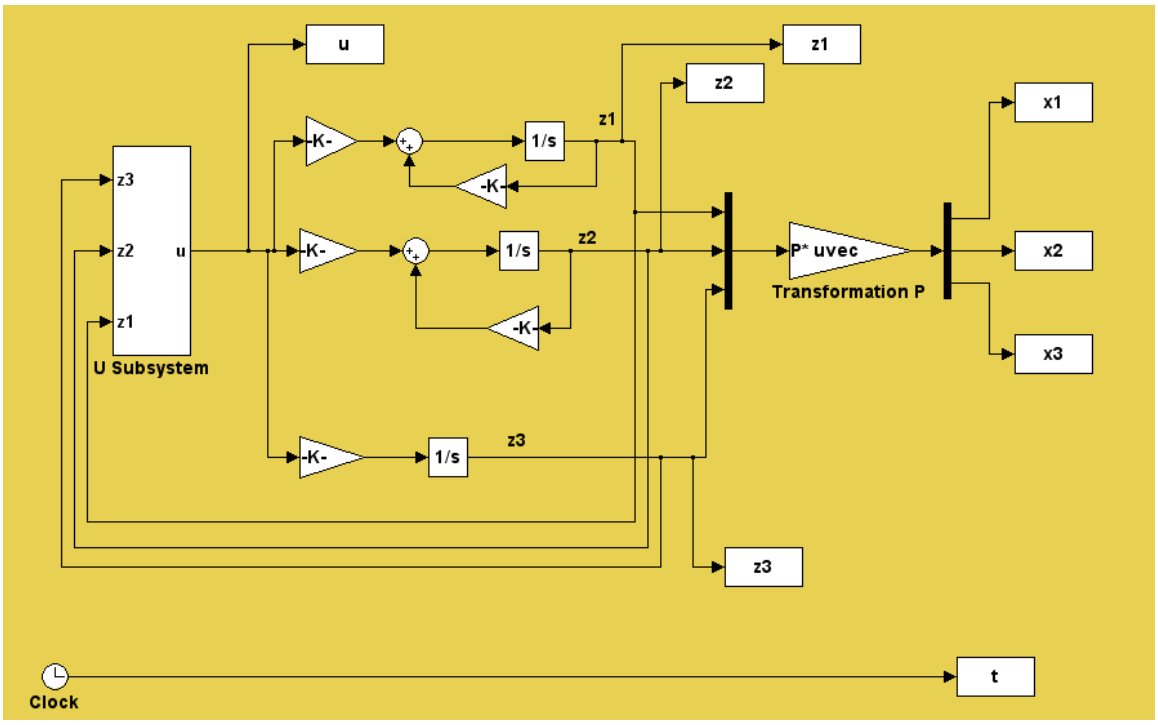

Figure 6. 34 Simulink block diagram of the CPTO controller

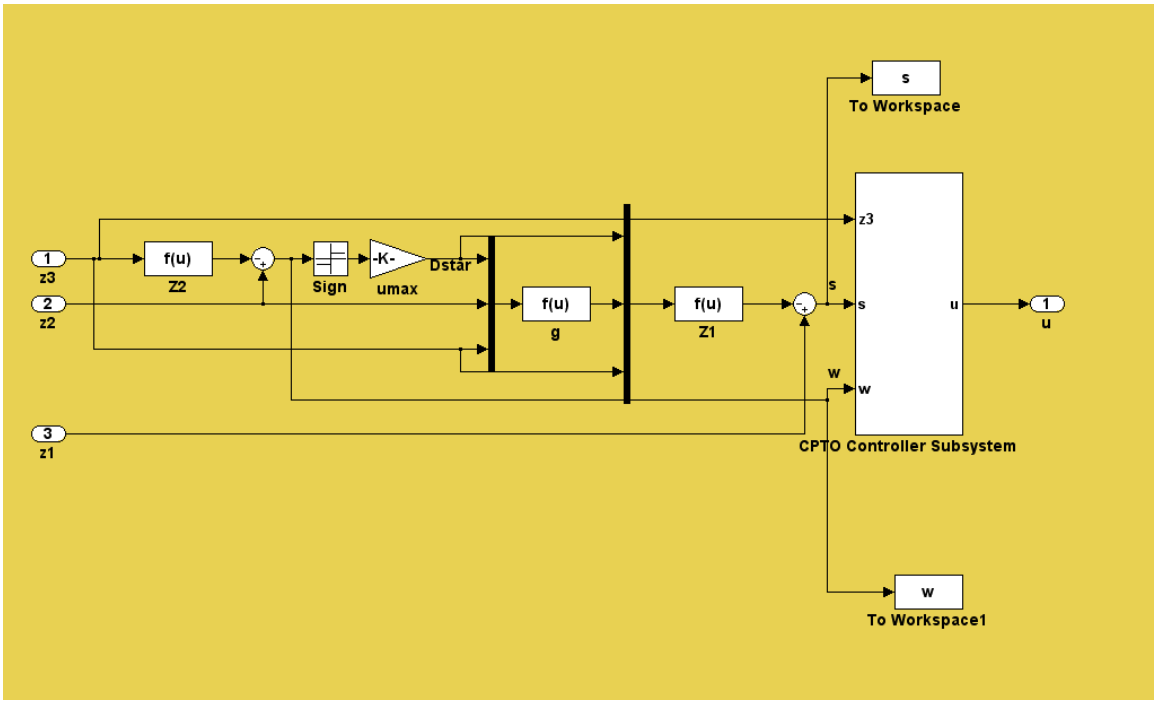

Figure 6. 35 Simulink sub-block "U subsystem" the CPTO controller

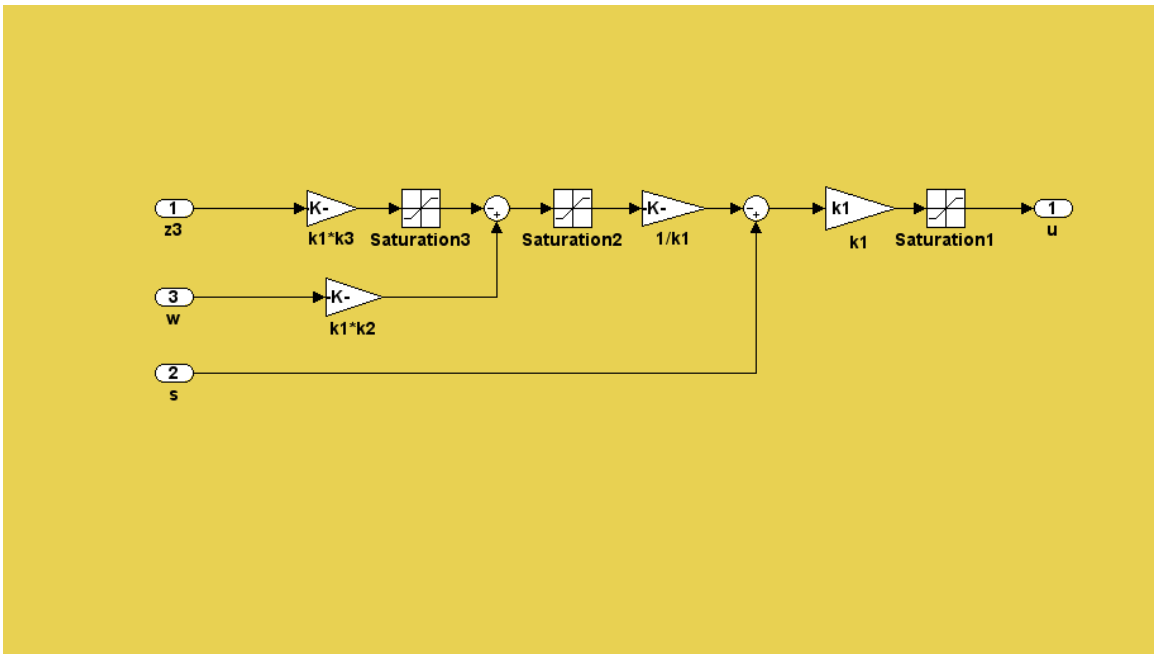

Figure 6. 36 The CPTO controller subsystem

6.4.2. The Simulink block diagrams of TOC

Since the TOC and the CPTO controller are controlling the same plant, then the plant must be common between the two controllers. We, thus, have two subsystems denoted as “U subsystem”, one for the TOC, shown in Figure 6.27, and the other for the CPTO controller, which is shown in Figure 6.25. In Figures 6.27 and 6.28 the details of the time-optimal control law (4.76) are shown.

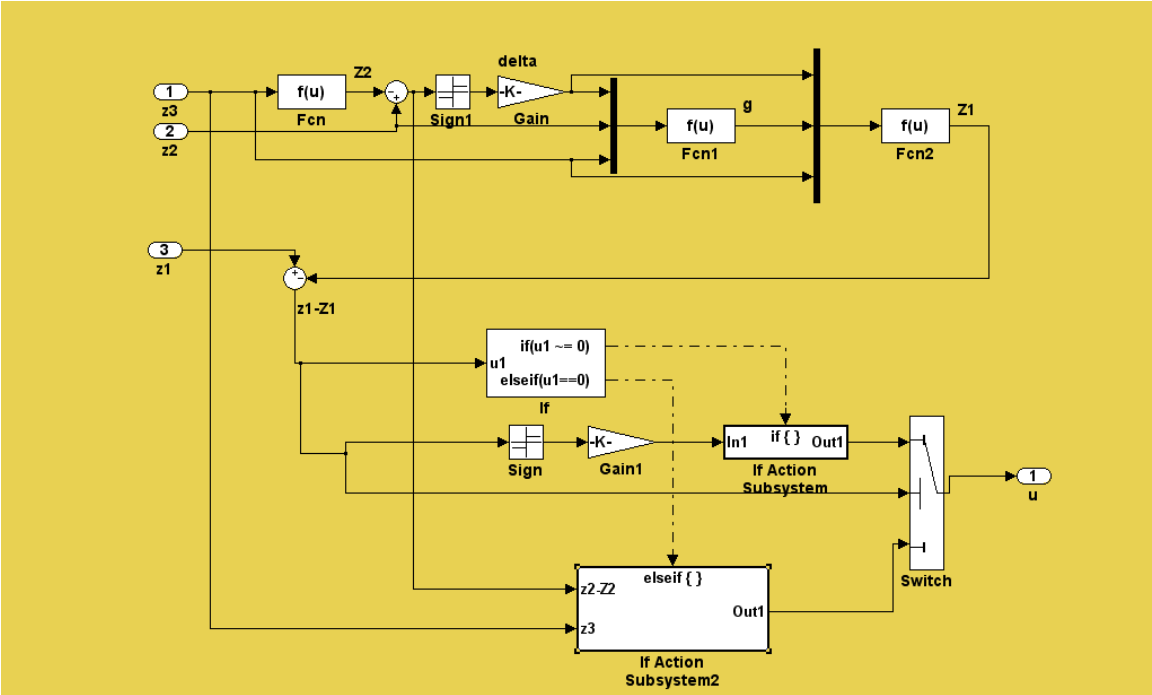

Figure 6.37 A sub-block diagram “U subsystem” of the TOC

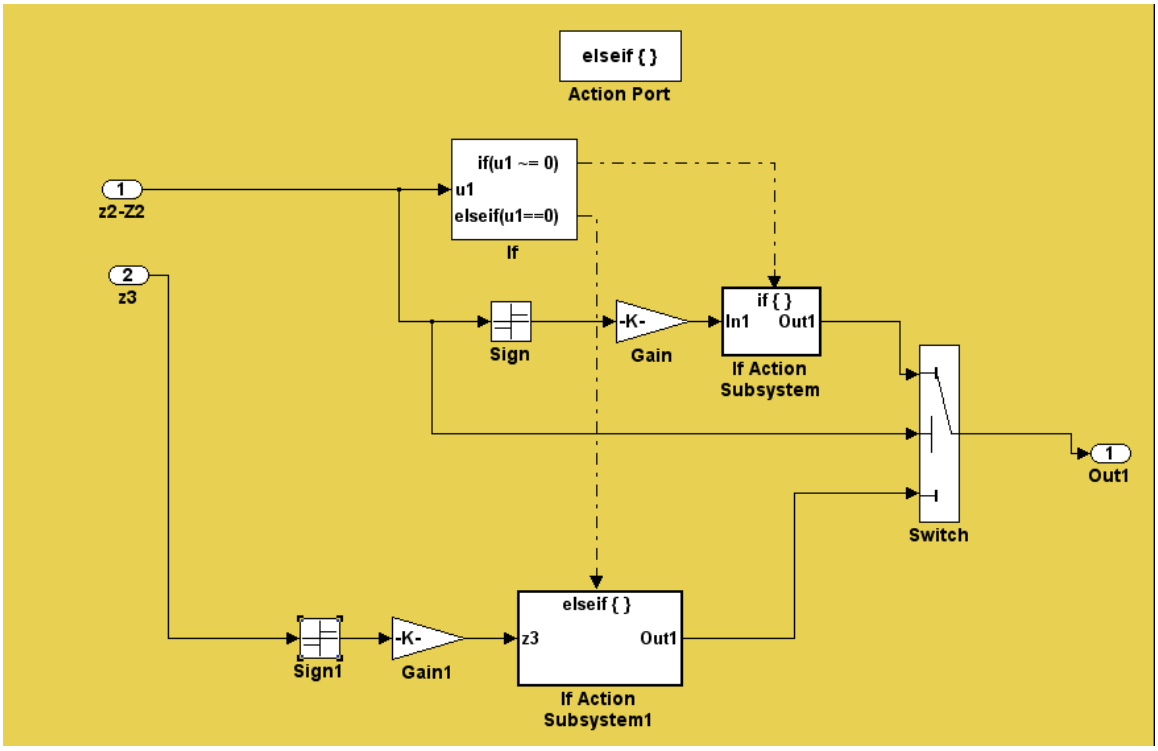

Figure 6. 37 A sub-block diagram “If action subsystem 2” of “Usub-system”

CHAPTER 7

CONCLUSIONS AND RECOMMENDATIONS

7.1. Conclusions

In this thesis, we have designed nonlinear control algorithm, Continuous Proximate Time-Optimal (CPTO) control law, for a plant having three real roots, noting that the proposed model of the Hard Disk Drive servomechanism is in this form. It has been believed that the time optimal control problem for such a plant does not have an easy analytical solution. We proposed an analytical solution to the TOC problem, based on the similarity transformation. The similarity transformation, basically, decouples the system, so that the analysis can be carried out easily in the transformed domain. We, thus, design the CPTO control law in the transformed domain, and then, by using inverse transformation, we obtain the desired results in the original domain.

We have also designed a linear state feedback controller in order to compare it with the CPTO control law regarding the performance of the two controllers.

Simulation results show that response times are indeed near time-optimal for different initial conditions. We remark that when the state is outside the final region the CPTO control law performs almost exactly the same as the ideal time-optimal control. Moreover, the CPTO controller converges to a linear controller when it comes to the region near the origin, noting that it has smooth switching rather than instantaneous switching of the ideal time-optimal control law.

We have shown through specific examples that the CPTO controller behaves well when considering the flexibility of the read/ write armature, for a wide range of frequencies. Moreover, we have shown that the CPTO controller is robust for certain plant parameter variations, providing that the control law is designed based on worst-case considerations.

A Comparison of the performance of the CPTO controller when changing its gain constants has been made.

Lastly, from the simulation results, we conclude that the designed CPTO controller is really suited for the Hard Disk Drive applications.

7.2. Recommendations for Future Work

There are still many other directions which can be explored. In particular, the following topics are suggested:

- Stability proof for the CPTO control law of the third order plant should be obtained.

- In our Hard Disk Drive modeling, we have neglected the flexibility. The technique should be developed for a system having flexibility as well. Although, we carried out some robustness analysis compensating the effect of the flexibility.
- Adaptive versions of the CPTO controller should be developed.
- The technique should be extended to develop continuous proximate time-optimal controllers for other third order plants having complex eigenvalues, unstable eigenvalues, etc.
- The theory developed in this thesis assumed that all the states are measured and the measurements are error free. In most control systems, however, not all the states can be measured and the state estimator is needed to obtain estimates of the unmeasured states.

NOMENCLATURE

A	Ampere
ARC	Adaptive Robust Control
CPTO	Continuous Proximate Time-Optimal
δ	Percentage Error
DOB	Disturbance Observer
DOF	Degree of Freedom
H	Henry
HDD	Hard Disk Drive
HOT	Higher Order Terms
Hz	Hertz
I	Current in the VCM circuit (A)
J	Moment of inertia of the head and head carriage ($Kg\ m^2$).
K_b	Back electromotive force gain (*volt sec*).
K_t	Overall armature constant ($N\ m/\ A$).
L	Inductance of the VCM
MSC	Mode Switching Controller
P. O.	Percent Overshoot
PTOS	Proximate Time-Optimal Servomechanism
r	Length of the head carriage.
R	Resistance of the VCM
RPT	Robust Perfect Tracking
SMPTOS	Slide Mode Combined with Proximate Time-Optimal Servomechanism
T	Tesla
TOC	Time-Optimal Control
TPI	Track Per Inch
T_s	Settling Time
V_1	Switching Surface
V_2	Switching Curve

VCM	Voice Coil Motor
ω	Frequency
y	Position of the read/ write head (track)
ζ	Damping Ratio

REFRENCES:

[1] D. E. Kirk “Optimal Control Theory” Prentice Hall 1970

[2] L.S. Pontrygin, V.G. Boltyanskii, R.V. Gamkrelidse, E.F. Mishchenko, “The mathematical theory of optimal processes” New York Macmillan. 1964

[3] Workman M. L., 1987, “Adaptive Proximate Time-Optimal Servomechanisms” Ph.D. thesis, Stanford University.

[4] Workman, M. L., 1987, “Adaptive Proximate Time-Optimal Control: Continuous Time Case” Proc. 1987 American Control Conference, Minneapolis, MN, pp. 589–594.

[5] Chen, B. M., Lee, T. H, Venkataramanan, V., “Hard Disk Drive Servo Systems” Springer 2002.

[6] Franklin G. F., Powell, J. D, Workman M L., “Digital Control of Dynamical Systems” 3rd edition Addison-Wesley. 1998

[7] L. Yi and M. Tomizuka. “Two-Degree-of-Freedom Control with Robust Feedback Control for Hard Disk Drive Servo Systems” IEEE/ASME transaction on mechatronics, Vol. 4, No 1, March 1999

[8] Kalyon M., “Continuous Proximate Time-Optimal Control of Servomechanisms” Ph.D. thesis, University of Michigan 1993.

[9] M. Kalyon, “Near Minimum Time Optimal Track-to-Track Seek Control of HDD by Continuous Proximate Time-Optimal Control,” in Proc. Mechatronics 2004, Ankara, Turkey, Aug. 30 2004, pp. 24-57.

[10] Kalyon, M., "Design of Continuous Time Controllers Having Almost minimum Time Response," ASME Dyn. Syst. Meas. Control, 124, June, pp 252-260. 2002.

[11] Kalyon, M., "Continuous Proximate Time-Optimal Control of an Aerodynamically Unstable rocket", Journal of Guidance, Control, and Dynamics 20, pp 1049-1052. 1997,

[12] Dorf R. C, and Bishop R. H., "Modern Control Systems" 9th edition Prentice-Hall, 2001.

[13] Goh T.B. et al, "Design and Implementation of a Hard Disk Drive Servo System Using Robust and Perfect Tracking Approach" IEEE Trans Cont Sys Tech, 9, pp. 221-233, 2001.

[14] McDonald, D. C. "Multiple Mode Operation of Servomechanisms" Rev. Sci. Ins., Vol. 23, pp. 22-30, January 1952.

[15] McDonald, D. C. "Intentional Nonlinearization of Servomechanisms" Proc. Symp. On Nonlinear Circuit Analysis, Polytechnic Inst. of Brooklyn, NY, pp. 402-411. 1953.

[16] Wu, S. T., "Time-Optimal Control and High-Gain Linear State Feedback" Int. J. of Control, 72, pp. 764-772. 1999.

[17] Pao, L. Y., and Franklin, G. F., "Proximate Time-Optimal Control of Third-Order Servomechanisms," IEEE Trans. Autom. Control, 38, pp. 560-580. 1993.

[18] Pao, L. Y., and Franklin, G. F., "Robustness of Proximate time-Optimal Control" IEEE Trans. Autom. Control, 39, pp. 1963-1966. 1994.

[19] Pao L. Y., "Proximate Time-optimal Control for High-Order Servomechanisms" Ph. D. thesis, Stanford University, November 1991.

[20] Ho, H.T., “Fast Servo Bang-Bang Seek Control”, IEEE Transactions on Magnetics, 33, No. 6, pp. 4522-4527. 1997.

[21] Yamaguchi T., Soyama Y., Hosokawa H., Tsuneta K. and Hirai H. “Improvement of Settling Response of Disk Drive Head Positioning Servo Using Mode Switching Control with Initial Value Compensation. IEEE Trans. Magn. 32: 1767-72, 1996.

[22] T. Yamaguchi, H. Numasato and H. Hirari “A mode switching control of motion control and its application to disk drives: Design of optimal mode switching conditions” IEEE/ASME Trans. Mechatron., 3:202-9. 1998.

[23] Iwashiro, M., Yatsu, M. and Suzuki, H. “Time optimal track-to-track seek control by model deadbeat control” IEEE Trans Magn., 35, pp. 904-9. 1999.

[24] Newman, W. S., “Robust near time-optimal control” IEEE Trans Auto Cont 35, pp. 841-844. 1990

[25] You, K. H., Lee, E. B., ”Robust, Near Time-Optimal Control of Nonlinear Second Order Systems with Model Uncertainty” Proceedings of IEEE Int. Conf. on Cont. App., Alaska, USA September 25-27, 2000

[26] Zhou, J., Zhou, R., Wang, Y., Guo, G. “Improved proximate time-optimal sliding-mode control of hard disk drives” IEE Proceedings- Contr. Theory and App. , 148 , 6:516 -522, Nov. 2001

[27] Zhang D. Q. and Guo G. X. “Discrete-time sliding mode proximate time optimal seek control of hard disk drives” IEE Proc.-Control Theory and App., Vol. 147, No. 4:440-446 July 2000

[28] Choi H. T., Kim B. K., Suh I. H. and Chung W. K. “Design of Robust High-Speed Motion Controller for a Plant with Actuator Saturation” ASME Dyn. Syst. Meas. Control, 122, September, pp 535-541. 2000.

[29] K. Liu, B.M. Chen, and Z. Lin “On the problem of robust and perfect tracking for linear systems with external disturbances” Int. J. Control, Vol. 74, No. 2, 158-174, 2001.

[30] B.M. Chen “Robust and H∞ Control” London Springer 2000.

[31] Ogata K., “ Modern Control Engineering” Prentice-Hall 1970

[32] La-orpacharapan C. and Pao L. Y., " Fast Seek Control for Flexible Disk Drive Systems with Back EMF and Inductance," Proc. American Control Conf., Denver, CO, pp. 3077-3082, June 2003.

[33] Ananthanarayanan K. S. “Third-Order Theory and Bang-Bang Control of Voice Coil Actuators” IEEE Trans. Mag**.** Vol. 18, No. 3, 1982.

[34] Halliday D., Resnick R. and Walker J., “Fundamentals of Physics” 5th edition, John Wiley and Sons, Inc. 1997.

[35] Naidu, D. S., “Optimal Control Systems” CRC Press. 2003.

[36] Burghes, D. N., and Graham, A., “Introduction to control theory including optimal control” John-Wiley & Sons. 1980.

[37] Bonger, I., and Kazda, O. F., “An Investigation of the Switching Criteria for Higher Order Contactor Servomechanisms” AIEE Transactions, 73, pp. 118–127. 1954

[38] Athans, M., and Falb, P. L., “Optimal Control: An Introduction to the Theory and Its Applications”, McGraw-Hill, New York. 1966

[39] Rauch, L. L. and Howe, R. M., "A Servo with Linear Operation in Region About The Optimum Discontinuous Switching Curve" Proc. Symp. On Nonlinear Circuit Analysis, Polytechnic Int. Brooklyn, NY April, 1956.

[40] http://www.storagereview.com/map/lm.cgi/seek.

[41] MathWorks, Inc. Version 6.5. Simulink, dynamic system simulation for Matlab, 2002.

[42] Venkataramanan, V., Peng K., Chen, B. M. and Lee, T. H., "Discrete-Time Composite Nonlinear Feedback Control With an Application in Design of a Hard Disk Drive Servo System" IEEE Trans. Cont. Sym. Tech., Vol. 11, No. 1, pp. 16-23. 2003.

[43] Li, Y., and Horowitz R., "Active Vibration Control of a PZT Actuated Suspension in Hard Disk Drives" Proc. 2002 American Control Conference, Anchorage, AK, pp. 1366–1371.

Vita

Mohammad Samer Charifa was born on August 29, 1978 in Aleppo, Syria. In 1996, he graduated from the high school. Then, he attended Aleppo University, where he received his Bachelor of Science degree in Mechanical Engineering in September 2001. In the summer of 2002, he came to Saudi Arabia where he joined King Fahd University of Petroleum & Minerals to work towards his Master of Science in Mechanical Engineering.